Fall 2016

Methodology for analysis of stress, creep, and fatigue behavior of compliant mechanisms

Joshua Allen Crews

Department: Mechanical and Aerospace Engineering

METHODOLOGY FOR ANALYSIS OF STRESS, CREEP, AND FATIGUE BEHAVIOR OF COMPLIANT MECHANISMS

by

JOSHUA ALLEN CREWS

A DISSERTATION

Presented to the Faculty of the Graduate School of the

MISSOURI UNIVERSITY OF SCIENCE AND TECHNOLOGY

In Partial Fulfillment of the Requirements for the Degree

DOCTOR OF PHILOSOPHY

in

MECHANICAL ENGINEERING

2016

Approved
L. R. Dharani, Advisor
A. Midha, Co-Advisor
V. Birman
K. Chandrashekhara
J.S. Thomas

PUBLICATION DISSERTATION OPTION

This dissertation has been prepared in the form of five papers for publication as follows:

Paper I, Pages 9 – 49, is intended for submission to the JOURNAL OF STRAIN ANALYSIS.

Paper II, Pages 50 – 83, is intended for submission to the JOURNAL OF MECHANICAL DESIGN.

Paper III, Pages 84 – 125, is intended for submission to MECHANISMS AND MACHINE THEORY.

Paper IV, Pages 126 – 169, is intended for submission to POLYMERS AND POLYMER COMPOSITES.

Paper V, Pages 170 – 206, is intended for submission to ENGINEERING FAILURE ANALYSIS.

ABSTRACT

A methodology is developed for analyzing stress within homogeneous and metallic-reinforced, fixed-free compliant segments and small-length flexural pivots. Boundary conditions related to the inclusion of metallic reinforcing components within a polymer compliant segment are investigated. The analysis method outlined herein relies on key outputs from the pseudo-rigid-body models (PRBMs). A method is presented for the redesign of compliant mechanisms to include metallic reinforcement to reduce stress while maintaining force-deflection behavior. Examples are provided in which a compliant segment is redesigned to include metallic reinforcement by using the stress equations developed from the PRBM. The effect of bonding between the polymer casing and the metallic reinforcement is addressed by presenting theoretical calculations as well as results obtained from deflection testing of compliant segments with near-frictionless tangential behavior and by testing segments with an intentional bond between the casing and insert. Fatigue, creep, and stress relaxation test results are presented to show the improvement in performance provided by the inclusion of metallic reinforcement. Lastly, fractography provides an overall view of the fracture behavior, including fracture initiation sites and propagation behavior of both homogeneous and metallic-reinforced compliant segments. The results show that the fatigue, creep and stress relaxation behavior of a compliant segment can be significantly improved by redesigning the segment to include a metallic reinforcing member.

ACKNOWLEDGMENTS

I would like to express my sincere appreciation to my advisor, Professor Lokeswarappa R. Dharani, for encouraging me to continue my education in the field of mechanical engineering and for providing endless support during my doctoral research efforts. I am grateful for the education and guidance provided by him, both academically and professionally.

I would like to express equal gratitude to my co-advisor, Professor Ashok Midha, for sharing invaluable knowledge gained over years of development in the field of compliant mechanisms. I am also grateful for the patience, motivation, and personal encouragement offered by him throughout the research effort.

I would also like to thank my Advisory Committee members Professor Victor Birman, Professor K. Chandrashekhara, and Professor Jeffery Thomas for their generous donation of time and effort.

Lastly, I would like my wife Crystal Crews; my son Carter Crews; and my daughter Charlotte Crews for their endless love, patience, encouragement, and support while pursuing this challenging degree.

TABLE OF CONTENTS

LIST OF ILLUSTRATIONS

Page

PAPER I

PAPER II

PAPER III

PAPER IV

PAPER V

LIST OF TABLES

SECTION

1. INTRODUCTION

1.1. COMPLIANT MECHANISMS

A mechanism is a mechanical device whose links and movable joints allow the transfer or transformation of motion, force, or energy [1], [2]. Unlike a rigid-body mechanism, a compliant mechanism is a type of mechanism that transfers or transforms motion, force, or energy through the deflection of its links or segments [3], [4]. Compliant mechanisms are typically classified as fully compliant or partially compliant. A fully compliant mechanism contains no links or traditional kinematic pairs; therefore, all transfers or transformation of motion, force, or energy occur due to deflection of its members [2], [5]. In contrast, a partially compliant mechanism contains at least one kinematic pair and one link. Therefore, a partially compliant mechanism gains some of its motion through the deflection of at least one member and some of its motion through the rotation or translation of a kinematic pair such as a slider or pin joint [2].

Many unique advantages are provided by compliant mechanisms, some of which are included below [2], [4], [6], [7]:

1. Reduced cost due to their limited part count and minimal assembly required
2. Excellent corrosion resistance, if constructed from engineering plastics
3. Precise motion provided by the elimination of joints, which prevents backlash and wear

4. Energy storage made possible by maintaining segments in the deformed state

A select few disadvantages of compliant mechanisms are included below [2], [6], [7]:

1. The design of compliant mechanisms is more complex than the design of rigid-body mechanisms due to large deflections and energy storage associated with compliant segments.
2. Compliant mechanisms constructed of engineering plastics and subjected to cyclic loads or deflections may fail prematurely from fatigue.
3. Compliant mechanisms constructed of engineering plastics and subjected to long-term exposure to loads or deflections may fail from creep or stress relaxation

1.2. PSEUDO-RIGID-BODY MODEL

Extensive research has been conducted into the development and use of a pseudo-rigid-body model (PRBM) to aid in the design of compliant mechanisms. The overall approach of the PRBM method is to model a compliant segment's tip deflection by replacing the compliant segment with a rigid body analog. The analogous rigid-body mechanism was conceptualized by introducing strategically placed kinematic pairs and torsional springs in an attempt to mimic the forces and deflections of the compliant mechanism in question. Development and further refinement of the PRBM method for various segment types have been a major focus of researchers since its introduction. Howell and Midha [5], [8] developed a PRBM for fixed-free compliant segments. Howell and Midha [9] included equations used to identify the location of pin joints, called characteristic pivots, and initial equations to determine the torsional spring

stiffness. Howell went on to develop additional PRBMs for other compliant segment types, notably the fixed-guided and initially curved fixed-pinned segment types [2], [10]. Equations for torsional spring stiffness were further refined by Pauly and Midha [11] and by Midha et al. [12]. Kuber extended the PRBM concept by developing a method of analyzing deflections of compliant segments containing spring steel inserts [7].

Compliant mechanisms, as mentioned above, are designed to transfer motion, force, or energy through deflection of their members. It would be unusual for a mechanism to be designed for a single load cycle. Mechanisms are often designed to accomplish a single task or a set of similar tasks in a repeated fashion. As such, it is anticipated that mechanisms are used in machine design applications or consumer products where deflection and associated stress cycles will occur many times in a relatively predictable fashion [2]. Repeated stress cycles can ultimately result in fatigue failure. This is in distinct contrast to structural design in which members are designed to sustain relatively constant loads with minimal deflection for a long period of time.

The consistent nature of the stress cycles in compliant mechanisms lends well to fatigue analysis via the stress-life model [2]. The stress-life approach to fatigue analysis is based upon the relationship between cyclic stress and the number of cycles to failure. Therefore, the model tends to decrease in accuracy with increased variation in stress from one cycle to another. The relationship between stress and number of cycles to failure for a particular material is represented by its associated Wöhler fatigue curve. The Wöhler fatigue curve (S-N curve) plots the number of cycles to failure (N) versus stress amplitude (S).

The dissertation consists of five papers that address specific tasks aimed at improving the fatigue, creep, and stress relaxation behavior of compliant segments by introducing metallic reinforcement. Each paper begins with a thorough review of background information related to compliant mechanism design and analysis techniques, namely the PRBM.

1.3. MOTIVATION AND SCOPE OF INVESTIGATION

This section presents the academic and industrial motivation as well as objectives of this investigation. The academic and industrial motivations share a common goal: to provide a concise design guide for metallic-reinforced compliant mechanisms to be used by students, academic professionals, and industry professionals as a reference for compliant segments used in applications containing cyclic loads, sustained loads, or deflections.

1.3.1. Academic Motivation. A main objective of this research effort is to bridge the gap between currently available, large-deflection analysis tools such as the PRBM and small-deflection bending stress equations commonly used in structural design. This information enables students and academic researchers to accurately predict stresses within compliant mechanisms subjected to cyclic or sustained load conditions and large deflections. A thorough understanding of stresses within compliant segments will unlock additional research areas for compliant mechanisms. Specific academic objectives for this research are listed below:

1. Advance existing research in the area of pseudo-rigid-body model analysis by developing equations for stresses within both homogeneous and metallic-reinforced compliant segments. This effort aims to transfer the

compliant segment stiffness and deflections from the well-established pseudo-rigid-body model into bending stress and axial stress equations widely accepted for use in static analysis of beams and columns.

2. Provide detailed testing methods, procedures, and fixture designs related to the empirical study of force-deflection behavior, fatigue behavior, and creep behavior of both homogeneous and metallic-reinforced compliant segments. It is hoped that techniques identified and validated in this research effort can be replicated or used as a foundation to conduct similar investigations requiring physical testing of compliant mechanisms.
3. Present a detailed comparison between theoretical calculations for fatigue life (based on PRBM stress equations) and experimental testing results for specific load cases applied to fixed-free segments and small-length flexural pivots.

1.3.2. Industrial Motivation. A second but related objective of this research effort is to provide a design guideline and concise equations that engineers can use to perform stress analysis while incorporating compliant mechanisms into industrial applications. Current uses of compliant mechanisms are focused heavily in the consumer product market. Compliant mechanisms have not been fully utilized in industrial design due to at least two perceived drawbacks: nonlinear deflections inherent to compliant mechanisms that are difficult to calculate, and plastic materials that are often viewed as weak and that may be restricted to temporary applications due to fear of fatigue and/or creep failures. A guideline that can be used to design compliant segments reinforced with high-strength spring steel will unlock additional applications for compliant

mechanisms by reducing stress and improving fatigue and creep behavior. Specific industrial objectives for this research are listed below:

1. Present equations for redesigning a compliant segment to include metallic reinforcement while maintaining identical force-deflection behavior and reduced stress compared to the original homogeneous segment
2. Evaluate the effects of manufacturing errors that may lead to unintentional bonding between the insert and the polymer casing
3. Evaluate stresses in fixed-free and small-length flexural pivot segments for two cases: frictionless insert and bonded insert
4. Document the fatigue fracture behavior of reinforced and homogeneous compliant segments

1.4. DISSERTATION STRUCTURE

This research effort is organized into five papers that align with the motivations listed section 1.3:

1. Paper I and II align with the first academic motivation by advancing existing research of the PRBM concept by developing equations for stresses within compliant segments. The backbone to stress-based design of fixed-free and small-length flexural pivot compliant segments are presented in Papers I and II, respectively.
2. Paper III aligns with the first industrial motivation by developing a methodology to improve stress relaxation, creep, and fatigue performance of a compliant segment without altering the overall function of the parent compliant mechanism. The method developed in Paper III enables a

designer to replace the segment with a redesigned segment that maintains overall functionality while reducing stresses. The method matches the flexural rigidity of the metallic-reinforced segment to that of the homogenous compliant segment while optimizing the polymer casing thickness to reduce stress.

3. Paper III also aligns with the second and third industrial objectives by evaluating stresses and force-deflection behavior within compliant segments containing a frictionless reinforcing insert as well as when using an intentionally bonded insert.

4. Papers IV and V align with the second academic motivation and the fourth industrial motivation by focusing on stress relaxation, creep, and fatigue testing of both homogeneous and reinforced compliant segments. Paper V documents the fatigue fracture behavior of reinforced and homogeneous compliant segments. Fractured fatigue will be examined to document the fracture behavior. Fractography results include evaluation of the initiation site, fracture propagation behavior, and location of final fracture. An overall assessment of the fracture behavior, including likely fracture initiation sites for the subject geometry, is presented.

Finally, a summary of the investigation, conclusions of key findings, and recommendations for future work are presented.

PAPER

I. STRESS ANALYSIS OF A FIXED-FREE COMPLIANT SEGMENT USING THE PSEUDO-RIGID-BODY MODEL (PRBM) CONCEPT

J. Crews, A. Midha, and L.R. Dharani[1]

Department of Mechanical and Aerospace Engineering, Missouri University of Science and Technology, Rolla, MO 65409-0050

ABSTRACT: A method is presented to analyze stress in ambient temperature fixed-free compliant segments subjected to end loads or displacement boundary conditions. The analysis method outlined herein relies on key outputs from the pseudo-rigid-body models (PRBMs). Simplified equations for stress are presented for both homogeneous and metallic-reinforced segments. Stresses in both the polymer compliant segment and the metallic reinforcing element are addressed to provide a comprehensive stress analysis method. The stress analysis method is demonstrated by using two example design cases: one homogeneous compliant segment and one reinforced with a spring steel element. The results showed that introducing metallic reinforcement increases the flexural rigidity but does not reduce the bending stress in the casing unless the cross-sectional thickness is reduced.

Keywords: compliant segment, compliant mechanism, stress analysis, mechanism

---

[1] Corresponding author

E-mail address: dharani@mst.edu

1. INTRODUCTION

A mechanism is a mechanical device whose links and movable joints allow the transfer or transformation of motion, force, or energy [1], [2]. Unlike a rigid-body mechanism, a compliant mechanism is a type of mechanism that transfers or transforms motion, force, or energy through the deformation of its links or segments [3], [4]. Compliant mechanisms are typically classified as either fully compliant or partially compliant. A fully compliant mechanism contains no links or traditional kinematic pairs; therefore, all transfer or transformation of motion, force, or energy occurs due to deflection of its members [1], [2]. In contrast, a partially compliant mechanism contains at least one kinematic pair and one link. A partially compliant mechanism gains some of its motion through the deflection of at least one member and some of its motion through the rotation or translation of a kinematic pair, such as a slider or pin joint [1].

Compliant mechanism designs offer several advantages, including reduced cost due to limited part count and minimal assembly required, excellent corrosion resistance if constructed from engineering plastics, precise motion via elimination of backlash and wear associated with mechanical joints, and energy storage enabled by deformation of the segments or links [1], [3], [5], [6]. They also have disadvantages, including increased design complexity due to large link deformations and energy storage, and susceptibility to failure by creep, stress relaxation, or fatigue if constructed from engineering plastic [1], [3], [5], [6].

Designers of compliant mechanisms are challenged in three distinct areas: kinematic synthesis, stress analysis, and material selection. This paper highlights the relationship between kinematics, stress analysis, and material selection by building upon

well-established analytical models for fixed-free segments to provide equations for stress analysis of compliant mechanisms, both homogeneous (unreinforced) and reinforced.

The pseudo-rigid-body model (PRBM) was developed by earlier researchers to aid in the kinematic design of compliant mechanisms. A brief overview of this model is presented next.

2. OVERVIEW OF THE PRBM METHOD

The PRBM is a tool used to analyze compliant mechanisms by calculating deflections of each compliant member or segment. The overall approach is to model a compliant segment's tip deflection by replacing the compliant segment with a rigid body analog. The rigid body analog is developed by placing a pivot point, called a characteristic pivot, within two rigid segments. The sum of the rigid segment lengths is equal to the length of the original compliant segment. The length proportion of each segment is governed by the location of the characteristic pivot. Previous research has identified characteristic radius factors used to calculate the location of the characteristic pivot, and therefore the length of each rigid segment within the PRBM representation.

Refinement of the PRBM for various segment types has been a major focus of researchers since its introduction. Midha et al. presented an efficient method to apply the PRBM to fixed-guided compliant segments with an inflection point [7]. Howell and Midha [8], Howell [9], [10] and Howell et al. [11] developed the PRBM for the fixed-free compliant segment, as shown in Figure 1. The compliant segment is modeled using two rigid links joined by a characteristic pivot. The location of the characteristic pivot is represented by the characteristic radius factor, γ. The stiffness of the compliant segment is maintained within the PRBM by placing a torsional spring at the location of the characteristic pivot. The stiffness of the torsional spring is related to the stiffness of the original compliant segment by using a beam stiffness coefficient.

Howell and Midha [8] presented a method to identify the location of pin joints, called characteristic pivots, and equations to determine the torsional spring stiffness that accurately represents the compliant segment stiffness. Howell went on to develop

additional PRBMs for other compliant segment types, notably the fixed-guided and initially-curved fixed-pinned segment types [1], [10]. Howell showed that it is possible to optimize the characteristic radius such that the path of the beam-end calculated using the PRBM is within 0.5% of the path calculated using closed-form elliptic integrals [9].

Several key variables such as the beam stiffness coefficient, deflection, and characteristic radius factor derived in the PRBM are used to calculate the bending moment and subsequently the bending stress in compliant segments. A summary of PRBM variables is included in Table 1.

Individual components of the PRBM have been researched and refined to improve its accuracy. Equations for torsional spring stiffness were refined by Pauly and Midha [12] and Midha et al. [13]. The development and refinement efforts noted above have resulted in the PRBM being a recognized and accepted method to accurately predict the characteristic deflection domain of homogeneous compliant segments.

Inasmuch as equations for deflection compliant segments are critical to synthesis of compliant mechanisms, equations for bending stress are critical to designing robust compliant mechanisms. This paper presents a method for stress analysis of homogeneous compliant segments designed with uniform cross sections, as shown in Figure 2. Additionally, this paper presents equations of bending stress developed for composite compliant segments of uniform cross section containing a metallic reinforcement centered about the neutral axis. The subject stress analysis is based on the PRBM for fixed-free compliant segments, both homogeneous [9] and reinforced [6]. Results from stress analysis performed using the equations developed from PRBM concepts may be

used in conjunction with fatigue curves, creep curves, or stress-relaxation curves for the selected material to more accurately predict the performance of compliant segments.

Material selection and stress analysis are interlinked, critical tasks within the design process. Manufacturing compliant segments and mechanisms using polymeric materials offers both significant advantages and disadvantages. The designer is faced with balancing cost, ease of manufacture, and material performance. Material performance requirements are typically driven by the need to make a segment both strong and flexible [1]. One way to measure a material's strength-flexibility performance is to compare the allowable strength to the elastic modulus [1]. A comparison between two materials with equal strength shows that the material with lower modulus will attain higher failure strain than the material with a higher modulus.

In practice, compliant segments are typically manufactured using thermoplastics and an injection molding process. The most common engineering materials are elastic solids, while most plastics exhibit viscoelastic behavior to some degree. A material exhibiting a viscoelastic response has a strain-dependent stress-strain relationship. The response contains an elastic component and a viscous component. The viscoelastic, or time-dependent, strain response introduces additional complexity during the design phase of polymeric compliant mechanisms. In addition to design difficulties arising from viscoelasticity, plastics generally do not perform as predictably as metals in the areas of fatigue, creep, or stress relaxation [14].

Kuber introduced the concept of placing a strong reinforcing material within a compliant casing constructed of a relatively weak casing material in an effort to prevent creep and fatigue failures [6]. He extended the PRBM concept by developing a method

of analyzing deflections of small-length flexural pivots, fixed-free compliant segments, and fixed-guided compliant segments containing spring steel inserts. He validated the final results using the finite element method and experimental tests. Experimental tests showed that the PRBM method predicted the force-deflection response with an accuracy of 0.87%.

The experimental validation performed by Kuber on the force-deflection behavior of reinforced fixed-free segments applies directly to the stress equations presented herein, with strain and hence stress as functions of deflection [6]. Therefore, the stress analysis presented in this paper is validated by the deflection (strain) validation performed by Kuber [6]. The final outcome is a methodology for stress analysis of both homogeneous and reinforced composite fixed-free compliant segments.

Research efforts, briefly detailed above, have focused on establishing a simple and effective method of analyzing the relationship between beam-end deflections and applied forces. The following sections expand upon previous research efforts by presenting stress equations derived from PRBM force-deflection equations and nomenclature for both homogeneous [2] and reinforced compliant segments [6] of uniform cross section.

3. PRBM-BASED STRESS ANALYSIS FOR HOMOGENEOUS, FIXED-FREE COMPLIANT SEGMENTS SUBJECTED TO END FORCES

Compliant mechanisms, such as partially compliant four-link mechanisms, are typically designed to provide a specific motion. The design process typically initializes with kinematic synthesis to mathematically establish the geometry of links and segments that provide the intended displacement, velocity, or acceleration.

The result of kinematic synthesis is a mechanism that can accomplish the intended motion from a geometric standpoint. However, kinematic synthesis does not take stress or robustness into account. Subsequent stress analysis is required to design a robust mechanism that can both meet the motion requirements and application-specific requirements such as material restrictions.

One key variable used in calculating the moments and stresses is the load factor, *n*. The load factor is the ratio of the axial force to the transverse force. The tensile stress is reduced and the compressive stress is increased by a compressive axial stress component if the load factor is greater than zero. The corresponding load angle ϕ is greater than $\pi/2$ radians (90 degrees). Conversely, the tensile stress is increased and the compressive stress is decreased by a tensile axial stress component if the load factor is less than zero. The corresponding load angle is less than $\pi/2$ radians (90 degrees).

The maximum tensile and compressive stresses in a compliant segment with a positive load factor are given by $\sigma_{max,t}$ and $\sigma_{max,c}$, respectively:

$$\sigma_{max,t} = \frac{Mc}{I} - \frac{nP}{A}, \tag{1}$$

$$\sigma_{max,c} = -\frac{Mc}{I} - \frac{nP}{A}. \quad (2)$$

Bending stress calculations become complex when applied to compliant segments due to the need for nonlinear beam analysis methods for accurate calculation of the large deflections and beam-end coordinates to determine the bending moment. The PRBM method provides simplified equations that accurately predict the beam-end coordinates. Large deflection behavior (i.e., much greater than the beam thickness) cannot be accurately calculated using Euler-Bernoulli beam theory [15]. The deflection behavior, specifically the relationship between the beam-end deflection and the applied transverse force, can be more accurately calculated using the PRBM.

Howell [1] presented two example calculations for stress in a homogeneous, fixed-free compliant segment with zero and positive load factors. After comparison between the stress calculation based on PRBM, elliptic integral approach, and finite element method, he concluded that the accuracy of the PRBM force-deflection analysis resulted in accurate stress analysis solutions.

The case for the homogeneous, fixed-free compliant segment presented below is similar to Howell's work [1] in that it relies on the PRBM. However, the analysis method and equations below expand the scope to cover negative load factors ($n \leq 0$) and reinforced composite segments. Additionally, the analysis has been refined to give succinct equations for stress based on pseudo-rigid-body angle inputs or tip deflection inputs. Lastly, the equations for homogeneous fixed-free compliant segments are solved in terms of PRBM variables that lend themselves well to subsequent calculation of stress in reinforced compliant segments.

This stress analysis applies to fixed-free compliant segments subjected to a non-following load and operating at steady-state ambient temperatures. Analyses of metallic-reinforced segments operating at elevated or varying temperatures must consider the material properties related to the operating temperature, as well as stresses related to differences between the coefficient of thermal expansion of the casing and reinforcement materials. Additional analysis may also be required to assess the effect of stress raisers caused by the introduction of metallic reinforcement.

This method applies to segments with a non-following load applied to the free end. A non-following load is a load that maintains consistent orientation to the base coordinate system and does not rotate with the beam-end. The load configuration of a segment in the free-state is shown in Figure 3. The vertical and horizontal components of the end load F are given as P and nP, respectively. The end load can be calculated using the vertical component and the load factor:

$$\mathrm{F} = \mathrm{P}\sqrt{1 + \mathrm{n}^2}. \tag{3}$$

A dimensionless quantity η, related to the load factor, is used to simplify subsequent equations:

$$\eta = \sqrt{1 + \mathrm{n}^2}. \tag{4}$$

The load angle does not change with deflection due to the definition of a non-following load. The load configuration in the deflected state is shown in Figure 4. The

transverse force component for use in subsequent torsional spring force calculations is given by F_t:

$$F_t = F[\mathrm{Sin}(\phi - \Theta)]. \tag{5}$$

The first step in calculating the moment required to attain a specified displacement is to evaluate the stiffness of the torsional spring, K. It must be carefully evaluated to ensure that the force-deflection response of the PRBM matches that of the compliant segment. The stiffness is given in moment per unit rotation (in.-lbf./degree). The stiffness (in terms of the stiffness coefficient K_Θ, flexural rigidity EI, characteristic radius factor γ, and the segment length l) is given by [6]:

$$K = K_\Theta \gamma \left[\frac{EI}{l}\right]. \tag{6}$$

The stiffness coefficient, as refined by Kuber [6], is a function of the load factor and the pseudo-rigid-body angle. The stiffness coefficient for a load configuration with a positive load factor is given by [6]:

$$\begin{aligned} K_\Theta = \frac{1}{\Theta}(&0.004233 - 0.012972n + 2.567095\Theta + 0.003993n^2 \\ &- 0.037173\Theta^2 - 0.000297n^3 + 0.179970\Theta^3 \\ &- 0.034678n\Theta + 0.003467n^2\Theta - 0.009474n\Theta^2), \end{aligned} \tag{7}$$

$$\text{for } 0 \le n \le 10 \text{ and } 0 < \Theta \le 65°.$$

The stiffness coefficient for a load configuration with a negative load factor is given by [6]:

$$K_\Theta = \frac{1}{\Theta}(0.000651 - 0.008244n + 2.544577\Theta - 0.004767n^2 + 0.071215\Theta^2 - 0.000104n^3 + 0.079696\Theta^3 + 0.069274n\Theta + 0.061507n^2\Theta - 0.347588n\Theta^2), \quad \text{for } -4 < n < 0 \text{ and } 0 < \Theta < 0.8\phi. \tag{8}$$

The moment of the torsional spring represents the moment applied to the torsional spring such that the link rotates by a pseudo-rigid-body angle. The pseudo-rigid-body angle represents the rotation of the rigid link used within the PRBM for a compliant segment.

The beam-end coordinates are calculated using the characteristic radius $l\gamma$ and pseudo-rigid-body angle shown in Figure 1. The beam-end coordinates, horizontal and vertical, are provided below in terms of the beam length, characteristic radius factor, and the pseudo-rigid-body angle:

$$a = l[\gamma(\cos(\Theta) - 1) + 1], \tag{9}$$

$$b = l\gamma\sin(\Theta). \tag{10}$$

The torsional spring constant, or force per unit angular displacement based on elementary spring theory, is given by

$$K = \frac{F_t \gamma l}{\Theta}. \tag{11}$$

The torsional spring constant is a function of transverse force and moment arm. The moment arm, in the case of a fixed-free compliant segment, is equal to the characteristic radius.

Using Equations 5, 6, and 11, the relationship between end force, load angle, and pseudo-rigid-body angle is obtained as

$$F = \frac{K_\Theta EI\Theta}{l^2 \mathrm{Sin}(\phi - \Theta)}. \tag{12}$$

The vertical load component can be calculated using Equations 3, 6, and 12:

$$P = \frac{K_\Theta EI\Theta}{\eta l^2 \mathrm{Sin}(\phi - \Theta)}. \tag{13}$$

The maximum moment can be determined using the vertical load component, load factor, and tip coordinates as

$$M = P(a + nb). \tag{14}$$

The use of Equations 13 and 14 enables the final calculation of the moment required to achieve the specified vertical and horizontal displacements at the tip as

$$M = \frac{K_\Theta EI\Theta}{\eta l^2 Sin(\phi - \Theta)}(a + nb). \quad (15)$$

Equation 15 shows that the moment required to achieve a specified tip deflection, via the specified pseudo-rigid-body angle, is proportional to the moment of inertia. By combining Equations 9, 10, and 15, the moment required to achieve a specific pseudo-rigid-body angle is obtained as

$$M = \frac{K_\Theta EI\Theta}{\eta l Sin(\phi - \Theta)}\{\gamma[\cos(\Theta) + n\sin(\Theta) - 1] + 1\}. \quad (16)$$

Calculation of the required applied moment enables the analysis of stresses in a fixed-free compliant segment using either tip-displacement or pseudo-rigid-body angle boundary conditions.

Equations 13 and 14 may be substituted into Equations 1 and 2 to provide the maximum tensile and compressive stresses in a homogeneous, fixed-free compliant segment in terms of the tip deflection and a load factor greater than zero:

$$\sigma_{max} = \pm\frac{K_\Theta E\Theta}{\eta l^2 Sin(\phi - \Theta)}\left[\frac{h(a + nb)}{2} \mp \frac{nI}{wh}\right]. \quad (17)$$

Using Equations 9 and 10, the total tensile and compressive stresses within a fixed-free compliant segment deflected to achieve a specific pseudo-rigid-body angle for a load factor greater than zero are given by

$$\sigma_{max} = \pm \frac{K_{\Theta} E \Theta}{\eta l \sin(\phi - \Theta)} \left[\frac{h\{\gamma(\cos(\Theta) + n\sin(\Theta) - 1) + 1\}}{2} - \frac{nI}{whl} \right]. \quad (18)$$

The equations derived in Section 2 provide a concise method to calculate the stresses in a fixed-free compliant segment constructed of a homogeneous polymer material subjected to either deflection or pseudo-rigid-body angle boundary conditions. The following section will present a similar analysis of a metallic-reinforced, composite compliant segment.

4. PRBM FOR A REINFORCED, COMPOSITE, FIXED-FREE COMPLIANT SEGMENT SUBJECTED TO END FORCES

The PRBM can also be used to analyze compliant mechanisms containing metallic reinforcement. The method below was developed specifically for a reinforced compliant segment designed such that the centroid of the reinforcement is located on the neutral axis of the casing. Figure 5 depicts nomenclature related to the cross section of a reinforced compliant segment. The subscript '1' denotes variables associated with the casing and the subscript '2' denotes variables associated with the reinforcement

The load applied to each component of the compliant segment must be calculated separately in order to assess the moment and subsequently the stress within each component. The load distribution between the two beam components is proportional to the flexural rigidity of each component. The component with the highest bending stiffness, or flexural rigidity, will support the highest bending load. The stiffness of the casing K_1 and the stiffness of the reinforcement K_2 are given by [6]

$$K_i = K_\theta \gamma \left[\frac{E_i I_i}{l}\right] \qquad i = 1,2. \tag{19}$$

In the case of a reinforced compliant segment, the total equivalent stiffness K_t^e of the torsional spring is the sum of the effective stiffness of the casing and the effective stiffness of the reinforcement:

$$K_t^e = (K_1 + K_2). \tag{20}$$

The reinforced segment is analyzed as two separate beams with identical transverse deflection [6]. This method is consistent with the calculation of linear springs in parallel. The equivalent torsional spring stiffness includes the flexural modulus and moment of inertia of each of the beam components which is given by

$$K_t^e = \frac{K_\theta \gamma}{l}(E_1 I_1 + E_2 I_2). \tag{21}$$

The moment required to rotate the torsional spring by a given pseudo-rigid-body angle for a metallic strip totally enclosed by a polymer casing was given by Kuber [6]. The force required at the end of the reinforced segment to cause a pseudo-rigid-body angle can be calculated:

$$K_t^e \Theta = F_t \gamma l \tag{22}$$

The load carried by the casing F_1 and the load carried by the reinforcement F_2 are given by

$$F_i = \frac{K_\Theta E_i I_i \Theta}{l^2 \mathrm{Sin}(\phi - \Theta)} \qquad i = 1,2. \tag{23}$$

Using Equation 23 and Equation 3, the value of the vertical load component P_1 applied to the casing and the vertical load component P_2 applied to the reinforcement can be written as

$$P_i = \frac{K_\Theta E_i I_i \Theta}{\eta l^2 Sin(\phi - \Theta)} \qquad i = 1,2. \tag{24}$$

The moments applied to the casing M_1 and reinforcement M_2 to achieve the specified displacement at the tip are given by

$$M_i = P_i(a + nb) \qquad i = 1,2. \tag{25}$$

Incorporating Equations 9 and 10 into Equation 25 provides the corresponding moments required to achieve a specific pseudo-rigid-body angle:

$$M_i = \frac{K_\Theta E_i I_i \Theta}{\eta l Sin(\phi - \Theta)} \{\gamma[\cos(\Theta) + n\sin(\Theta) - 1] + 1\} \qquad i = 1,2. \tag{26}$$

The moment calculation enables the use of Equations 1 and 2 to determine the maximum tensile and compressive stresses in a reinforced composite segment, respectively.

The maximum tensile and compressive stresses in the polymer casing and reinforcement, in terms of tip displacement, are given by

$$\sigma_{max,i} = \pm \frac{K_\Theta E_i \Theta}{\eta l^2 Sin(\phi - \Theta)} \left[\frac{h(a + nb)}{2} \mp \frac{nI_i}{w_1 h_1 - w_2 h_2}\right] \qquad i = 1,2. \tag{27}$$

Using Equations 11, 12 and 27, the total tensile and compressive stresses are obtained for a fixed-free compliant segment deflected to achieve a specific pseudo-rigid-body angle for a load factor greater than zero:

$$\sigma_{max,i} = \pm \frac{K_\Theta E_i \Theta}{\eta l \sin(\phi - \Theta)} \left[\frac{h_i\{\gamma(\cos(\Theta) + n\sin(\Theta) - 1) + 1\}}{2} \mp \frac{nI_i}{(w_1 h_1 - w_2 h_2)l} \right] \qquad i = 1,2. \tag{28}$$

Equation 1 showed that the total stress in a fixed-free compliant segment subjected to an end force includes a bending stress component as well as an axial stress component.

One objective in calculating the bending stress was to identify the variables that may be optimized to reduce the stress in the beam, resulting in improved performance. Separate analyses are performed for the polymer and insert, related by identical deflections along the neutral axis at the tip of each segment.

The bending stress within the polymer casing $\sigma_{max,b,1}$ in terms of tip displacement and pseudo-rigid-body angle are given by the respective equations:

$$\sigma_{max,b,1} = \frac{K_\Theta E_1 \Theta}{\eta l^2 \mathrm{Sin}(\phi - \Theta)} \left[\frac{h(a + nb)}{2} \right], \tag{29}$$

$$\sigma_{max,b,1} = \pm \frac{K_\Theta E_1 \Theta}{\eta l \sin(\phi - \Theta)} \left[\frac{h_1\{\gamma[\cos(\Theta) + n\sin(\Theta) - 1] + 1\}}{2} \right]. \tag{30}$$

Equations 29 and 30 confirm that the maximum bending stress in the casing, for a given segment deflection and elastic modulus, is a function of the distance from the neutral axis to the extreme fiber of the polymer and not the moment of inertia. Therefore, the introduction of an insert does not directly reduce the bending stress in the polymer portion of the beam, as the moment of inertia of the polymer is not included in the final equation. This is true in the case of a reinforced compliant segment deflected to achieve the same displacement or pseudo-rigid-body angle as that of a homogeneous segment.

The maximum bending stress in a casing subjected to a specified deflection is not directly reduced by the introduction of a high-strength insert because the distance from the neutral axis to the extreme fiber remains constant. However, the flexural rigidity increases as the result of the introduction of metallic reinforcement. The increase in flexural rigidity for the segment results in an increase in the force required to produce the desired deflection.

While the maximum bending stress is not reduced, the total stress may be reduced due to the reduction in axial stress provided by the reinforcement in the case of a nonzero load factor. While the bending stress is not directly reduced by the introduction of metallic reinforcement due to the constant tip deflection boundary condition, the axial force P on the casing and the cross-sectional area A of the casing are reduced by the introduction of the metallic reinforcement.

5. DESIGN APPROACH WITH RESPECT TO STRESS USING PRBM FOR A REINFORCED, COMPOSITE, FIXED-FREE COMPLIANT SEGMENT SUBJECTED TO END FORCES

The stress analysis method above resulted in succinct equations for stress within homogeneous and composite fixed-free compliant segments. A designer can use the stress analysis method to design a homogeneous, fixed-free compliant segment in the following six ways, each facilitated by Equations 1 through 18:

1. Input a material's allowable stress and cross section dimensions and calculate the maximum allowable tip displacement
2. Input a material's allowable stress and cross section dimensions and calculate the maximum allowable pseudo-rigid-body angle
3. Input a material's allowable stress and tip displacement and calculate the segment's cross section dimensions
4. Input a material's allowable stress and pseudo-rigid-body angle and calculate the segment's cross section dimensions
5. Input a segment's tip deflection and cross section dimensions and calculate the maximum tensile and compressive stresses. These stresses can be used along with a safety factor to select an appropriate material of construction
6. Input a segment's pseudo-rigid-body angle and cross section dimensions and calculate the maximum tensile and compressive stresses. These stresses can be used along with a safety factor to select an appropriate material of construction

Similarly, a designer can use the stress analysis method to design a composite fixed-free compliant segment in the following six ways, each facilitated by Equations 19 through 30:

1. Input the allowable stress and cross section dimensions of both the casing and reinforcement and calculate the maximum allowable tip displacement
2. Input the allowable stress and cross section dimensions of both the casing and reinforcement and calculate the maximum allowable pseudo-rigid-body angle
3. Input the allowable stress of both the casing and reinforcement along with the tip displacement and calculate the segment's cross section dimensions
4. Input the allowable stress of both the casing and reinforcement along with the pseudo-rigid-body angle and calculate the segment's cross section dimensions
5. Input a segment's tip deflection and cross section dimensions of the casing and reinforcement and calculate the maximum tensile and compressive stresses. These stresses can be used along with a safety factor to select an appropriate material of construction
6. Input a segment's pseudo-rigid-body angle and cross section dimensions of the casing and reinforcement and calculate the maximum tensile and compressive stresses. These stresses can be used along with a safety factor, to select an appropriate material of construction

6. EXAMPLE RESULTS AND DISCUSSION

The following examples show that the stress analysis method is a simply way for a designer to leverage design information from the PRBM to calculate the stress in a fixed-free compliant segment, either homogeneous or metallic-reinforced.

6.1 EXAMPLE 1: HOMOGENEOUS, FIXED-FREE COMPLIANT SEGMENT

A homogeneous, fixed free compliant segment has been designed and constructed from urethane with the following properties and dimensions:

E = 433,843 psi (2,985.43 MPa)

Θ = 30 deg (0.524 rad)

n = 0

h = 0.2473 in (6.28 mm)

w = 1.502 in. (38.15 mm)

l = 9.8 in. (248.9 mm)

γ = 0.85

The first step is to calculate the stiffness coefficient using Equation 7, which is duplicated below for clarity:

$$K_\Theta = \frac{1}{\Theta}(0.004233 - 0.012972n + 2.567095\Theta + 0.003993n^2 - 0.037173\Theta^2 - 0.000297n^3 + 0.179970\Theta^3 - 0.034678n\Theta + 0.003467n^2\Theta - 0.009474n\Theta^2), \quad (7)$$

for $0 \leq n \leq 10$ and $0 < \Theta \leq 65°$,

$$K_\Theta = \frac{1}{0.524}(0.004233 + 2.567095(0.524) - 0.037173(0.524)^2 + 0.179970(0.524)^3) = 2.61. \quad (31)$$

A load factor of zero allows for simplification of Equation 19. Additionally, a zero load factor results in a load angle of 90° (π/2 radians). The tensile stress is shown below:

$$\sigma_{max} = \frac{(2.61)(433{,}843)(0.524)}{(9.8)\sin\left(\frac{\pi}{2} - 0.524\right)}\left[\frac{0.2473\{0.85(\cos(0.524) - 1) + 1\}}{2}\right] = 7{,}660 \text{ psi (51.8 MPa)}. \quad (32)$$

The flexural rigidity, *EI* is calculated for subsequent use in Example 2, wherein the flexural rigidity of a homogeneous segment is compared to that of a reinforced, composite segment:

$$EI = 433{,}843\left[\frac{1.502(0.2473^3)}{12}\right] = 821.285 \text{ lbf} - \text{in}^2 \ (2.36\text{x}10^6 \text{ N} - \text{mm}^2). \quad (33)$$

6.2 EXAMPLE 2: REINFORCED, COMPOSITE, FIXED-FREE COMPLIANT SEGMENT

The polyurethane fixed free compliant segment described in Example 1 was redesigned to include an AISI 1095 spring steel insert 0.050 inches (1.27 mm) thick and

1.000 inches (25.4 mm) wide. The properties and dimensions of the polymer segment detailed in Example 1 are unchanged, with the exception of the introduction of the metallic reinforcement with E = 30×10^6 psi (206.8 GPa).

The tensile stress in the polymer casing is calculated using Equation 28, which is duplicated below for clarity:

$$\sigma_{max,t,1} = \frac{K_\Theta E_1 \Theta}{\eta l \sin(\phi - \Theta)} \left[\frac{h_1\{\gamma(\cos(\Theta) + n\sin(\Theta) - 1) + 1\}}{2} - \frac{nI_1}{(w_1 h_1 - w_2 h_2) l} \right], \tag{28}$$

$$\sigma_{max,t,1} = \frac{(2.61)(433{,}843)(0.524)}{(9.8)\sin\left(\frac{\pi}{2} - 0.524\right)} \left[\frac{0.2473\{0.85(\cos(0.524) - 1) + 1\}}{2} \right] = 7{,}660 \text{ psi } (51.8 \text{ MPa}). \tag{34}$$

The stress in the polymer casing is less than the flexural strength of thermoset urethane [16], which indicates that static failure is not expected. Similarly, the tensile stress in the reinforcement is calculated using Equation 34, which is duplicated below for clarity:

$$\sigma_{max,t,2} = \frac{K_\Theta E_1 \Theta}{\eta l \sin(\phi - \Theta)} \left[\frac{h_1\{\gamma(\cos(\Theta) + n\sin(\Theta) - 1) + 1\}}{2} - \frac{nI_1}{w_2 h_2 l} \right], \tag{35}$$

$$\sigma_{max,t,2} = \frac{(2.61)(30x10^6)(0.524)}{(9.8)\sin\left(\frac{\pi}{2} - 0.524\right)}\left[\frac{0.050\{0.85(\cos(0.524) - 1) + 1\}}{2}\right] = 107{,}099 \text{ psi } (738.4 \text{ MPa}). \quad (36)$$

This stress is within the working stress limit of AISI 1095 steel [17], which indicates that static failure is not expected. Since the maximum stresses in both the polymer casing and steel reinforcement are less than the working limits, static failure is not expected in the reinforced, composite segment. However, the stress in Example 2 is the same as the stress in Example 1 because the distance from the neutral axis to the outside surface of the segment is unchanged with the introduction of the metallic reinforcement.

The flexural rigidity of the reinforced segment is calculated and compared to the flexural rigidity from Example 1 to determine the change resulting from the introduction of the metallic reinforcement:

$$EI = 433{,}843\left[\frac{1.502(0.2473^3)}{12} - \frac{1.000(0.050^3)}{12}\right] + 30x10^6\left[\frac{1.000(0.050^3)}{12}\right] = 1{,}129.27 \text{ lbf} - \text{in}^2 \ (3.24x10^6 \text{ N} - \text{mm}^2). \quad (37)$$

Example 2 shows that the introduction of metallic reinforcement increases the flexural rigidity but does not reduce the bending stress in the casing unless the cross-sectional thickness is reduced.

7. CONCLUSIONS

A method and supporting equations for analysis of stress in fixed-free compliant segments subjected to beam-end loads or displacement boundary conditions has been derived. The analysis method outlined herein relies on key outputs from the accurate, well-established, and well-accepted pseudo-rigid-body models (PRBMs).

Final, simplified equations for stress are presented for both homogeneous and reinforced segments. Equations are presented for both the polymer compliant segment and for the metallic reinforcing element to enable a comprehensive stress analysis tool.

The stress analysis method and equations were demonstrated within two example compliant segment design cases: one homogeneous compliant segment and one reinforced with a spring steel reinforcing element.

The example stress analysis showed that the introduction of metallic reinforcement increases the flexural rigidity but does not reduce the bending stress in the casing unless the cross-sectional thickness is reduced.

8. ACKNOWLEDGMENTS

The authors would like to acknowledge the contributions of Dr. Sushrut Bapat, Dr. Jun Wei, and graduate students Vamsi Lodagala and Pratheek Bagivalu Prasanna for participating in early discussions of this work. These discussions helped identify the needs and develop the bounds of this research effort.

9. REFERENCES

[1] Howell, L. L., Compliant Mechanisms, John Wiley & Sons, Inc., New York, New York, 2001.

[2] Howell L. L. and Midha A., “A Method for the Design of Compliant Mechanisms with Small-Length Flexural Pivots,” Journal of Mechanical Design, Trans. ASME, Vol. 116, No. 1. - 1994. - pp. 280-290.

[3] Midha, A., T. W. Norton and L. L. Howell, "On the Nomenclature, Classification, and Abstractions of Compliant Mechanisms," Journal of Mechanical Design, Trans. ASME, Vol. 116, No. 1, March 1994, pp. 270-279.

[4] Salamon, B. A., “Mechanical Advantage Aspects in Compliant Mechanisms Design,” MS Thesis, Purdue University, October 1989.

[5] Bapat, S. G., "On the design and analysis of compliant mechanisms using the pseudo-rigid-body model concept,” Doctoral Dissertation. Paper 2376. Missouri University of Science and Technology, 2015.

[6] Kuber, R. S., "Development of a methodology for pseudo-rigid-body models of compliant segments with inserts, and experimental validation," Master’s Thesis. Paper 5363. Missouri University of Science and Technology, 2013.

[7] Midha, A., Bapat, S.G., Mavanthoor, A., and Chinta, A., “Analysis of a Fixed-Guided Compliant Beam with an Inflection Point Using the Pseudo-Rigid-Body Model Concept,” Journal of Mechanisms and Robotics, Trans. ASME, Vol. 7, Aug. 2015, pp. 031007-1-10.

[8] Howell, L. L., and Midha, A., “Parametric Deflection Approximations for End-Loaded, Large-Deflection Beams in Compliant Mechanisms,” Journal of Mechanical Design, Trans. ASME, Vol. 117, No. 1, March 1995, pp. 156-165.

[9] Howell, L.L., “The Design and Analysis of Large-Deflection Members in Compliant Mechanisms,” MS Thesis, Purdue University, August 1991.

[10] Howell, L. L., “A Generalized Loop Closure Theory for the Analysis and Synthesis of Compliant Mechanisms,” Ph.D. Dissertation, Purdue University, 1993.

[11] Howell, L. L., Midha, A., and Norton, T. W., “Evaluation of Equivalent Spring Stiffness for use in a Pseudo-Rigid-Body Model of Large-Deflection Compliant Mechanisms,” Journal of Mechanical Design, Trans. ASME, Vol. 118, No. 1, March 1986, pp. 126-131

[12] Pauly, J., and A. Midha, "Improved Pseudo-Rigid-Body Model Parameter Values for End-Force-Loaded Compliant Beams," Proceedings of the 28th Biennial ASME Mechanisms and Robotics Conference, Salt Lake City, Utah, September 2004, pp. DETC 2004-57580 – 1-5.

[13] Midha, A.; Kuber, R. S.; Chinta, V.; Bapat, S. G., "A Method for a More Accurate Calculation of the Stiffness Coefficient in a Pseudo-Rigid-Body Model (PRBM) of a Fixed-Free Beam Subjected to End Forces," Proceedings of the ASME 2014 International Design Engineering Technical Conferenced & Computers and Information in Engineering Conference, Vols. DETC35366-1-10, Buffalo, NY, 2014.

[14] Rosen, S.L., "Fundamental Principals of Polymeric Materials," 2nd Edition, John Wiley & Sons, Inc., New York, New York, 1993.

[15] Bisshopp, K.E., and Drucker, DC. "Large Deflection of Cantilever Beams," Quarterly of Applied Mathematics, Vol. 3, No. 3, pp. 272.

[16] Innovative Polymers, Incorporated. "IE-3075 Data Sheet," Accessed September 1, 2015. http://www.innovative-polymers.com/images/specs/Classic-Shore-D/IE-3075.pdf.

[17] ASM International ASM handbook. - 2015. - Vols. Volume 1, D02, A13.

10. FIGURES AND TABLES

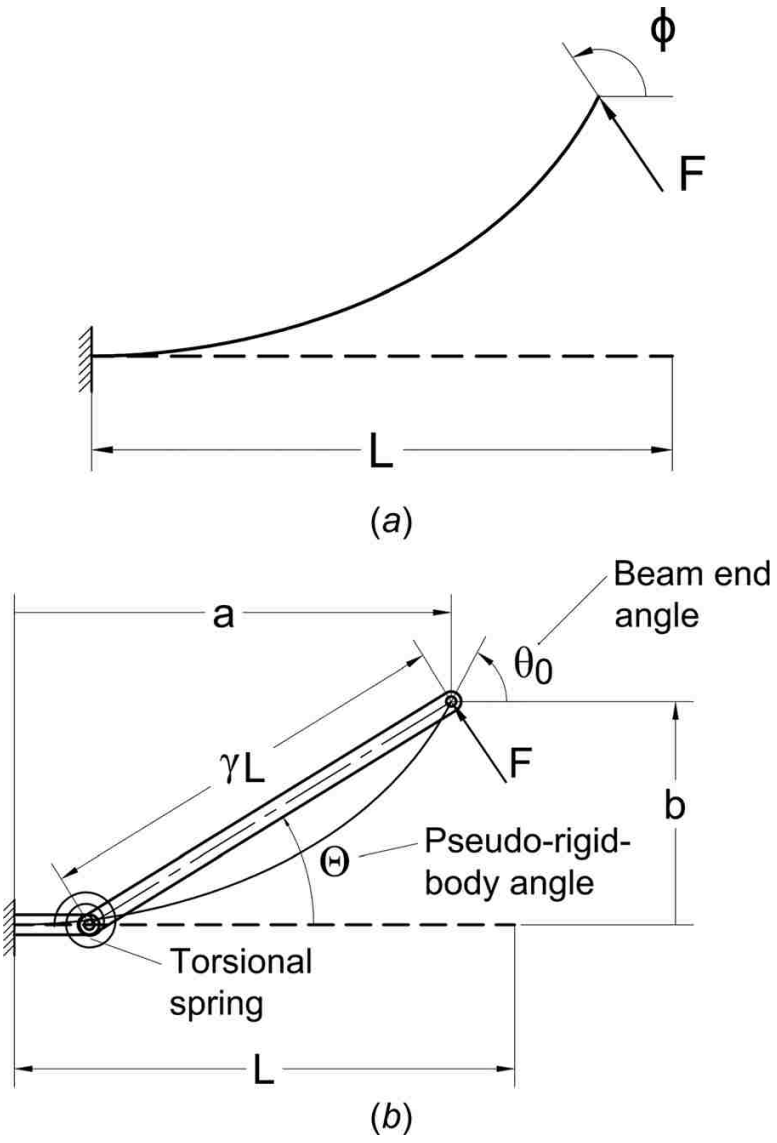

Figure 1: PRBM of fixed-free compliant segment shown in initial position (a) and deformed position (b) [7]

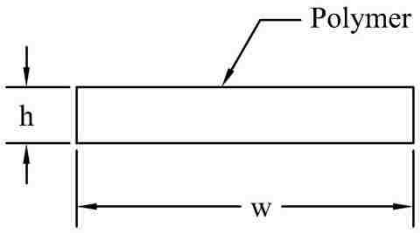

Figure 2: Cross Section of a Homogeneous Compliant Segment

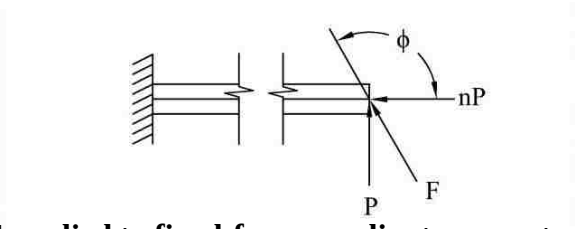

Figure 3: End-load, F applied to fixed-free compliant segment

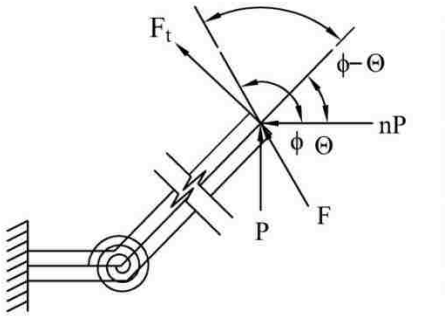

Figure 4: Nomenclature of fixed-free compliant segment in deflected state

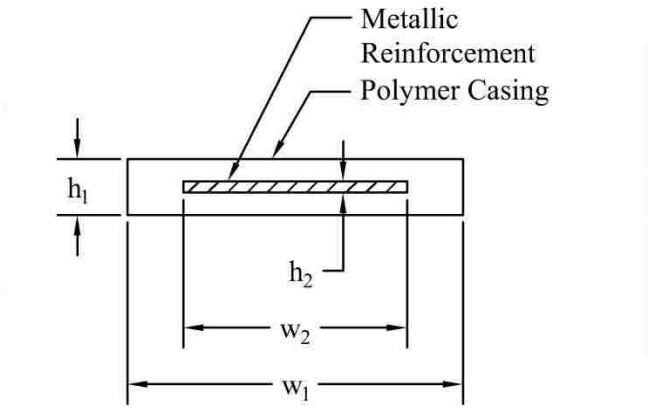

Figure 5: Cross Section of Metallic Reinforced Compliant Segment

Table 1: Nomenclature

Variable	Description
K_t^e	Equivalent Stiffness of Reinforced Segment
K	Stiffness of Torsional Spring
a	Horizontal Distance from Fixed-end to beam tip
b	Transverse Deflection of the Beam Tip
l	Length
E	Flexural Modulus
I	Moment of Inertia
Θ	Pseudo-Rigid-Body Angle
ϕ	Load Angle
n	Load Factor
P	Vertical Component of End Load
F	End Load
F_t	Transverse Load Component
A	Cross-sectional Area
w	Cross-sectional Width
h	Cross-sectional Height

II. STRESS ANALYSIS OF A SMALL-LENGTH FLEXURAL PIVOT COMPLIANT SEGMENT USING THE PSEUDO-RIGID-BODY MODEL (PRBM)

J. Crews, A. Midha and L.R. Dharani[1]

Department of Mechanical and Aerospace Engineering, Missouri University of Science and Technology, Rolla, MO 65409

ABSTRACT: A method based on the pseudo-rigid-body model (PRBM) is presented for analysis of stress in small-length flexural pivot compliant segments subjected to end loads or displacement boundary conditions. The analysis method provides the designer with a tool to ensure that stress levels are maintained that are appropriate for the intended application and materials of construction. Simplified equations for stress are presented for both homogeneous polymer and metallic-reinforced composite segments. The method is demonstrated with two example case studies, one homogeneous compliant segment and one reinforced with spring steel. The introduction of metallic reinforcement increases the flexural rigidity, but does not reduce the bending stress in the casing of a small-length flexural pivot unless the cross-sectional thickness is reduced.

Keywords: compliant segment, compliant mechanism, stress analysis, mechanism, small-length flexural pivot

---

[1] Corresponding author

E-mail address: dharani@mst.edu

1. INTRODUCTION

A mechanism is a device containing links and movable joints that allow the transfer or transformation of motion, force, or energy [1], [2]. A compliant mechanism transfers or transforms motion, force, or energy through the deformation of its links or segments [3], [4]. A compliant link containing two distinct segments, one much shorter and more flexible than the other, is said to contain a small-length flexural pivot. A small-length flexural pivot is one segment within a compliant link. The compliant length of a small-length flexural pivot is usually 10% or less of the total link length [1], which differentiates the small-length flexural pivot from a fixed-free compliant segment, in which the entire link length is compliant.

Introducing compliance into mechanism design offers several advantages, including reduced cost due to limited part count and minimal assembly and light weight and excellent corrosion resistance if constructed from engineering plastics [1], [3], [5], [6]. Compliant mechanisms also have disadvantages such as design complexity due to nonlinear deflections and also nonlinear material properties if constructed from engineering plastic. Plastic materials are typically more susceptible to creep deformation, stress relaxation, and fatigue fracture [1], [3], [5], [6].

Designers of compliant mechanisms are generally challenged in three distinct areas: kinematic synthesis, stress analysis, and material selection. This paper highlights the relationship between kinematics, stress analysis, and material selection by building upon pseudo-rigid-body models for small-length flexural pivots to provide equations for stress within compliant mechanisms, both homogeneous (unreinforced) and reinforced.

The so-called pseudo-rigid-body model (PRBM) has been developed by earlier researchers to aid in the kinematic design of compliant mechanisms. A brief overview of this model is presented next.

The PRBM approach aims to develop an analogous rigid-body mechanism by introducing strategically placed kinematic pairs and torsional springs in an attempt to mimic the force-deflection behavior of the compliant mechanism in question.

Refinement of the PRBM for various segment types has been a major focus of researchers since its introduction. Howell and Midha [2] developed a small-length flexural pivot, the segment type to which this research effort applies. Figure 1 shows the PRBM of a small-length flexural pivot. Howell and Midha [7] presented a method used to place pin joints, called characteristic pivots, at locations within the PRBM to provide an accurate prediction of the beam tip. Midha et al. [8] presented an efficient method to apply the PRBM to fixed-guided compliant segments with an inflection point.

Individual components of the PRBM have been researched and refined to improve the accuracy of the PRBM. Equations for torsional spring stiffness were further refined by Pauly and Midha [9] and by Midha et al. [10]. The development and refinement efforts noted above have resulted in the PRBM becoming a recognized method to accurately predict the characteristic deflection domain of homogeneous compliant segments.

While force-deflection relationships are critical for the synthesis of compliant mechanisms, stress analysis is critical to the successful design of robust compliant mechanisms that can sustain load conditions in practical applications. This paper presents a baseline method and equations to perform stress analysis of homogeneous small-length

flexural pivots designed with uniform cross sections. Subsequently, the baseline method is extended to small-length flexural pivots of uniform cross sections containing a metallic reinforcement centered about the neutral axis. One of the primary objectives of this paper is to provide a method of stress analysis for bi-material compliant segments derived from PRBM concepts to be used in conjunction with fatigue curves, creep curves, or stress relaxation curves to accurately predict and improve the performance of compliant segments.

Material selection and stress analysis are often complimentary tasks within design activities related to any engineered product. However, material selection for compliant mechanisms is often more complex due to the inherent need for flexibility while maintaining strength. The designer of any compliant mechanism must carefully consider and balance the environmental factors, material strength, and flexibility while remaining cognizant of cost and manufacturability. Engineering plastics are commonly used to manufacture compliant segments due to their cost effectiveness, light weight, flexibility, and manufacturability. One way to measure a segment's strength and flexibility performance is to compare the strength to the modulus of elasticity [1]. A polymeric material with a high strength-to-modulus ratio can attain higher strain amplitudes without yielding than a material with a low strength-to-modulus ratio.

While most commonly recognized engineering materials are elastic solids (such as metals), most plastics are viscoelastic and exhibit a time-dependent stress-strain relationship. Viscoelasticity is easily detected by performing tensile tests at various strain rates. The resulting stress strain curves show variations in amplitude and shape of the stress-strain curve as well as variations in the ultimate strength of the material. The

viscoelastic response contains an elastic component and a viscous component. The viscoelastic strain response introduces additional complexity during the design phase of polymeric compliant mechanisms because the designer must consider the acceleration and velocity of each segment in addition to forces. In addition to design difficulties arising from viscoelasticity, plastics generally do not perform as predictably as metals in areas of fatigue, creep or stress relaxation [11].

Kuber introduced the concept of bi-material compliant segments - specifically plastic casings with spring steel reinforcement - as a way to improve fatigue and creep resistance [5]. He extended the PRBM concept by developing a method of analyzing deflections of small-length flexural pivots, fixed-free compliant segments, and fixed-guided compliant segments containing spring steel inserts [5].

The following sections present a detailed description of the PRBM and its previously developed application for determining deflection behavior of a small-length flexural pivot, and a method to extend the model to provide stress analysis of both homogeneous and metallic-reinforced composite compliant segments.

2. PSEUDO-RIGID-BODY MODEL FOR A SMALL-LENGTH FLEXURAL PIVOT COMPLIANT SEGMENT SUBJECTED TO END FORCES

The PRBM analysis method has been shown to accurately represent the force-deflection behavior of compliant mechanisms by addressing them segment-by-segment. The PRBM method accurately represents the force deflection of a compliant segment by replacing the compliant segment with a rigid body analog. The rigid body analog is developed by placing a pivot point, called a characteristic pivot, at the center of the small length flexural pivot, between two rigid links. The sum of the individual rigid segment lengths is equal to the total length of the original compliant segment. A graphical representation of the PRBM for a small-length flexural pivot is shown in Figure 1. Figure 2 depicts nomenclature related to the cross section of a homogeneous small-length flexural pivot. Figure 3 depicts nomenclature related to the cross section of a reinforced compliant segment. The subscript '1' denotes variables associated with the casing and the subscript '2' denotes variables associated with the reinforcement.

Howell and Midha [2] developed the pseudo-rigid-body model (PRBM) for the small-length flexural pivot, shown in Figure 1. The small-length flexural pivot is located between a fixed base and a relatively rigid link. The stiffness of the small-length flexural pivot is maintained within the PRBM by placing a torsional spring at the location of the characteristic pivot. The stiffness of the torsional spring is related to the stiffness of the compliant segment.

Several key variables, such as the torsional spring stiffness and pseudo-rigid-body angle derived in the PRBM method, are used to calculate the bending moment and subsequently, the bending stress in the small-length flexural pivot. A summary of PRBM variables is included in Table 1.

This paper builds upon the force-deflection analysis of the PRBM, developed by prior researchers as described above, by leveraging PRBM variables to obtain key stress equations for both homogeneous and reinforced small-length flexural pivots affixed to free rigid links.

3. PRBM-BASED STRESS ANALYSIS FOR HOMOGENEOUS, INITIALLY-STRAIGHT SMALL-LENGTH FLEXURAL PIVOTS

Compliant mechanisms, as opposed to engineered structures, are typically designed to achieve a specified motion to complete a specified task. One commonly used example is a simple archer's bow [12]. Designers of compliant mechanism rely heavily on kinematic synthesis to establish the geometry of each segment to provide displacement, velocity, or acceleration. While kinematic synthesis provides a mechanism design that can perform the intended task, it does not ensure that the mechanism can sustain operation for the desired product life span. Stress analysis, used in parallel with kinematic synthesis, allows the designer to design a robust mechanism that can both meet the motion requirements and product life span.

Design considerations such as the slenderness of the small-length flexural pivot can have a significant effect on the accuracy of stress analyses. This research assumes that the thickness of the small-length flexural pivot is 10% or less of the total length. The total stress within the small-length flexural pivot is equal to the sum of the bending stress and the axial stress [13]. The tensile and compressive stresses within the segment are either increased or decreased depending on the load factor, n.

The tensile stress, σ_t, is reduced and the compressive stress, σ_c, is increased by a compressive axial stress component if the load factor is greater than zero. The corresponding load angle ϕ is greater than $\pi/2$ radians (90 degrees). Conversely, the tensile stress is increased and the compressive stress is decreased by a tensile axial stress component if the load factor is less than zero. The corresponding load angle is less than $\pi/2$ radians (90 degrees).

The maximum tensile and compressive stresses in a compliant segment with a nonzero load factor are given by

$$\sigma_{max,t}, \sigma_{max,c} = \pm\frac{Mc}{I} - \frac{nP}{A}. \quad (1)$$

The bending stress component of total stress is dependent on the applied moment. Without the use of the PRBM, accurate calculation of the applied moment acting upon a compliant segment requires nonlinear beam analysis methods for accurate calculation of the large deflections and beam-end coordinates to determine the bending moment. The PRBM method is a simplified analysis technique capable of accurately determining the force-deflection response of a compliant segment.

Howell presented an example calculation for stress in a homogeneous small-length flexural pivot with a load factor of zero [1]. The stress analysis presented below applies to a small-length flexural pivot subjected to a non-following load at the free end of the segment. The stress analysis for homogeneous, small-length flexural pivots presented below is similar to Howell's work in that it relies on the PRBM. This paper presents a similar analysis, but uses a set of baseline equations solved in terms of PRBM variables that lend themselves well to subsequent calculation of stress in metallic-reinforced compliant segments. Additionally, the analysis method and equations below expand the scope to cover nonzero load factors and reinforced segments. The end result is two sets of equations for stress, one based on pseudo-rigid-body angle inputs, and the other based on tip deflection inputs.

Non-following loads applied to compliant segments are addressed in this research effort. A non-following load does not rotate with the segment's tip upon deflection. A non-following load configuration applied to a small-length flexural pivot in the free state is shown in Figure 4a. The non-following load configuration applied to a small-length flexural pivot in the deflected state is shown in Figure 4b. The vertical and horizontal components of the end load, *F*, are given as *P* and *nP*, respectively. The end load can be calculated using the vertical component and the load factor:

$$\mathrm{F} = \mathrm{P}\sqrt{1 + \mathrm{n}^2}. \tag{2}$$

A dimensionless quantity, η, related to the load factor, is used to simplify subsequent equations:

$$\eta = \sqrt{1 + \mathrm{n}^2}. \tag{3}$$

The first step in calculating the bending stress in a small-length flexural pivot is to determine the magnitude of the moment applied at the end of the beam. The moment is calculated with respect to a specified end displacement, *b*, or pseudo-rigid-body angle, Θ, and the transverse force component, F_t, of the non-following load.

The moment arm lengths can be determined using Figure 1. The non-following load components, *P* and *nP*, are applied at the vertical and horizontal coordinates of the beam tip, *a* and *b*, respectively:

$$a = \left(\frac{l}{2}\right) + \left(L + \frac{l}{2}\right)\cos(\Theta), \tag{4}$$

$$b = \left(L + \frac{l}{2}\right)\sin(\Theta). \tag{5}$$

Accurate analysis of the torsional spring stiffness ensures that the PRBM force-deflection response matches that of the small-length flexural pivot. Equation 7 presents the stiffness of the torsional spring that provides a force-deflection response in the PRBM that closely matches the force-deflection response of the homogeneous small-length flexural pivot [12]. The stiffness is presented in terms of the flexural modulus, moment of inertia, and small-length flexural pivot length. The stiffness is given in moment per unit rotation (i.e., in.-lbf./degree):

$$K = \frac{EI}{l}. \tag{6}$$

The transverse force component is determined using the PRBM geometry shown in Figure 4b:

$$F_t = F[\mathrm{Sin}(\phi - \Theta)]. \tag{7}$$

Based on elementary spring theory, torsional spring stiffness (K) is written in terms of the transverse force, pseudo-rigid-body angle, and the moment arm. Solving for the transverse force provides the following:

$$F_t = \frac{K\Theta}{\left(\frac{l}{2} + L\right)}. \quad (8)$$

Equations 7 and 8 enable the calculation of the non-following force *F* applied at the end of the beam:

$$F = \frac{K\Theta}{Sin(\phi - \Theta)\left(\frac{l}{2} + L\right)}. \quad (9)$$

The vertical load component *P* can be calculated using Equations 2 and 9:

$$P = \frac{K\Theta}{\eta Sin(\phi - \Theta)\left(\frac{l}{2} + L\right)}. \quad (10)$$

The maximum moment can be determined using the vertical load component, load factor, and tip coordinates (*a*, *b*):

$$M = P(a + nb). \quad (11)$$

The maximum tensile and compressive stresses, $\sigma_{t\ max}$ and $\sigma_{c\ max}$, are calculated using Equation 1 and Equation 11 as follows:

$$\sigma_{max} = P\left[\pm\frac{(a + nb)c}{I} - \frac{n}{A}\right]. \quad (12)$$

Using Equations 4-6 and 10 in Equation 12, a succinct equation for the maximum tensile and compressive stresses $\sigma_{t\ max}$ and $\sigma_{c\ max}$, in a homogeneous, small-length flexural pivot segment can be obtained:

$$\sigma_{max} = \frac{E\Theta}{\eta l Sin(\phi - \Theta)\left(\frac{l}{2} + L\right)}\left\{\pm\frac{\left[\left(L + \frac{l}{2}\right)\left(\cos(\Theta) + n\sin(\Theta)\right) + \frac{l}{2}\right]h}{2} - \frac{nI}{wh}\right\}. \quad (13)$$

The next section builds upon previous research [5] on metallic-reinforced compliant segments and the stress analysis presented above for homogeneous compliant segments to derive a method of stress analysis for metallic-reinforced small-length flexural pivots.

4. PRBM-BASED STRESS ANALYSIS FOR METALLIC-REINFORCED, INITIALLY-STRAIGHT SMALL-LENGTH FLEXURAL PIVOTS

The PRBM can also be used to analyze compliant mechanisms containing metallic reinforcement. The method below was developed specifically for a reinforced compliant segment designed such that the centroid of the reinforcing element is located on the neutral axis of the polymer casing. The stress analysis presented below applies to mechanisms operating at steady-state ambient temperatures. Analyses of metallic-reinforced segments operating at elevated or varying temperatures must include material properties related to the operating temperature, as well as stresses related to differences between the coefficient of thermal expansion of the casing and reinforcement materials. Additional analysis may also be required to assess the effect of stress raisers caused by the introduction of metallic reinforcement.

The load applied to each component of the compliant segment must be calculated separately in order to assess the moment and subsequently the stress within each component. The load distribution between the two beam components is proportional to the flexural rigidity of each component [14]. The component with the higher bending stiffness, or flexural rigidity, will support the higher bending load.

The reinforced segment is analyzed as two separate segments with identical transverse deflection [5]. For the sake of brevity, subscript i is used, where $i = 1$ corresponds to the casing and $i = 2$ corresponds to the reinforcement. The stiffness of the casing K_1 and the stiffness of the reinforcement K_2 are given by [5]:

$$K_i = \frac{E_i I_i}{l}. \tag{14}$$

In the case of a reinforced compliant segment, the total equivalent stiffness of the torsional spring K_t^e is the sum of the stiffness of the casing and the effective stiffness of the reinforcement. The reinforced segment is analyzed as two separate segments with identical transverse deflections [5]. This method is consistent with the calculation of springs in parallel. The equivalent torsional spring stiffness shown below includes the modulus and moment of inertia for each of the beam components:

$$K_t^e = \frac{E_1 I_1 + E_2 I_2}{l}. \tag{15}$$

Equations 2, 8, and 15 enable the calculation of the non-following force *F* applied at the end of the beam:

$$F = \frac{\Theta K_t^e}{\mathrm{Sin}(\phi - \Theta)\left(\frac{l}{2} + L\right)}. \tag{16}$$

The non-following force is distributed between the casing F_1 and the reinforcement F_2 based on the respective flexural rigidity, *EI*, and is given by the following:

$$F_i = \frac{\Theta E_i I_i}{l\mathrm{Sin}(\phi - \Theta)\left(\frac{l}{2} + L\right)}. \tag{17}$$

The vertical load component applied to the casing P_1 and the vertical load component applied to the reinforcement P_2 can be calculated using Equations 2 and 9:

$$P_i = \frac{\Theta E_i I_i}{\eta l \mathrm{Sin}(\phi - \Theta)\left(\frac{l}{2} + L\right)}. \tag{18}$$

The moment applied to the casing M_1 and the moment applied to the reinforcement M_2 to achieve the specified displacement at the tip is given by the following:

$$M_i = P_i(a + nb). \tag{19}$$

Stresses in the casing and the reinforcement can be calculated using the vertical loads and moments. The maximum tensile and compressive stresses in the casing are given by the following:

$$\sigma_{max,i} = \pm P_i\left[\frac{(a + nb)c_i}{I_i} - \frac{n}{A_i}\right]. \tag{20}$$

Equations 4, 5, and 18 are substituted into Equation 20 to provide the final, succinct equation for the maximum tensile and compressive stresses, $\sigma_{t\ max,1}$ and $\sigma_{c\ max,2}$, in the casing of a reinforced small-length flexural pivot:

$$\sigma_{max,1} = \frac{E_1\Theta}{\eta l \mathrm{Sin}(\phi-\Theta)\left(\frac{l}{2}+L\right)}\left\{\pm\frac{\left[\left(L+\frac{l}{2}\right)\left(\cos(\Theta)+n\sin(\Theta)\right)+\frac{l}{2}\right]h_1}{2} - \frac{nI_1}{w_1h_1-w_2h_2}\right\}. \quad (21)$$

Equations 4, 5, and 18 are substituted into Equation 20 to provide the final, succinct equation for the maximum tensile and compressive stresses, $\sigma_{t\ max,2}$ and $\sigma_{c\ max,2}$, in the reinforcement of a reinforced small-length flexural pivot:

$$\sigma_{max,2} = \frac{E_2\Theta}{\eta l \mathrm{Sin}(\phi-\Theta)\left(\frac{l}{2}+L\right)}\left\{\pm\frac{\left[\left(L+\frac{l}{2}\right)\left(\cos(\Theta)+n\sin(\Theta)\right)+\frac{l}{2}\right]h_2}{2} - \frac{nI_2}{w_2h_2}\right\}. \quad (22)$$

Equation 21 confirms that the maximum bending stress in the casing for a given segment deflection and material properties is a function of the distance from the neutral axis to the extreme fiber of the polymer and not the moment of inertia. Therefore, the introduction of an insert does not directly reduce the bending stress in the polymer portion of the beam, as the moment of inertia of the polymer is not included in the final equation. This is true in the case of a reinforced compliant segment deflected to achieve the same displacement or pseudo-rigid-body angle as that of a homogeneous segment.

The maximum bending stress in a casing subjected to a specified deflection is not directly reduced by the introduction of a high-strength insert because the distance from the neutral axis to the extreme fiber remains constant. However, the flexural rigidity increases. The increase in flexural rigidity for the segment results in an increase in the force required to produce the desired deflection.

While the maximum bending stress is not reduced, the total stress consisting of bending and axial components may be reduced due to the reduction in axial stress provided by the reinforcement, in the case of a nonzero load factor. While the bending stress is not directly reduced by the introduction of metallic reinforcement due to the constant tip deflection boundary condition, the axial force, P, and the area, A, are both reduced by the introduction of the metallic reinforcement.

5. RESULTS AND DISCUSSION

This section provides two examples of stress analysis of small-length flexural pivots. The first example presents the use of the equations derived herein to analyze the stress in a homogeneous small-length flexural pivot. The second example presents the use of the equations derived herein to analyze the stress in a metallic-reinforced small-length flexural pivot.

5.1 EXAMPLE 1 - HOMOGENEOUS, SMALL-LENGTH FLEXURAL PIVOT

A homogeneous, small-length flexural pivot has been designed and constructed from urethane with the following properties and dimensions:

E = 433,843 psi (2,985.43 MPa)

Θ = 30 deg (0.524 rad)

n = 0

h = 0.1 in. (3.18 mm)

w = 1.502 in. (38.15 mm)

L = 16 in. (406.4 mm)

l = 1 in. (25.4 mm)

Equation 13 can be used to calculate the tensile stress in the small-length flexural pivot. A load factor of zero (n = 0) allows for simplification of Equation 13. Additionally, a zero load factor results in a load angle of 90° (π/2 radians). The tensile stress is shown below:

$$\sigma_{max} = \frac{433{,}843(0.524)}{\mathrm{Sin}\left(\frac{\pi}{2} - 0.524\right)(0.5 + 16)}\left[\frac{[(16 + 0.5)\cos(0.524) + 0.5]0.1}{2}\right]. \quad (23)$$

The resulting tensile stress of 11,765 psi (81.12 MPa) is relatively high compared to the flexural strength of some engineering plastics [15]. Therefore, it is desirable to introduce metallic reinforcement to reduce the stresses in this small-length flexural pivot.

5.2 EXAMPLE 2 - REINFORCED, SMALL-LENGTH FLEXURAL PIVOT

The polyurethane small-length flexural pivot from Example 1 has been redesigned to include an AISI 1095 spring steel insert. The reinforced small-length flexural pivot was designed with the following properties and dimensions:

E_1 = 433,843 psi (2,985.43 MPa)

E_2 = 30,000,000 psi (206.8 GPa)

Θ = 30 deg (0.524 rad)

n = 0

h_1 = 0.1 in. (3.18 mm)

h_2 = 0.015 in. (0.381 mm)

w_1 = 1.502 in. (38.15 mm)

w_2 = 1 in. (25.4 mm)

L = 16 in. (406.4 mm)

l = 1 in. (25.4 mm)

Equation 21 and Equation 22 can be used to calculate the tensile and compressive stresses in the casing and the reinforcement of a metallic-reinforced small-length flexural pivot. A load factor of zero (n = 0) allows Equation 21 to be simplified. Additionally, a

zero load factor results in a load angle of 90° (π/2 radians). The tensile stress is shown below:

$$\sigma_{max,1} = \frac{433{,}843(0.524)}{\mathrm{Sin}\left(\frac{\pi}{2} - 0.524\right)(0.5 + 16)}\left[\frac{[(16 + 0.5)\cos(0.524) + 0.5]0.1}{2}\right], \quad (24)$$

$$\sigma_{max,2} = \frac{30{,}000{,}000(0.524)}{\mathrm{Sin}\left(\frac{\pi}{2} - 0.524\right)(0.5 + 16)}\left[\frac{[(16 + 0.5)\cos(0.524) + 0.5]0.015}{2}\right]. \quad (25)$$

The stress in the polymer casing of Example 2 is the same as the stress in Example 1 (11,765 psi or 81.12 MPa) because the distance from the neutral axis to the outside surface of the segment is unchanged with the introduction of the metallic reinforcement. The stress in the metallic reinforcement is 14,223 psi (98.06 MPa).

The example of stress analysis shows that the introduction of metallic reinforcement does not reduce the bending stress in the casing. Future research will focus on optimizing the cross-sectional dimensions to reduce the thickness and therefore the bending stresses in the metallic-reinforced small-length flexural pivot while achieving acceptable force-deflection behavior.

6. CONCLUSIONS

A method for analyzing stress in a small-length flexural pivot subjected to beam-end loads has been derived and provided in simplified, usable form. The analysis method built upon the accurate, well-established, and readily-available pseudo-rigid-body models (PRBMs) previously developed for force-deflection analysis.

The final, simplified equations for stress are presented for both homogeneous and reinforced segments. Equations are presented for the polymer compliant segment as well as the metallic reinforcing element to enable a comprehensive stress analysis tool. The stress analysis method and equations were demonstrated using two example compliant segment design cases, one homogeneous compliant segment and one reinforced with a spring steel element.

The example stress analysis showed that the introduction of metallic reinforcement increases the flexural rigidity, but does not reduce the bending stress in the casing unless the cross-sectional thickness is reduced. Future work will focus on presenting a method to optimize the cross section design when introducing metallic reinforcement to reduce the stress in the polymer casing.

7. ACKNOWLEDGMENTS

The authors would like to acknowledge the contributions of Dr. Sushrut Bapat, and graduate students Vamsi Lodagala and Pratheek Bagivalu Prasanna, graduate for participating in early discussions of this work. These discussions helped identify the needs and develop the bounds of this research effort.

8. REFERENCES

[1] Howell, L. L., *Compliant Mechanisms*, John Wiley & Sons, Inc., New York, New York, 2001.

[2] Howell, L. L., and A. Midha, "A Method for the Design of Compliant Mechanisms with Small-Length Flexural Pivots," *Journal of Mechanical Design*, Trans. ASME, Vol. 116, No. 1, March 1994, pp. 280-290.

[3] Midha, A., T. W. Norton and L. L. Howell, "On the Nomenclature, Classification, and Abstractions of Compliant Mechanisms," *Journal of Mechanical Design*, Trans. ASME, Vol. 116, No. 1, March 1994, pp. 270-279.

[4] Salamon, B. A., "Mechanical Advantage Aspects in Compliant Mechanisms Design," MS Thesis, Purdue University, October 1989.

[5] Kuber, Raghvendra Sharadchandra, "Development of a methodology for pseudo-rigid-body models of compliant segments with inserts, and experimental validation," Masters Theses. Paper 5363. Missouri University of Science and Technology, 2013.

[6] Bapat, Sushrut Gangadhar, "On the design and analysis of compliant mechanisms using the pseudo-rigid-body model concept," Doctoral Dissertation. Paper 2376. Missouri University of Science and Technology, 2015.

[7] Howell, L. L., and A. Midha, "Parametric Deflection Approximations for End-Loaded, Large-Deflection Beams in Compliant Mechanisms," *Journal of Mechanical Design*, Trans. ASME, Vol. 117, No. 1, March 1995, pp. 156-165.

[8] Midha, A., Bapat, S.G., Mavanthoor, A., and Chinta, A., "Analysis of a Fixed-Guided Compliant Beam with an Inflection Point Using the Pseudo-Rigid-Body Model Concept," *Journal of Mechanisms and Robotics*, Trans. ASME, Vol. 7, Aug. 2015, pp. 031007-1-10.

[9] Pauly, J., and A. Midha, "Improved Pseudo-Rigid-Body Model Parameter Values for End-Force-Loaded Compliant Beams," *Proceedings of the 28th Biennial ASME Mechanisms and Robotics Conference*, Salt Lake City, Utah, September 2004, pp. DETC 2004-57580 – 1-5.

[10] Midha, A.; Kuber, R. S.; Chinta, V.; Bapat, S. G., "A Method for a More Accurate Calculation of the Stiffness Coefficient in a Pseudo-Rigid-Body Model (PRBM) of a Fixed-Free Beam Subjected to End Forces," Proceedings of the ASME 2014 International Design Engineering Technical Conferenced & Computers and Information in Engineering Conference, Vols. DETC35366-1-10, Buffalo, NY, 2014.

[11] Rosen, S.L., "*Fundamental Principals of Polymeric Materials*," 2nd Edition, John Wiley & Sons, Inc., New York, New York, 1993.

[12] Howell, L.L., Magleby, S.P., Olsen, B.M., Handbook of Compliant Mechanisms, John Wiley & Sons, Ltd., West Sussex, United Kingdom, 2013.

[13] Spiegel, L., and Limbrunner, G.F., *Applied statics and strength of materials*. Merril, New York, New York 1991.

[14] Baumeister, T, and Marks, L., Standard Handbook for Mechanical Engineers, 7th ed. McGraw Hill, New York, New York, 1967.

[15] Innovative Polymers, Incorporated. "IE-3075 Data Sheet," Accessed September 1, 2015. http://www.innovative-polymers.com/images/specs/Classic-Shore-D/IE-3075.pdf.

9. FIGURES AND TABLES

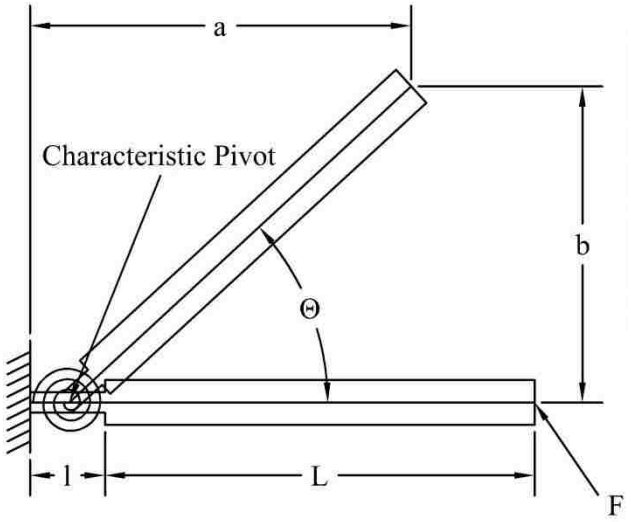

Figure 1: PRBM of Small-length flexural pivot compliant segment shown in initial position and deformed position

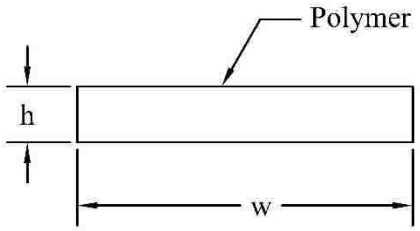

Figure 2: Cross Section of a Homogeneous Compliant Segment

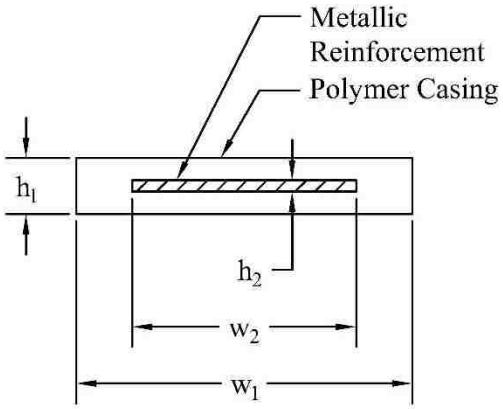

Figure 3: Cross Section of Metallic Reinforced Compliant Segment

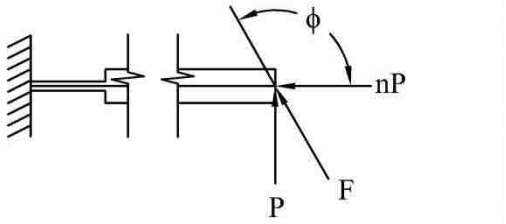

a)

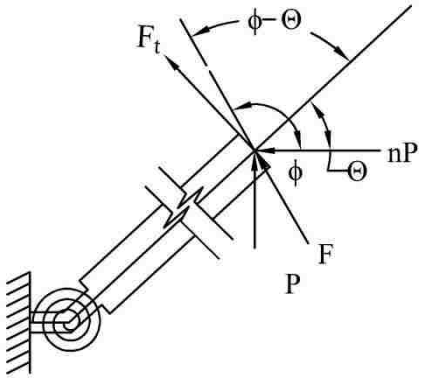

b)

Figure 4: Non-Following End-Load, F Applied to a Small-length flexural pivot in the a) Free State and b) Deflected state

Table 1: Nomenclature

Variable	Description
K_t^e	Equivalent Stiffness of Reinforced Segment
K	Stiffness of Torsional Spring
b	Transverse Deflection of the Beam Tip
l	Length of Small-length flexural pivot
L	Length of Rigid Segment
E	Flexural Modulus
I	Moment of Inertia
Θ	Pseudo-Rigid-Body Angle
ϕ	Load Angle
n	Load Factor
P	Vertical Component of End Load
F	End Load
F_t	Transverse Load Component
A	Cross-sectional Area
w	Cross-sectional Width
h	Cross-sectional Height

III. REDUCTION OF STRESS IN PLASTIC COMPLIANT MECHANISMS BY INTRODUCING METALLIC REINFORCEMENT

J. Crews, A. Midha and L.R. Dharani[1]

Department of Mechanical and Aerospace Engineering, Missouri University of Science and Technology, Rolla, MO 65409

ABSTRACT: A method is provided and validated for redesigning compliant segments to improve fatigue, creep, and stress relaxation performance. The method reduces the bending stress in the polymer portion of the compliant segment without the need for overall mechanism redesign by introducing metallic reinforcement and by matching the force-deflection response of the redesigned segment to that of the baseline segment. An example redesign case study is presented and validated with experimental testing using a unique deflection testing device designed for fixed-free compliant mechanisms.

Keywords: compliant segment, compliant mechanism, stress analysis, mechanism, design, bending stiffness, flexural rigidity, thermoset, pseudo-rigid-body model

[1] Corresponding author

E-mail address: dharani@mst.edu

1. INTRODUCTION

A mechanism is a mechanical device whose links and movable joints allow the transfer or transformation of motion, force, or energy [1], [2]. A compliant mechanism is a type of mechanism that transfers or transforms motion, force, or energy through the deformation of its links or segments in place of, or in addition to moveable joints [3], [4]. Figure 1 shows a rigid-body mechanism and an equivalent compliant mechanism concept applied to automotive suspension.

Introducing compliance into mechanism design offers reduced cost due to limited part count and minimal assembly labor, elimination of backlash and wear associated with mechanical joints, and energy storage resulting from deformation of the segments [1], [3], [5], [6]. Compliant segments, commonly constructed of engineering plastics, also have disadvantages including increased design complexity due to geometric and material nonlinearities, and susceptibility to failure by creep, stress relaxation, or fatigue [1], [3], [5], [6].

Designers of compliant mechanisms constructed of engineering plastics are generally challenged to design a mechanism that offers the needed motion while ensuring that failure doesn't occur due to static or dynamic loads. Failure prevention, via the design of a robust compliant mechanism, relies on both stress analysis and material selection [7].

A compliant segment that has experienced failure could traditionally be redesigned to reduce stress by either limiting the deflection of the failed link or by introducing a material with higher strength. The drawback to the traditional approach of limiting deflection is that the force-deflection behavior of the compliant mechanism

function would be affected, as compliant segments are generally designed with large deflections specifically tailored to support the function of the parent mechanism.

This paper provides a validated method for redesigning compliant segments that have failed due to common stress-related failure modes including fatigue, creep, and stress relaxation. The method focuses on introducing metallic reinforcement centered within a polymer casing. The outcome of the proposed redesign method is a reduction of the bending stress in the polymer portion of the compliant segment without the need for overall mechanism redesign. This outcome is accomplished by matching the force-deflection response of the redesigned segment to that of the failed segment.

Previous work has shown that a pseudo-rigid-body model (PRBM) can be employed to calculate the bending stress in compliant segments [1], [6], [8]. The PRBM is a tool originally developed to analyze deflections of compliant links or segments. Howell and Midha [9], Howell [10], [11], and Howell et al. [12] developed the PRBM for the fixed-free compliant segment shown in Figure 2. The approach of the PRBM method is to model a compliant segment's tip deflection by replacing the compliant segment with a rigid body analog. The rigid body analog is developed by placing a pivot point, called a characteristic pivot, between two rigid links. The PRBM of a fixed-free compliant segment is described in more detail in the following section.

2. ANALYSIS OF STRESS USING THE PRBM

Stress analysis is a challenging step in the design process for robust compliant mechanisms. Previous work by Howell [1] highlighted two common loading modes and associated stresses within a compliant segment as axial and bending. The predominant loading configuration of compliant mechanisms, typically designed for motion via specified deflections of segments or links, is a force applied at the end of a segment. In most cases the direction of the applied force contains a transverse component that significantly exceeds the axial component. The direction of end-forces applied to compliant segments leads to the bending stress component substantially exceeding the axial stress component such that axial component may be neglected [1].

Analysis of bending stress in compliant segments is complicated by the need for an accurate calculation of the applied bending moment. Howell [1] presented several stress analyses related to fixed-free compliant segments and small-length flexural pivots with load factors of zero. Kuber [6] introduced the concept of using metallic reinforcement in polymeric compliant segments as a way to improve performance. Crews [8] expanded the PRBM approach by providing simplified equations of stress within fixed-free compliant segments and small-length flexural pivots, both homogeneous and metallic-reinforced.

The method described herein utilizes the PRBM to show that the bending stress in a compliant segment subjected to a specified displacement is a function of the distance from the neutral axis to the extreme fiber and that simply introducing metallic reinforcement does not reduce stress. Additionally, it is shown that the moment required to achieve a specified tip deflection is proportional to the moment of inertia. Therefore,

an increase or decrease in the moment of inertia must be accompanied by a proportional increase or decrease in the applied moment to achieve the desired tip deflection.

Bending stress σ_b is defined in terms of the applied moment M, moment of inertia I, and distance c from the neutral axis to the surface of the compliant segment:

$$\sigma_b = \frac{Mc}{I}. \tag{1}$$

Calculation of bending stress is initiated by calculating the moment needed to achieve the specified deflection. The applied moment, with respect to the desired deflection, can be determined using the PRBM. The load configuration of the segment in the free-state and deflected state is shown in Figure 3. The vertical and horizontal components of the end load F are given as P and nP, respectively. The end load can be calculated using the vertical component and the load factor:

$$F = P\sqrt{1 + n^2}. \tag{2}$$

A dimensionless quantity η, related to the load factor, is used to simplify subsequent equations:

$$\eta = \sqrt{1 + n^2}. \tag{3}$$

The load angle ϕ does not change with deflection due to the definition of a non-following load. The load configuration in the deflected state is shown in Figure 3b. The

transverse force component for use in subsequent torsional spring force calculations is given by F_t:

$$F_t = F[\mathrm{Sin}(\phi - \Theta)]. \tag{4}$$

The first step in calculating the moment required to attain a specified displacement is to evaluate the stiffness of the torsional spring, *K*. The stiffness is given in moment per unit rotation (in.-lbf./degree). The stiffness, in terms of the stiffness coefficient K_Θ, flexural rigidity *EI*, characteristic radius factor γ and the segment length *l* is given by [6]:

$$K = K_\Theta \gamma \left[\frac{EI}{l}\right]. \tag{5}$$

The stiffness coefficient, as refined by Kuber [6], is a function of the load factor and the pseudo-rigid-body angle, Θ. The stiffness coefficient for load configurations with a positive load factor is given by the following [6]:

$$\begin{aligned} K_\Theta = \frac{1}{\Theta}(&0.004233 - 0.012972n + 2.567095\Theta + 0.003993n^2 \\ &- 0.037173\Theta^2 - 0.000297n^3 + 0.179970\Theta^3 \\ &- 0.034678n\Theta + 0.003467n^2\Theta - 0.009474n\Theta^2), \\ &\text{for } 0 \le n \le 10 \text{ and } 0 < \Theta \le 65°. \end{aligned} \tag{6}$$

The stiffness coefficient for load configurations with a negative load factor is given by the following [6]:

$$K_\Theta = \frac{1}{\Theta}(0.000651 - 0.008244n + 2.544577\Theta - 0.004767n^2 + 0.071215\Theta^2 - 0.000104n^3 + 0.079696\Theta^3 + 0.069274n\Theta + 0.061507n^2\Theta - 0.347588n\Theta^2), \quad \text{for } -4 < n < 0 \text{ and } 0 < \Theta < 0.8\phi. \tag{7}$$

The moment of the torsional spring represents the moment applied to the torsional spring such that the link rotates by a pseudo-rigid-body angle. The pseudo-rigid-body angle represents the rotation of a rigid link used within the PRBM for a compliant segment. The torsional spring constant, or force per unit angular displacement, is given by:

$$K = \frac{F_t \gamma l}{\Theta} \tag{8}$$

The torsional spring constant is a function of transverse force and the length of the moment arm. The length of the moment arm is equal to the characteristic radius γl for the case of a fixed-free compliant segment. The use of Equations 4, 5, and 8 provides the relationship between end force, load angle, and pseudo-rigid-body angle:

$$F = \frac{K_\Theta E I \Theta}{l^2 \mathrm{Sin}(\phi - \Theta)}. \tag{9}$$

The vertical load component is calculated using Equations 2, 5 and 9:

$$P = \frac{K_\Theta EI\Theta}{\eta l^2 Sin(\phi - \Theta)}. \quad (10)$$

The maximum moment is determined using the vertical load component, load factor, and tip coordinates:

$$M = P(a + nb). \quad (11)$$

The use of Equations 10 and 11 enables the calculation of the moment required to achieve the specified vertical and horizontal displacements at the tip:

$$M = \frac{K_\Theta EI\Theta}{\eta l^2 Sin(\phi - \Theta)}(a + nb). \quad (12)$$

Equation 12 shows that the moment required to achieve a specified tip deflection, via the specified pseudo-rigid-body angle, is proportional to the moment of inertia. Next, the moment can be inserted into the equation for bending stress and the maximum stress can be calculated:

$$\sigma_b = \pm \frac{Mc}{I}, \quad (13)$$

$$\sigma_{max} = \pm \frac{K_{\Theta} E \Theta (a + nb)}{\eta l^2 Sin(\phi - \Theta)} [c]. \quad (14)$$

The stiffness coefficient is a function of the deflection via the inclusion of the pseudo-rigid-body angle. The load factor, load angle, and dimensionless quantity η, are characteristics of the applied load. The modulus *E* is a material property. Inspection of Equation 14 shows that if the length, material, or specified deflection is not changed during the redesign then the stress is proportional to the distance from the neutral axis to the surface of the segment, *c*.

3. REDESIGN OF HOMOGENEOUS COMPLIANT MECHANISMS TO REDUCE STRESS AND MAINTAIN FUNCTION

Initial activities subsequent to failure of a compliant mechanism fit into the process known as failure analysis. The goal of a failure analysis is to determine the primary cause failure. Causes of failure may include inadequate design, improper material selection, material defect, manufacturing defect, or the application of loads beyond the original design condition.

This paper focuses on redesign of compliant mechanisms that have failed due to either inadequate design or improper material selection. The scope is further refined within the category of inadequate design to focus on redesign of failures caused by improper consideration of creep, stress relaxation, or fatigue. The scope is also refined within the category of improper material selection to focus on compliant mechanisms constructed from engineering plastics including, but not limited to polypropylene, acetal, or nylon.

Compliant mechanisms are designed for a specific motion enabled by deflection of segments or links. Therefore, redesigning one failed link may have a restraining effect on the overall mechanism functionality. It is advantageous to redesign failed segments or links within compliant mechanisms while minimizing the effect on the overall mechanism functionality. One way to redesign a failed link without requiring the need for redesign of the mechanism is to match the force-deflection response of the redesigned link to that of the failed link. The forces and loads within connecting links and the overall compliant mechanism remain the same.

The segment's flexural rigidity, the product of the modulus and the moment of inertia, provides a parameter to quantify the segment's resistance to bending. The

methodology presented herein maintains the force-deflection response of the original homogeneous segment while including metallic reinforcement thereby reducing the stress. This methodology enables a direct comparison of stress in two compliant segments: one with and one without metallic reinforcement, but both exhibiting the same force-deflection behavior.

Kuber [6] introduced the concept of placing a high-modulus reinforcing material within a compliant casing constructed of a relatively low-modulus material in an effort to reduce stress. The introduction of metallic reinforcement within a plastic compliant mechanism increases the flexural rigidity due to the relatively high flexural modulus of the reinforcing material. It becomes possible to match the flexural rigidity of the redesigned link to that of the baseline link by reducing the segment's cross-sectional thickness. The reduction in segment thickness offsets the increase in flexural rigidity caused by the metallic reinforcing element. This research effort expands the concept by showing that the high-modulus reinforcement enables a reduction in casing thickness and the distance from the neutral axis and the surface of the beam, thereby reducing bending stress. Cross sections of homogeneous and reinforced compliant segments are shown in Figure 4a and Figure 4b, respectively. It should be noted that the thickness, h_1 of the reinforced compliant segment is less than the thickness, h of the original homogeneous compliant segment.

The bending stiffness of the baseline homogeneous compliant segment is equal to the product of the modulus of elasticity and the moment of inertia. The bending stiffness of the reinforced compliant segment is the sum of the individual components of the segment, namely the polymer casing and the metallic reinforcement. The subject method

provides a consistent bending stiffness between the baseline homogeneous compliant segment and the redesigned, reinforced compliant segment. The left and right hand sides of Equation 15 contain the bending stiffness of the baseline segment and the bending stiffness of the redesigned segment, respectively:

$$E_1 I = E_1 I_1 + E_2 I_2. \tag{15}$$

where the subscript 1 denotes the polymer casing and subscript 2 denotes the reinforcing element.

The moment of inertia of the casing, I_1, is related to the moments of inertia of the reinforcement I_2 and the baseline segment I. Equation 16 provides the required moment of inertia for the polymer casing with respect to the moments of inertia of the baseline segment and reinforcing element, as well as the ratio of the modulus of the insert material to the modulus of the casing material. The baseline segment and polymer casing of the redesigned, reinforced segment are assumed to be constructed of the same material in this case. Equation 16, derived from Equation 15, confirms that the moment of inertia of the polymer casing must be reduced after the introduction of the reinforcing element to ensure that the bending stiffness is unaffected when compared to the baseline:

$$I_1 = I - \frac{E_2}{E_1} I_2. \tag{16}$$

The cross-sectional dimensions of the polymer component should be optimized to contain the lowest height, which corresponds to the smallest distance from the neutral

axis to the extreme fiber. The calculations below represent the optimization of the moment of inertia of the casing, without changing the width of the beam. The moment of inertia of the casing is calculated as follows:

$$I_1 = \frac{bh^3}{12} - \frac{E_2}{E_1}\left(\frac{b_2 h_2^3}{12}\right). \tag{17}$$

The width of the optimized section is equal to that of the baseline segment. The left hand side of Equation 17 can be expanded to include the width and height dimensions of the optimized cross section:

$$I_1 = \frac{bh_1^3}{12} - \frac{b_2 h_2^3}{12}. \tag{18}$$

The use of Equations 17 and 18 enable calculation of the cross-sectional height of the reinforced segment that provides a consistent bending stiffness when compared to the baseline segment:

$$\frac{bh_1^3}{12} - \frac{b_2 h_2^3}{12} = \frac{bh^3}{12} - \frac{E_2}{E_1}\left(\frac{b_2 h_2^3}{12}\right), \tag{19}$$

$$h_1 = \sqrt[3]{h^3 + \frac{b_2 h_2^3}{b}\left(1 - \frac{E_2}{E_1}\right)}. \tag{20}$$

The bending stress in the polymer portion of the beam can be indirectly reduced by the introduction of a metallic insert because the distance from the neutral axis to the extreme fiber of the polymer is reduced to maintain a consistent deflection behavior. The corresponding reduction in bending stress will improve the segments stress relaxation, creep, and fatigue performance.

4. EFFECT OF BONDING BETWEEN THE CASING AND METALLIC REINFORCEMENT

Manufacturing methods used to create metallic-reinforced compliant segments may lead to unintentional bonding between the insert and the polymer casing. This section presents a comparison between the flexural rigidity corresponding to two boundary conditions of the metallic insert: "frictionless" and "bonded" to the casing. The flexural rigidity is assessed using a parallel spring analogy [6] for the "frictionless" insert and by using the equivalent area method for the "bonded" insert [13]. The "frictionless" and "bonded" cases represent limits of the range of boundary conditions that may be encountered in reinforced compliant segments. The actual boundary condition may be "partially-bonded".

The calculations presented in Section 3 were derived under the assumption that the reinforced segment behaved as two independent segments: the polymer casing and the metallic reinforcement. The assumption was that the two segments were modeled as springs in parallel with identical tip deflections [6].

The parallel-spring approach realizes another assumption that the interface between the segments is frictionless and that the shear stresses within one component of the segment do not translate into shear stresses of the other component.

The following calculations arrive at the effective bending stiffness assuming perfect bonding; an assumption commonly used while analyzing fiber reinforced composites [13]. The method, called equivalent area method, transforms the composite cross section into an equivalent cross section of a single material to enable analysis using beam theory. The bending stiffness of the composite beam is maintained by refining the dimensions of the cross section based on the ratio of the modulus of the constituent

materials. It is more desirable to adjust the width of the cross section as opposed to the height to enable the use of bending stress calculations which rely on the distance from the neutral axis to the outer surface of the segment. An equivalent-area representation of a metallic-reinforced compliant segment is shown in Figure 4c. The cross section of the material with the higher modulus is transformed into a cross section composed of the material with the lower modulus while retaining the bending stiffness.

The equivalence in bending stiffness between the metallic insert and the polymer cross section is given by the following:

$$E_2 \frac{b_2 h_2^3}{12} = E_1 \frac{b_{2,\text{transformed}} h_2^3}{12}. \tag{21}$$

The width of the transformed section of the metallic reinforcement shown in Figure 4c is given by the following:

$$b_{2,\text{transformed}} = \frac{E_2}{E_1} b_2. \tag{22}$$

The moment of inertia and flexural rigidity of the transformed section, which is composed of only the polymer material, are given by the following:

$$I_{\text{transformed}} = 2(I_1 + A_1 d_1^2) + \frac{E_2}{E_1}(I_2 + A_2 d_2^2), \tag{23}$$

$$E_1 I_{transformed} = E_1 \left((I_1 + a_1 d_1^2) + \frac{E_2}{E_1} (I_2 + a_2 d_2^2) \right). \quad (24)$$

The distances from the centroid of the polymer casing to the neutral axis and from the centroid of the reinforcing insert to the neutral axis are both equal to zero if the reinforcing insert is located at the neutral axis:

$$d_1 = d_2 = 0. \quad (25)$$

As such, Equation 24 can be simplified for the case of a reinforcing insert located such that its centroid is located on the neutral axis:

$$E_1 I_{transformed} = E_1 \left(I_1 + \frac{E_2}{E_1} (I_2) \right). \quad (26)$$

Equation 15 and Equation 26 show that the flexural rigidity is equivalent between the parallel spring method and the transformed section method for compliant segments containing reinforcing inserts whose centroids are aligned with the segment's neutral axis.

This equivalence shows that the degree of friction or bonding between the insert and the casing does not have an effect on the bending stiffness of the reinforced compliant segment if the reinforcement and the casing share a common neutral axis due to symmetry about the horizontal axis.

5. RESULTS AND DISCUSSION

5.1 EXAMPLE CASE STUDY

A fixed-free compliant segment constructed of thermoset polyurethane has failed from fatigue and needs redesign. The fixed-free segment is part of a compliant 4-link mechanism that serves a particular purpose within an engineered system. The segment is redesigned to include spring steel reinforcement. The force-deflection behavior of the compliant mechanism must not be affected so as to not alter system performance. The properties and dimensions of the failed, fixed-free compliant segment and metallic reinforcement are as follows:

E_1 = 433,843 psi (2,985.43 MPa)

E_2 = 30,000 ksi (206.8 GPa)

h = 0.2473 in. (6.28 mm)

h_2 = 0.050 in. (1.27 mm)

w = w_1 = 1.502 in. (38.15 mm)

w_2 = 1.003 in. (25.48 mm)

The use of Equation 20 with the properties and dimensions above provides the thickness of the polymer casing that would, with metallic reinforcement, maintain the same bending stiffness as the failed link:

$$h_1 = \sqrt[3]{(0.2473\text{in.})^3 + \frac{(1.0\text{ in.})(0.050\text{ in.})^3}{1.502\text{ in.}}\left(1 - \frac{30{,}000\text{ ksi}}{433.843\text{ ksi}}\right)} \quad (27)$$

$$= 0.211\text{ in.}\,(5.36\text{ mm}).$$

The reduction in thickness in the polymer casing enabled by the introduction of metallic reinforcement is approximately 15%. It was shown in Section 2 that the reduction in bending stress is proportional to the reduction in the distance from the neutral axis to the surface of the segment. Therefore, the stress reduction in the example above is 15%.

5.2 EXPERIMENTAL VALIDATION

Fixed-free compliant segment test specimens were constructed and tested to validate the ability of Equation 20 to optimize the thickness of the polymer casing in a redesigned, reinforced fixed-free compliant segment to maintain a consistent force-deflection behavior.

A test fixture was developed to measure the deflection of points spaced 2 inches (50.8 millimeters) along the length of each fixed-free compliant segment. The test fixture consists of a test arm machined from 6061-T6 aluminum, a hot-rolled steel base, a load applicator additively manufactured from Acrylonitrile Butadiene Styrene (ABS) plastic, and five dial indicators to measure deflection. A rendering of the deflection test device is shown in Figure 5.

The load applicator is designed to apply the clamp load to the homogeneous portion of the cross section. This helps to prevent axial constraint of the metallic reinforcement to the polymer casing at the free end of the fixed-free compliant segment. A 49.5 ounce (1,403.3 gram) weight is hung from the load applicator to provide a non-following load to the tip of the fixed-free compliant segment. The deflections are measured and recorded 15 seconds after the load is applied; the time experimentally determined to provide a stable dial measurement.

5.2.1 Material for Experimental Test Specimens . A castable urethane, IE-3075, was selected for this research effort because it is a commonly used plastic for prototyping, it is readily available and easy to work with, and because its modulus and flexural strength are comparable to other engineering plastics used in the construction of compliant mechanisms. The flexure strength and modulus of IE-3075 were determined by testing five samples in the 3-point bend configuration of ASTM D790-10.

IE-3075 can be used at room temperature and without the need for high temperature injection molding equipment. The urethane is based on a urethane-type repeated structural unit, a polymer prepared by the reaction of diisocyanate with hydroxyl containing compounds [14]. It is classified as a rigid plastic per ASTM definition [14] because it has a modulus of elasticity greater than 10,000 psi (68.948 MPa). The material properties of IE-3075 are similar to those of acetal. Acetal is a commonly used material in compliant mechanism construction [6]. Material properties of IE-3075 and acetal are shown in Table 1.

5.2.2 Test Specimen Fabrication. IE-3075 is a room-temperature casting urethane typically cast in a platinum-cured silicone mold. All casting was performed in custom cast molds constructed of platinum cured silicone. The mold making process is initiated by affixing a pattern, which is typically a compliant mechanism or segment constructed via 3d printing or machining, to a backing plate. The backing plate is constructed of ABS plastic because it naturally releases from cast silicone. Once the pattern is affixed to the backing plate, a mold box is placed on top of the backing board such that it provides liquid-tight walls surrounding the pattern. Platinum-cured silicone is a two-part system that requires thorough mixing and vacuum degassing prior to pouring it

into the mold box. The mold is inverted and the backing plate is removed once the silicone cures. Fill and vent tubes are affixed to the pattern. The exposed silicone is treated with a mold release to prevent the second mold half from adhering to the first. A second mold box is placed atop the first mold box. A second pour of silicone is poured into mold box to form the second half of the silicone mold. Once the second half is cured, the mold boxes are split, the vents and fill tubes are removed, the pattern is removed, and the silicone mold is complete.

The casting process used to make the final compliant segment or test specimen initiates by applying a mold release to the interior surfaces and mating surfaces of the silicone mold halves. The mold is closed and the urethane casting resin is prepared. The urethane casting resin must be thoroughly mixed and degassed similar to the silicone mold material. Vent tubes and the fill funnel are placed into the second mold half. The urethane is poured into the fill tube until it emerges in the vent tubes. The mold is split once the stated demold time has been reached. The cured specimen is removed from the mold and the sprues are removed to reveal the final product.

A reinforced compliant segment can be constructed using the same bottom mold half as the original, unreinforced compliant segment. A new top mold half is required in order to achieve the desired overall section thickness of 0.210 inches (5.334 mm). One additional step is added to the molding process described above to yield a reinforced compliant segment. A reinforcing strip is placed into two insert holders which are then placed into the mold as an assembly. The casting process then proceeds as described above. Once the demold time has been reached, the product is removed from the mold

and the insert holders are removed by cross-sectioning. Figure 6 shows an exploded assembly view of a mold setup for casting a metallic reinforced specimen.

The resulting reinforced compliant segment created using the example mold is shown in Figure 7. Insert holders, shown in yellow in Figures 6 and 7, are used to center the metallic reinforcement in the cast IE-3075. The yellow portions of the segment are removed by abrasive cross sectioning after demolding.

Reinforced specimens with intentional bonding between the casing and reinforcement are constructed by applying a release agent to the spring steel reinforcing member of the compliant segment specimens containing "frictionless" inserts and by neglecting to apply a release agent to the spring steel reinforcement of the compliant segments containing "bonded" inserts. The effectiveness of the bonding agent was qualitatively confirmed by manually extracting the reinforcement from a specimen containing an insert with release agent applied. The mix schedule developed for the final test specimens is shown in Table 2.

A total of 15 specimens were tested. Test specimens include: five homogeneous fixed-free compliant segments, five reinforced fixed-free compliant segments and five reinforced fixed-free compliant segments with intentional bonding between the reinforcement and the casing. Average dimensions for the test specimens are shown in Table 3. The urethane samples exhibited notable dimensional accuracy, with deviations from the desired thickness were less than 2%.

5.2.3 Deflection Test Results. Deflection testing and subsequent analysis of results show that the reinforced compliant segment designed using Equation 7 maintains the force-deflection relationship of the homogeneous compliant segment to within 1% at

the free end of the segment. Figure 8 shows a plot of deflection measurements obtained during experimental trials. Table 4 and Table 5 contain the average deflection measured on five test specimens of each type: homogeneous, reinforced with insert and release agent, and reinforced with insert and no release agent.

6. CONCLUSIONS

A straightforward method is presented to redesign a baseline compliant segment to reduce stress without requiring the need for additional redesign of the whole mechanism. The need for redesign of the entire mechanism is eliminated by matching the force-deflection response of the redesigned segment to that of the failed segment. The forces and loads within connecting links or segment, as well as the overall compliant mechanism remain the same.

The method is aimed at applications wherein the compliant segment is overstressed and has failed due to either inadequate design or improper material selection resulting in creep, stress relaxation, or fatigue. The introduction of metallic reinforcing elements as a critical step in the redesign method allows the designer to leverage the unique advantages offered by both the plastic and metallic materials.

It was highlighted that the bending stress in the polymer portion of the compliant segment can be indirectly reduced by the introduction of a high-modulus insert because the distance from the neutral axis to the extreme fiber of the polymer is reduced to maintain a consistent deflection behavior. The reduction in bending stress enabled by the introduction of metallic reinforcement will increase the number of stress cycles that the segment can be subjected to prior to fatigue failure. Additionally, similar performance improvements are expected in the areas of creep and stress relaxation behavior due to the reduction in bending stress. Future work should include stress relaxation, creep, and fatigue testing of fixed-free compliant test specimens similar to those used in the subject research.

Room-temperature urethane casting was introduced as a simple and economical construction technique for compliant mechanisms. This manufacturing technique enables the production of both homogeneous and reinforced compliant mechanisms at ambient temperature using relatively inexpensive materials and equipment.

A unique, simple, and accurate deflection testing device was introduced that enabled experimental testing and validation of the force-deflection response of fixed-free compliant segments.

Equivalence between results obtained using the parallel spring and equivalent area methods showed that the degree of bonding between the insert and casing does not affect the bending stiffness if the reinforcement and casing share a common neutral axis due to symmetry about the horizontal axis.

7. ACKNOWLEDGMENTS

The authors would like to acknowledge the contributions of Dr. Sushrut Bapat and graduate students Vamsi Lodagala and Pratheek Bagivalu Prasanna for participating in early discussions of this work. These discussions helped identify the needs and develop the scope of this research effort.

8. REFERENCES

[1] Howell, L. L., *Compliant Mechanisms*, John Wiley & Sons, Inc., New York, New York, 2001.

[2] Howell L. L. and Midha A., "A Method for the Design of Compliant Mechanisms with Small-Length Flexural Pivots," Journal of Mechanical Design, Trans. ASME, Vol. 116, No. 1. - 1994. - pp. 280-290.

[3] Midha, A., T. W. Norton and L. L. Howell, "On the Nomenclature, Classification, and Abstractions of Compliant Mechanisms," Journal of Mechanical Design, Trans. ASME, Vol. 116, No. 1, March 1994, pp. 270-279.

[4] Salamon, B. A., "Mechanical Advantage Aspects in Compliant Mechanisms Design," MS Thesis, Purdue University, October 1989.

[5] Bapat, S. G., "On the design and analysis of compliant mechanisms using the pseudo-rigid-body model concept," Doctoral Dissertation. Paper 2376. Missouri University of Science and Technology, 2015.

[6] Kuber, R. S., "Development of a methodology for pseudo-rigid-body models of compliant segments with inserts, and experimental validation," Masters Theses. Paper 5363. Missouri University of Science and Technology, 2013.

[7] Juvinall, R.C., Marshek, K.M., *Fundamentals of Machine Component Design*, 3rd. Edition, John Wiley & Sons, 2003.

[8] Crews, J. A., "Methodology for Analysis of Stress, Creep and Fatigue Behavior of Compliant Mechanisms," Doctoral Dissertation. Missouri University of Science and Technology, 2016.

[9] Howell, L. L., and Midha, A., "Parametric Deflection Approximations for End-Loaded, Large-Deflection Beams in Compliant Mechanisms," Journal of Mechanical Design, Trans. ASME, Vol. 117, No. 1, March 1995, pp. 156-165.

[10] Howell, L.L., "The Design and Analysis of Large-Deflection Members in Compliant Mechanisms," MS Thesis, Purdue University, August 1991.

[11] Howell, L. L., "A Generalized Loop Closure Theory for the Analysis and Synthesis of Compliant Mechanisms," Ph.D. Dissertation, Purdue University, 1993.

[12] Howell, L. L., Midha, A., and Norton, T. W., "Evaluation of Equivalent Spring Stiffness for use in a Pseudo-Rigid-Body Model of Large-Deflection Compliant Mechanisms," Journal of Mechanical Design, Trans. ASME, Vol. 118, No. 1, March 1986, pp. 126-131.

[13] Beer, F.P., Johnston, R.E. and DeWolf, J.T., *Mechanics of Materials*, McGraw Hill Companies, Inc. New York, New York, 2006.

[14] ASTM Standard D883, 2012e1, "Standard Terminology Relating to Plastics," ASTM International, West Conshohocken, PA, 2012, DOI: 10.1520/D0790-15E02, www.astm.org.

[15] Midha, A., Bapat, S.G., Mavanthoor, A., and Chinta, A., "Analysis of a Fixed-Guided Compliant Beam with an Inflection Point Using the Pseudo-Rigid-Body Model Concept," *Journal of Mechanisms and Robotics*, Trans. ASME, Vol. 7, Aug. 2015, pp. 031007-1-10.

[16] E.I. du Pont de Nemours and Company. "Delrin® Acetal Resin Product and Properties Guide," Copyright 2000.

[17] ASTM Standard D790, 2015e2, "Standard Test Methods for Flexural Properties of Unreinforced and Reinforced Plastics and Electrical Insulating Materials," ASTM International, West Conshohocken, PA, 2015, DOI: 10.1520/D0790-15E02, www.astm.org.

[18] Innovative Polymers, Incorporated. "IE-3075 Data Sheet." Accessed September 1, 2015. http://www.innovative-polymers.com/images/specs/Classic-Shore-D/IE-3075.pdf.

9. FIGURES AND TABLES

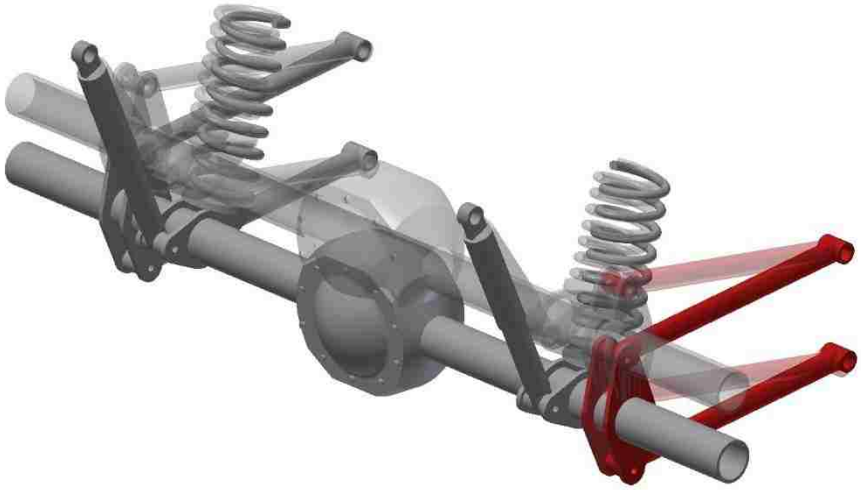

a)

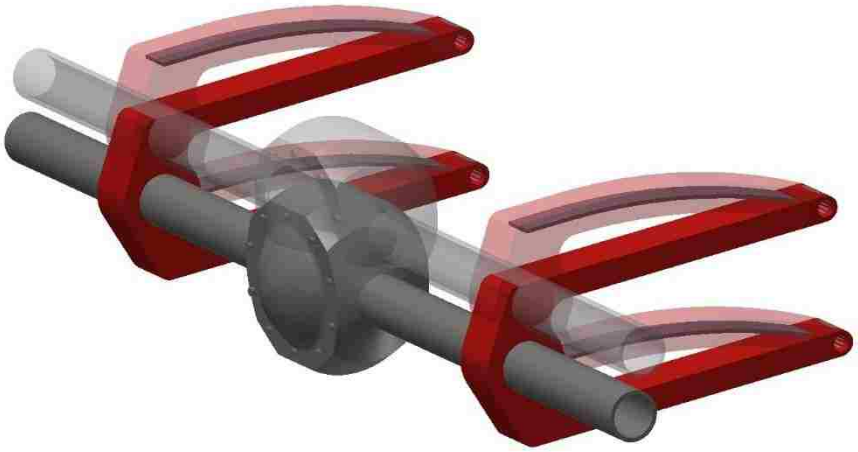

b)

Figure 1: Automotive Suspension Mechanism Examples a) Rigid-body 4-bar Mechanism Assembly and b) Compliant 4-bar mechanism assembly

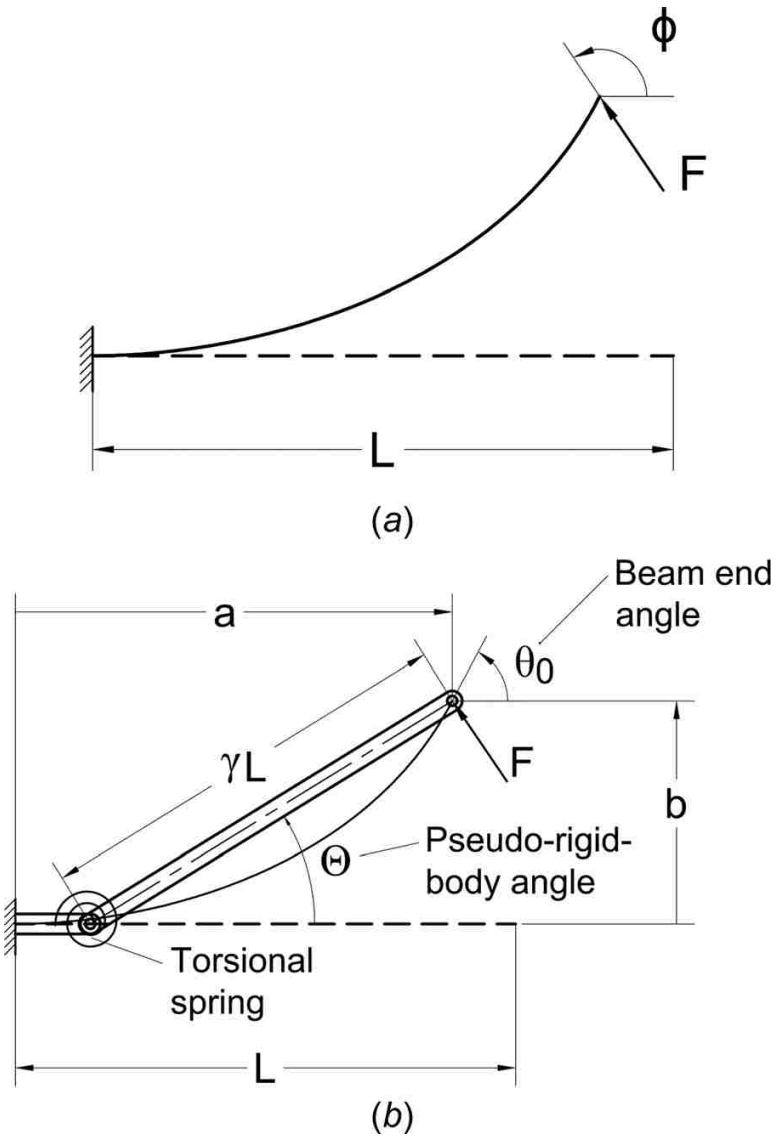

Figure 2: PRBM of fixed-free compliant segment shown in (a) initial position and (b) deformed position [15]

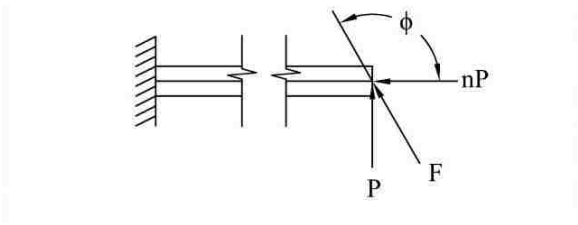

a)

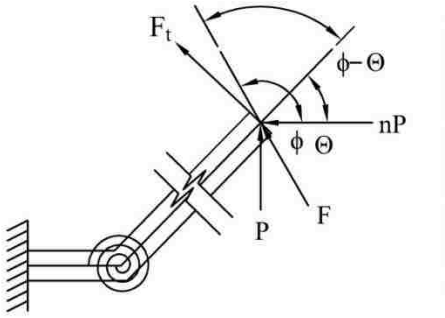

b)

Figure 3: Nomenclature of fixed-free compliant segment in the a) Free State and b) Deflected State

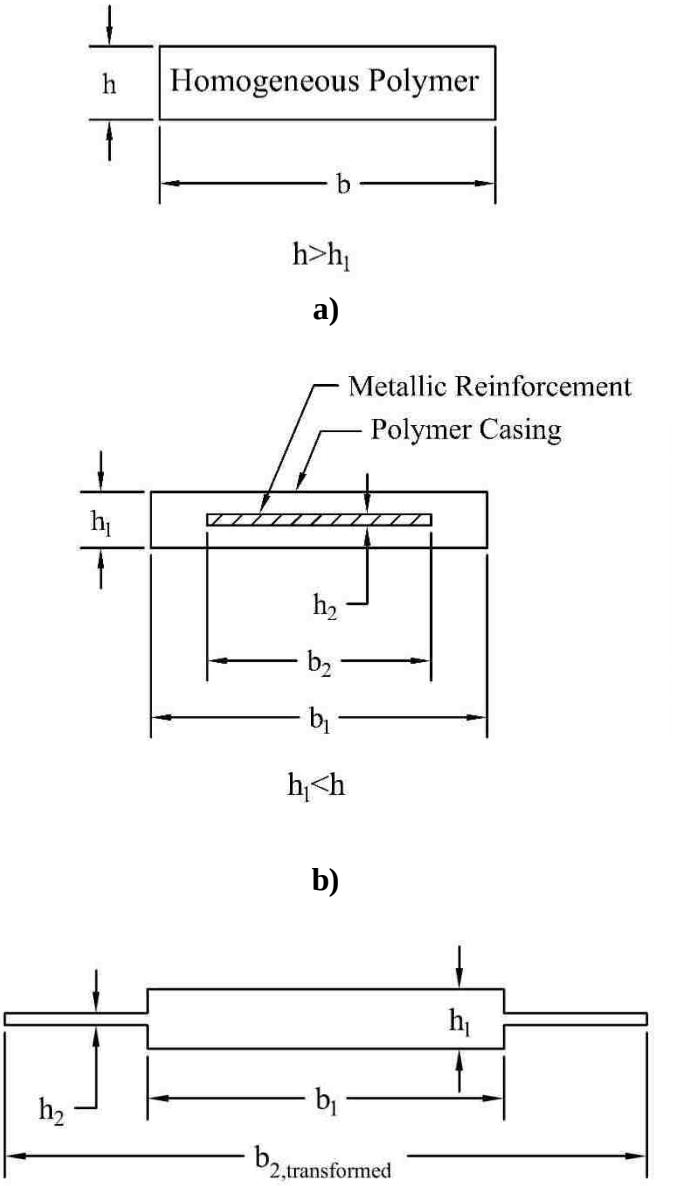

Figure 4: Cross sections of a) homogeneous compliant segment, b) metallic-reinforced compliant segment, and c) transformed cross section of metallic-reinforced compliant segment

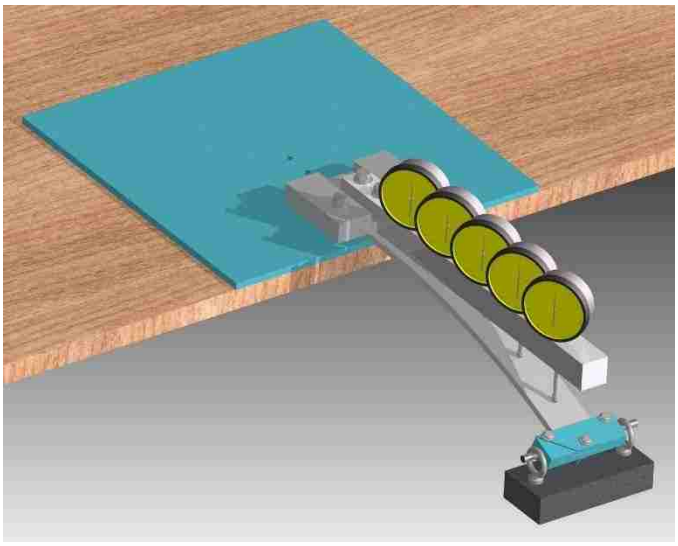

Figure 5: Deflection Test Device

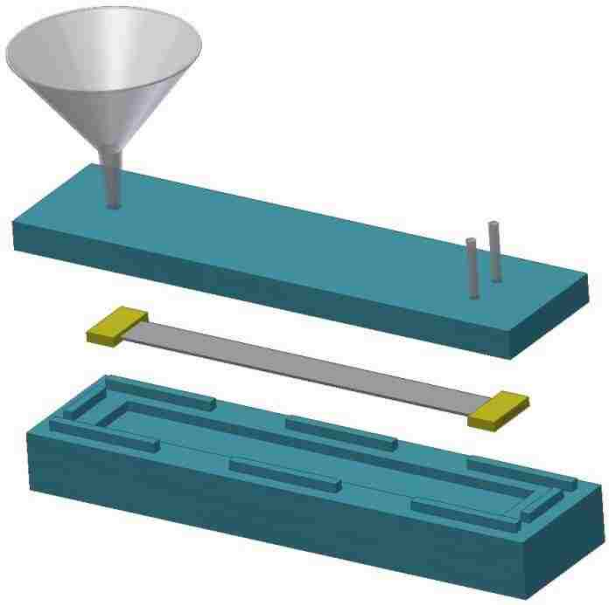

Figure 6: Assembly View of Silicone Mold used for Casting IE-3075 Urethane

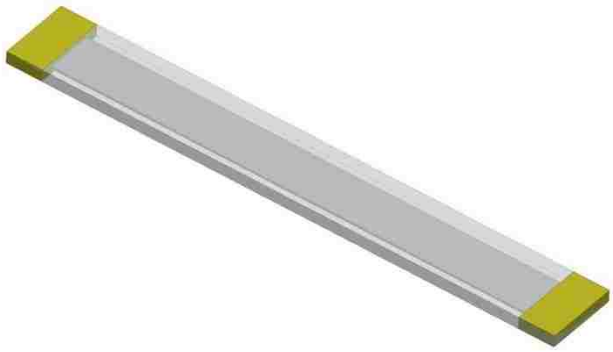

Figure 7: Cast IE-3075 Urethane Fixed-Free Compliant Segment

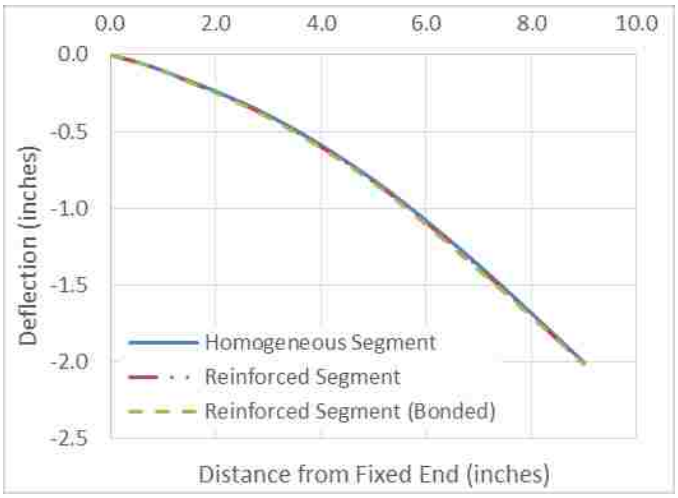

Figure 8: Measured Deflection of Homogeneous and Reinforced Segments with and without Intentional Bonding between the Casing and the Metallic Insert

Table 1: Material Properties of IE-3075 and Acetal

	IE-3075 Polyurethane	Delrin® Grade 100[2]
Flexure Strength (psi)	13,177	14,000
Flexural Modulus (psi)	433,843[3]	419,000
Izod Notched Impact Strength[4] (ft-lb/in)	0.7	2.2
Specific Gravity4	1.11	1.42

[2] All values for Delrin® obtained from literature [16]

[3] Tested in accordance with ASTM D790-15 [17]

[4] Izod and SG for IE-3075 obtained from literature [18]

Table 2: Urethane Mixing Schedule

Time (hh:mm:ss)	Task
00:00:00	2.4 oz resin and 2.15 oz hardener are combined in mixing cup
00:02:30	Mixing is complete and mixture is placed in vacuum degassing chamber
00:06:00	Mixture is removed from vacuum degassing chamber and poured into mold fill port
00:08:00	Mold filling operation complete
06:00:00	Demold to expose specimen

Table 3: Average Overall Dimensions of Homogeneous and Reinforced Test Specimens

Description	Average Thickness in. (mm)	Average Width in. (mm)
Homogeneous Specimens	0.2473 (6.28)	1.494 (37.95)
Reinforced Specimens	0.2070 (5.26)	1.503 (38.17)
Reinforced (bonded) Specimens	0.2077 (5.28)	1.505 (38.23)

Table 4: Deflection Measurements - Imperial Units

	Deflection Measurements (in.)					
Distance from Fixed End (in.)	0	1	3	5	7	9
Homogeneous	0	-0.105	-0.394	-0.816	-1.372	-2.007
Reinforced (not bonded)	0	-0.108	-0.404	-0.827	-1.386	-2.018
Reinforced (bonded)	0	-0.108	-0.409	-0.835	-1.403	-2.017

Table 5: Deflection Measurements - Metric Units

	Deflection Measurements (mm.)					
Distance from Fixed End (mm.)	0	1	3	5	7	9
Homogeneous	0	-2.66	-10.00	-20.73	-34.85	-50.97
Reinforced (not bonded)	0	-2.75	-10.27	-21.00	-35.20	-51.26
Reinforced (bonded)	0	-2.75	-10.38	-21.21	-35.64	-51.22

IV. CREEP AND STRESS RELAXATION BEHAVIOR OF HOMOGENEOUS AND REINFORCED COMPLIANT MECHANISMS AND SEGMENTS

J. Crews, L.R. Dharani[1], and A. Midha

Department of Mechanical and Aerospace Engineering, Missouri University of Science and Technology, Rolla, MO, 65409-0050

ABSTRACT: Two critical disadvantages of compliant mechanisms constructed of engineering plastics are poor creep and stress relaxation resistance. Metallic reinforcement is investigated as a method to improve the creep and stress relaxation behaviors of compliant mechanisms and compliant segments. The stress relaxation and creep behaviors of homogeneous compliant segments are compared to those of metallic reinforced compliant segments. Special specimens and fixtures were designed for conducting physical tests. Test results show that metallic reinforced compliant segments significantly outperform homogeneous compliant segments with respect to both creep and stress relaxation.

Keywords: Thermoset plastics, metallic-reinforcement, compliant mechanism, compliant segment, creep, stress relaxation

[1] Corresponding Author

E-mail address: dharani@mst.edu

1. INTRODUCTION

A mechanism is a set of interconnected, moving parts that work together to achieve a desired function [1]. An example of a simple rigid-body 4-bar mechanism is shown in Figure 1. The example shown in Figure 1 is the rear suspension from an automobile. The suspension contains a 4-bar mechanism, a shock absorber, and a spring. The shock absorber dampens the motion of the axle as it moves up and down. The spring offers resistance to motion to ensure that the axle translates the desired distance based on anticipated terrain. The 4-bar mechanism ensures that the axle follows the desired path as the automobile encounters terrain or anomalies along the roadway.

A compliant mechanism is a type of mechanism that achieves its functionality by transferring motion, force or energy through the deformation of its interconnected links or segments [2], [3]. An example of a compliant mechanism is shown in Figure 2. Figure 2 depicts another possible design for the rear suspension of an automobile. This conceptual design includes a compliant 4-bar mechanism. The 4-bar mechanism consists of three interconnected links connected to mounting points that make up the fourth link, known as the ground link. Compliance, or deformation in the mechanism, offers resistance to motion as the axle moves up and down, thus replacing the spring shown in Figure 1. Selection of an appropriate polymeric material may provide acceptable damping such that the shock absorber can be eliminated. The redesign of the mechanism shown in Figure 1 to include compliance as shown in Figure 2 allows for the reduction in moving parts, reduction in weight, and reduction in maintenance.

Plastic compliant mechanisms offer several advantages over their rigid-body counterparts such as reduced assembly time, light weight, ability to store energy, and

reduced wear due to elimination or reduction in number of kinematic pairs [3], [4], [5], [6].

Plastic compliant mechanisms also have disadvantages. Two critical disadvantages of compliant mechanisms constructed of engineering plastics are poor creep resistance and poor stress relaxation resistance [3], [4], [5], [6]. Therefore, the advantageous energy storage enabled by deformation of a compliant link or segment must be balanced with material considerations including stress relaxation and creep behavior.

Designers of compliant mechanisms are faced with performing two distinct tasks: kinetic synthesis to ensure that the functionality requirements are met, followed by load analysis and subsequent material selection to provide robustness [7]. In many cases performing the two design tasks requires multiple iterations with a need for compromise. This paper addresses the material selection task by providing creep and stress relaxation test data that compares homogeneous compliant segments to metallic reinforced compliant segments.

2. CREEP AND STRESS RELAXATION

2.1 CREEP

Creep is an increase in strain that occurs in some materials under constant application of a stress boundary condition. The severity of creep deformation is directly related to the applied stress, temperature, and time. Creep behavior can be shown by plotting strain versus time for one stress level, which is held constant throughout the test.

A mechanical analog to creep deformation in a viscoelastic solid contains a spring and dashpot connected in parallel which is known as the Voigt-Kelvin element [8]. The dashpot offers an initial resistance to deflection of the creep test specimen which results in a time-dependent strain response [8]. The initial response of the Voigt-Kelvin element is dependent on both the Newtonian viscosity of the dashpot and the shear modulus of the Hookean spring [8]. The amplitude of the Newtonian viscosity of the dashpot within the Voigt-Kelvin element is higher for a material exhibiting a highly viscoelastic response than for a material with a nearly-elastic viscoelastic response. Upon initial application of load to a Voigt-Kelvin element, the extension of the spring is restricted by the extension of the dashpot. The spring and dashpot extend over time, providing a simplistic representation of creep deformation [8].

2.2 STRESS RELAXATION

Stress relaxation is a decrease in stress that occurs in some materials under constant application of a strain boundary condition. The severity of stress relaxation is directly related to the applied strain, temperature, and time.

Compliant segments that are restrained in the deflected state or subjected to applied forces for an extended period of time are subject to stress relaxation or creep mechanisms, respectively [4]. One example of a compliant mechanism that is at risk of failing from stress relaxation is a compliant cantilever beam used to hold the brushes of an electric motor in contact with the armature [4]. The indication of failure in this case would be loss of functionality of the motor, and not necessarily breakage of the compliant beam.

Stress relaxation applied to compliant mechanisms is the reduction in stress that occurs when a plastic compliant mechanism is restrained in a deformed condition. The degree of stress relaxation in a material or structure is directly related to the applied strain amplitude, temperature, and time.

Stress relaxation is more prevalent than creep in compliant mechanisms because compliant mechanisms are generally designed with their functionality relying on motion via deflection of their links. This is unlike other engineering applications such as turbine blades that experience creep due to the application of relatively constant force over a long period of time and temperature.

A mechanical analog to stress relaxation in a viscoelastic solid contains a spring and dashpot connected in series known as the Maxwell element [8]. The dashpot offers an initial resistance to strain within the stress relaxation test specimen which results in a time-dependent stress response [8]. Similar to the Voigt-Kelvin Element for creep, the initial response of the Maxwell Element is dependent on the Newtonian viscosity of the dashpot and on the shear modulus of the Hookean spring [8]. The amplitude of the Newtonian viscosity of the dashpot within the Maxwell Element is higher for a material

exhibiting a highly viscoelastic response than for a material with a nearly-elastic viscoelastic response. Upon initial application of load to a Maxwell Element, the extension of the spring represents the initial deflection. The retraction of the spring and the extension of the dashpot with time provide a simplistic representation of stress relaxation for a constant strain [8]. Therefore the stress-strain relationship, or the stress-relaxation modulus, decreases with time as evidenced by a reduction of stress while maintaining a constant strain.

3. MATERIAL SELECTION FOR COMPLIANT MECHANISMS

Designers of compliant mechanisms are typically faced with selecting materials from two distinct categories, metals and engineering plastics, each with advantages and disadvantages [7].

Metals have more desirable creep resistance stress relaxation behavior at ambient temperature when compared to engineering plastics and are suitable for use as metallic reinforcement within a plastic compliant mechanism [6], [7].

Engineering plastics are attractive to designers due to their high strength-to-modulus ratio relative to metals. For example, the strength-to-modulus ratio of Polypropylene is approximately 25 whereas the ratio for 1010 hot rolled steel is approximately 0.87 [4]. A high strength-to-modulus ratio is desirable as it indicates that a material can be subjected to relatively high strain amplitude without exceeding the stress limits of the material. Plastics are also lightweight and relatively easy to manufacture.

Engineering plastics also have disadvantages including a susceptibility to stress relaxation and creep deformation at ambient temperature. Unlike steel, which is used as the reinforcing element in this research effort, plastics exhibit viscoelastic behavior. A viscoelastic response is a strain-dependent stress-strain relationship. The response contains an elastic component and a viscous component which are modeled as a spring and dashpot, respectively. The viscoelastic or time dependent strain response introduces additional complexity during the design phase of polymeric compliant mechanisms due to the nonlinearity in the material behavior with respect to time. The constitutive equations for linear viscoelastic materials can be expressed in terms of stress or strain to

address creep and stress relaxation, respectively. The constitutive equation related to creep of a linear viscoelastic material is given by the following [9]:

$$\varepsilon(t) = \int_{-\infty}^{t} D(t-\tau)\dot{\sigma}(\tau)d\tau, \quad (1)$$

where *D(t)* is the creep compliance, ε is strain, σ is stress and τ is a time constant. The constitutive equation related to stress relaxation of a linear viscoelastic material is given by the following [9]:

$$\sigma(t) = \int_{-\infty}^{t} E(t-\tau)\dot{\varepsilon}(\tau)d\tau, \quad (2)$$

where *E(t)* is the stress relaxation modulus.

As plastics generally do not perform as predictably as metals in the areas of creep or stress relaxation [8], this paper aims to leverage the advantages of both plastic and metal by testing segments that contains both metal and plastic. Kuber [6] introduced the concept of placing a strong reinforcing material within a compliant casing constructed of a relatively weak casing material in an effort to prevent creep and fatigue failures.

In the interest of directly comparing the performance of homogeneous and reinforced compliant segments, each segment was designed of offer a similar force deflection behavior. The methodology used throughout this effort was to maintain the force deflection behavior of the homogeneous segment by matching the bending stiffness (EI) of the reinforced segment to that of the homogeneous segment [7]. The bending

stiffness of the reinforced segment was matched to the bending stiffness of the homogeneous segment by reducing the cross-sectional thickness in the reinforced segment. The reduction in segment thickness also reduces the distance from the neutral axis to the extreme fiber resulting in a reduction in the bending stress in the plastic. Cross sections of homogeneous and reinforced compliant segments are shown in Figure 3 and Figure 4, respectively.

4. EXPERIMENTAL COMPARISON BETWEEN CREEP BEHAVIOR OF HOMOGENEOUS AND REINFORCED COMPLIANT SEGMENTS

Creep testing of both homogeneous and reinforced compliant segments was performed in accordance with ASTM D2990-09: Standard Test Methods for Tensile, Compressive, and Flexural Creep and Creep Rupture of Plastics [10]. More specifically, testing was performed in accordance with Section 6.3 Flexural Creep found within ASTM D2990-09.

The testing device consists of a test rack capable of testing multiple specimens simultaneously, one stirrup per test specimen, one weight per test specimen and one dial indicator to measure vertical displacement of the stirrup upon loading. The complete testing system is shown in Figure 5. The placement of the test specimen, stirrup, and dial indicator is shown in Figure 6.

Test setup includes measuring the cross-sectional dimensions of each test specimen, externally supporting the load to allow for specimen placement on the test rack, installation and alignment of the stirrup and lowering of the load to initiate contact with the specimen, and alignment of the dial indicator. The test specimen is simply-supported by the test rack.

Testing commences by removing the external load support, thus allowing the full load to be applied at the mid span of the specimen. The vertical displacement of the stirrup is recorded in accordance with Section 11.5 of ASTM D2990-09 [10]. Additional data was collected between the time intervals recommended by D2990 to monitor for sudden shifts in displacement caused by jostling of the test frame or dial indicator failure. Test loads ranging from 16.2 lbf (71.9 N) and 46.9 lbf (208.6 N) were applied to test specimen for 1000 hours. The intent of the creep testing was to apply the same loads to

both homogeneous and reinforced specimens and then compare the resulting increase in strain with respect to time. Load levels were selected based on both availability of test weights and a target stress range of 10% to 25% of the flexural strength. The actual stress range provided by the available test weights was 8.6% to 24.3% of the flexural strength.

5. EXPERIMENTAL COMPARISON BETWEEN STRESS RELAXATION BEHAVIOR OF HOMOGENEOUS AND REINFORCED COMPLIANT SEGMENTS

Stress relaxation testing was performed on five homogenous and five metallic reinforced compliant segments. Testing was performed in accordance with Test Method C-1 of ASTM E328-13: Standard Test Methods for Stress Relaxation for Materials and Structures [11]. It should be noted that the method for analysis of stress relaxation of plastics was withdrawn from ASTM D2991 and ASTM E328 in the 1990's due to the difficulty in application of standard techniques to plastics [12]. However, the aforementioned test method was used in this effort as it is a reputable standard for other materials, and the subject effort is a comparative study between homogeneous and reinforced compliant segments and not a design document or acceptance test.

The mandrel shown in Figure 7 was used for flexural stress relaxation testing. The mandrel radius is approximately 8.5 inches. The entire length of each specimen was in contact with the mandrel, meeting the standard test method requirement of contact length at least 20 times the specimen thickness. The percent remaining stress of the ratio of remaining stress to initial stress is equal to the ratio of the elastic strain on removal of the test stress to the initial strain [11]. The percent remaining stress is equal to 100% at the initiation of the test, as the stresses have yet to relax. However, as the stress within the strained sample relax, the percent remaining stress decreases.

Testing commences by conforming the specimen to the mandrel using a threaded clamping system.

6. TEST SPECIMENS

Test specimens were designed and fabricated to enable experimental creep and stress relaxation testing of compliant segments, both homogeneous and reinforced. A total of thirty specimens were produced and tested. Test specimens include: ten homogeneous creep specimens, ten reinforced creep specimens, five homogeneous stress relaxation specimens, and five reinforced stress relaxation specimens.

6.1 SELECTION OF MATERIAL FOR EXPERIMENTAL TESTING

A castable urethane, IE-3075, was selected as the material of construction for this research effort. IE-3075 is a commonly used plastic for prototyping and its modulus and flexural strength are similar to other engineering plastics [8]. These qualities make it a relevant material for consideration in the field of compliant mechanisms. Additionally, it can be cast at room temperature and without the need for high temperature injection molding equipment. IE-3075 is a rigid thermoset with material properties comparable to those of acetal, a commonly used material in compliant mechanism construction [6].

6.2 TEST SPECIMEN DESIGN

The dimensions of the homogeneous test specimens were selected based on available materials as well as requirements of applicable test standards [10], [11].
ASTM E328-13 does not give specific specimen dimensions. Specimens measuring 5.5 inches long by 1.5 inches wide by approximately 0.250 inches thick (homogeneous) and approximately 0.211 inches thick (reinforced) were tested.

The force-deflection behavior of the homogeneous and reinforced segments was designed to be equal to provide a comparison of two possible designs that could be

introduced into a compliant mechanism without altering the overall functionality [7]. The thickness of the polymer casing that would, with metallic reinforcement, maintain the same bending stiffness as the homogeneous specimens is calculated next [7].

The left and right hand sides of Equation 1 contain the bending stiffness of the homogeneous segment and the reinforced segment, respectively:

$$E_1 I = E_1 I_1 + E_2 I_2. \tag{3}$$

The moment of inertia of the polymer casing must be reduced after the introduction of the reinforcing element to ensure that the bending stiffness is unaffected. The moment of inertia is calculated as follows:

$$I_1 = I - \frac{E_2}{E_1} I_2. \tag{4}$$

The cross-sectional thickness of the polymer casing is optimized to provide the smallest distance from the neutral axis to the extreme fiber:

$$I_1 = \frac{w h^3}{12} - \frac{E_2}{E_1}\left(\frac{w_2 h_2^3}{12}\right). \tag{5}$$

The left hand side of Equation 3 is expanded to include the width and height dimensions of the optimized cross section:

$$I_1 = \frac{wh_1^3}{12} - \frac{w_2 h_2^3}{12}. \quad (6)$$

The use of Equations 3 and 4 provides the cross-sectional thickness required for a reinforced segment to result in a consistent bending stiffness when compared to the homogeneous segment:

$$\frac{wh_1^3}{12} - \frac{w_2 h_2^3}{12} = \frac{wh^3}{12} - \frac{E_2}{E_1}\left(\frac{w_2 h_2^3}{12}\right), \quad (7)$$

$$h_1 = \sqrt[3]{h^3 + \frac{w_2 h_2^3}{w}\left(1 - \frac{E_2}{E_1}\right)}. \quad (8)$$

The use of Equation 6 with the dimensions described above provides the design thickness of the reinforced segment:

$$h_1 = \sqrt[3]{(0.244\text{ in.})^3 + \frac{(1.003\text{ in.})(0.050\text{ in.})^3}{1.500\text{ in.}}\left(1 - \frac{30{,}000\text{ ksi}}{433.843\text{ ksi}}\right)}. \quad (9)$$

The theoretical casing thickness that will provide an equivalent bending stiffness between the homogeneous and reinforced test specimens is 0.207 in. (5.26 mm).

6.3 TEST SPECIMEN FABRICATION

IE-3075, a room-temperature casting urethane, was selected as the material of construction for test specimens. IE-3075 is cast in a platinum-cured silicone mold. The mold making process for compliant segments, both homogeneous and reinforced was introduced by Crews [7] and is summarized below.

A silicone mold is constructed by affixing an exemplar, or pattern with the desired physical dimensions to the bottom of an open-top mold box. The mold box is subsequently filled with a two part silicone system. Once the silicone is cured, the mold box is inverted and the bottom is carefully removed to expose the pattern. Fill and vent tubes are affixed to the pattern. The exposed silicone is treated with a mold release to prevent the second half of the mold from adhering to the first. A second batch of silicone is poured into mold box to form the second half of the silicone mold. Once the second half is cured, the mold boxes are split, the vents and fill tubes are removed, the pattern is removed, and the silicone mold is complete.

The casting process initiates by applying a mold release to the interior surfaces of the mold halves. The mold is closed and the urethane casting resin is prepared. Vent tubes and the fill funnel are placed into the mold. The mixed urethane is poured into the fill tube until it emerges in the vent tubes. Upon curing, the mold is split and the test specimen is removed from the mold. Figure 8 shows an assembly view of a mold setup for casting a metallic reinforced specimen [7].

A reinforced compliant segment can be constructed using the same bottom mold half as the original, unreinforced compliant segment [7]. A new top mold half is required in order to achieve the desired overall section thickness of 0.210 inches (5.334 mm). A

metallic reinforcing element is held by two plastic insert holders which are then placed into the mold as an assembly. The casting process then proceeds as described above. The plastic insert holders may be removed by abrasive cross sectioning, if desired. A completed, reinforced compliant segment created using the example mold is shown in Figure 9.

Properties and dimensions of homogeneous and metallic reinforced specimens for creep and stress relaxation testing are included in Table 1. Properties and dimensions of metallic reinforcing elements used in both stress relaxation and creep specimens are included in Table 2.

7. RESULTS AND DISCUSSION

Results from both creep and stress relaxation testing are presented and discussed in this section. Test results are presented for both homogeneous and metallic-reinforced, composite segments. The relative difference in creep and stress relaxation behavior of homogeneous and metallic-reinforced specimens is discussed.

7.1 CREEP TEST RESULTS

Creep curves are generally shown as plots of strain versus time for a given stress. However, in this case, the cross-sectional dimensions of the test specimens have been designed to provide a similar force-deflection response. This cross section design effort results in two test specimens, one homogeneous and one reinforced, with similar force deflection response but different stress levels and therefore different creep behavior. Plotting the strain versus time for a given load allows for direct comparison between the homogeneous and reinforced specimens as designed for similar deflection.

Figure 10 and Figure 11 show that the initial deflections are similar between the homogeneous and reinforced compliant segments. Table 3 shows that the magnitude of the deviation in initial deflections between the homogeneous and reinforced segments is between 1% and 2.9%. Figure 12 and Figure 13 show that the homogeneous specimens exhibited significantly higher strains than the reinforced specimens after 1,000 hours of exposure to the same loads.

While the amplitude of strain is significantly different, the positive slope of the strain rate for both the homogeneous and reinforced segments are similar at the conclusion of the 1,000 hour test. This positive slope indicates that the dashpot in the

Voigt-Kelvin Element is still extending, but at a rate that is significantly reduced from the beginning of the test.

7.2 STRESS RELAXATION TEST RESULTS

Stress relaxation behavior is generally presented in the form of the stress relaxation modulus versus test duration and by the ratio of remaining stress to initial stress. The stress relaxation modulus is calculated using the theoretical strain in the specimen while clamped to the mandrel, the strain retained in the specimen upon removal from the mandrel, and the flexural modulus of elasticity. The theoretical initial strain, ε_i, in the specimen while clamped to the mandrel is calculated by using [11]:

$$\varepsilon_i = \frac{h}{2R_i + h}, \tag{10}$$

where R_i is the radius of the mandrel.

The retained strain, ε_r, in the specimen upon removal from the mandrel is calculated using [11]:

$$\varepsilon_r = \frac{h}{2R_o - h} \tag{11}$$

where R_o is the radius of the outside of the specimen.

The ratio of remaining stress to initial stress is equal to the ratio of the elastic strain on removal of the test stress to the initial strain [11]. Figure 14 shows the percentage of stress remaining in the test specimen, given by

$$\%\sigma_r = \frac{\varepsilon_r}{\varepsilon_i} \text{ x } 100. \quad (12)$$

The homogeneous specimens had relaxed to near-zero stress approximately 800 hours after they were restrained to the mandrel. The reinforced specimens retained approximately 50% of the initial stress after 1,000 hours of testing.

Figure 15 shows the stress relaxation modulus, E_r, taken as an average of five specimens, for both homogeneous and reinforced test specimens. The stress relaxation modulus signifies the stress-strain relationship of a material when subjected to a displacement boundary condition over time. The stress relaxation modulus is calculated as follows:

$$E_r = \frac{\sigma(t)}{\varepsilon_i} \text{ x } 100. \quad (13)$$

The strain is constant, in the case of negligible viscous flow, and the stresses relax, resulting in a decrease in the modulus over time. The plots show that the homogeneous specimen had relaxed to a significantly lower amount than the reinforced specimen. The homogeneous specimens had essentially conformed to the mandrel

approximately 800 hours after they were restrained to the mandrel, as shown in Figure 16.

The metallic reinforced outperformed the homogeneous stress relaxation specimens during the ambient temperature, 1000 hour duration test. Near-total relaxation of stress in the homogeneous specimens signifies that the specimens exhibited approximately the same radius as the mandrel upon removal. Near-total stress relaxation as observed in the homogeneous specimens would constitute failure in a compliant mechanism held in a restrained state as the energy originally stored in the deflected segments would be unusable or non-transferable to kinetic energy upon removal of the restraint.

8. CONCLUSIONS

Creep and stress relaxation, as they relate to compliant mechanisms, were studied. It was highlighted that stress relaxation is more likely to occur than creep deformation because compliant mechanisms are generally designed with their functionality relying on motion via deflection of their links.

Results were presented from creep tests performed in accordance with ASTM D2990-09. Creep test results show that metallic-reinforced compliant segments exhibit improved creep resistance over homogeneous compliant segments of similar function. The initial deflections between the homogeneous and reinforced segments matched within 3%. Strains at the end of the 1000 hour creep test of homogeneous samples were approximately 1% and 4% for the lightest and heaviest loads, respectively. Corresponding strains at the end of the 1000 hour creep test of reinforced samples were approximately 0.5% and 1.6%.

Similar improvements in stress relaxation performance were realized by the introduction of metallic reinforcement. The homogeneous specimens had relaxed to near-zero stress approximately 800 hours after they were restrained to the mandrel. The reinforced specimens retained approximately 50% of the initial stress after 1,000 hours. A plot of specimen radius versus time shows that the homogeneous specimen had relaxed to a significantly lower amount than the reinforced specimen. The homogeneous specimens had essentially conformed to the mandrel approximately 800 hours after they were restrained to the mandrel.

9. REFERENCES

[1] Shigley, J.E., Uicker, J.J. Jr., *Theory of Machines and Mechanisms*, 5th printing, McGraw Hill Book Company, Singapore, 1988.

[2] Howell L. L. and Midha A., "A Method for the Design of Compliant Mechanisms with Small-Length Flexural Pivots," Journal of Mechanical Design, Trans. ASME, Vol. 116, No. 1. - 1994. - pp. 280-290.

[3] Midha, A., T. W. Norton and L. L. Howell, "On the Nomenclature, Classification, and Abstractions of Compliant Mechanisms," *Journal of Mechanical Design*, Trans. ASME, Vol. 116, No. 1, March 1994, pp. 270-279.

[4] Howell, L. L., *Compliant Mechanisms*, John Wiley & Sons, Inc., New York, New York, 2001.

[5] Bapat, S. G., "On the design and analysis of compliant mechanisms using the pseudo-rigid-body model concept," Doctoral Dissertation. Paper 2376. Missouri University of Science and Technology, 2015.

[6] Kuber, R. S., "Development of a methodology for pseudo-rigid-body models of compliant segments with inserts, and experimental validation," Masters Theses. Paper 5363. Missouri University of Science and Technology, 2013.

[7] Crews, J. A., "Methodology for Analysis of Stress, Creep and Fatigue Behavior of Compliant Mechanisms," Doctoral Dissertation. Missouri University of Science and Technology, 2016.

[8] Rosen, S.L., *Fundamental Principals of Polymeric Materials*, 2nd Edition, John Wiley & Sons, Inc., New York, New York, 1993.

[9] Sorvari, J. and Malinen, M., "Determination of the relaxation modulus of a linearly viscoelastic material," Mechanics of Time-Dependent Materials, 10:125-133, 2006.

[10] ASTM Standard D2990, 2009, "Standard Test Methods for Tensile, Compressive, and Flexural Creep and Creep-Rupture of Plastics," ASTM International, West Conshohocken, PA, 2009, DOI: 10.1520/D2990-09, www.astm.org.

[11] ASTM Standard E328, 2013, "Standard Test Methods for Stress Relaxation for Materials and Structures," ASTM International, West Conshohocken, PA, 2013, DOI: 10.1520/E0328-13, www.astm.org.

[12] Osswald, T. A., *Understanding Polymer Processing*. Hanser Gardner Publications, 2010.

10. FIGURES AND TABLES

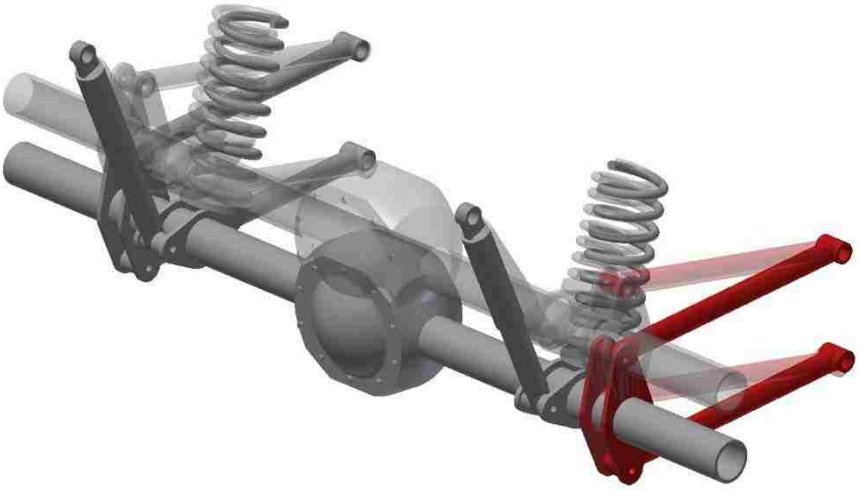

a)

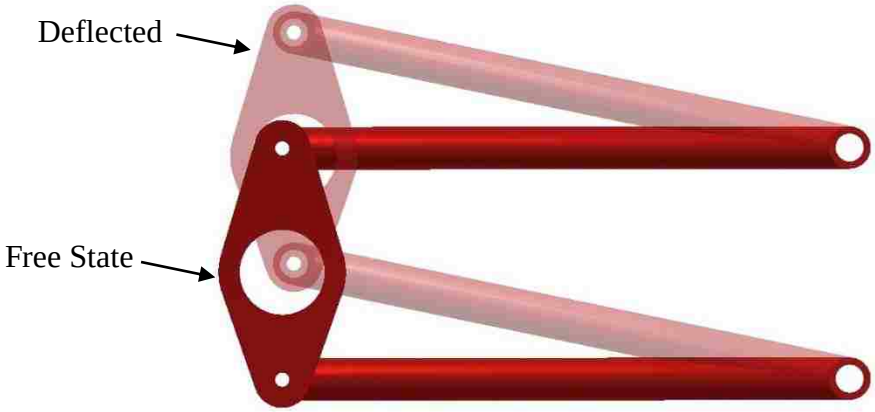

b)

Figure 1: Automotive Suspension Rigid-body Mechanism Example a) Rigid-body 4-bar Mechanism Assembly and b) Rigid-body Mechanism

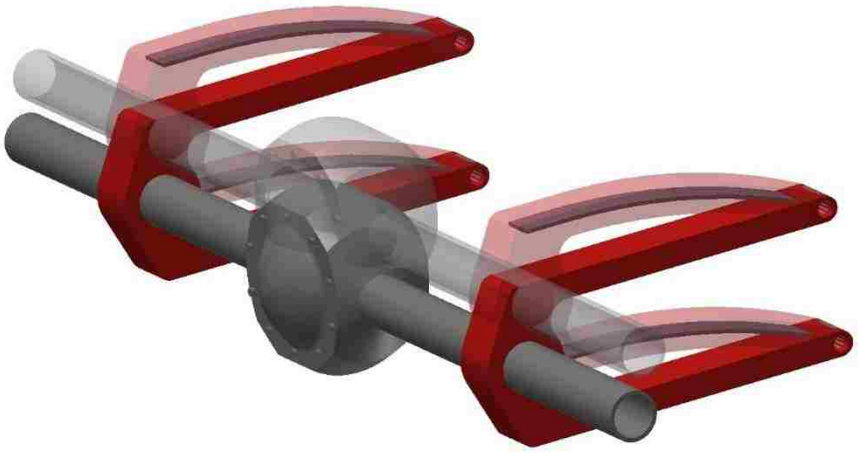

a)

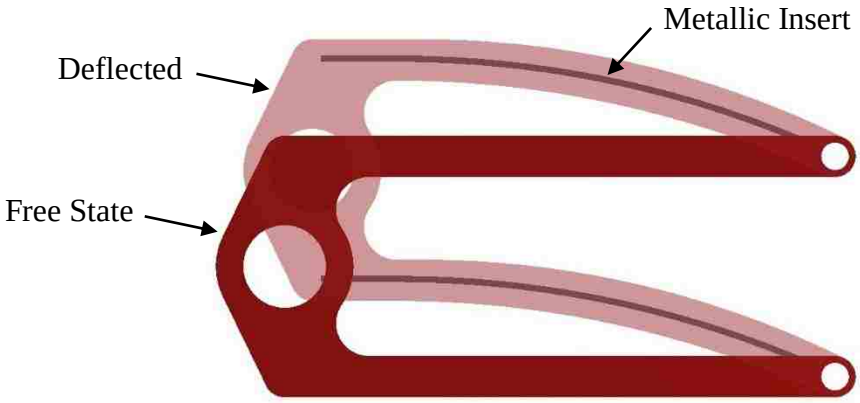

b)

Figure 2: Automotive Suspension Compliant Mechanism Example a) Compliant 4-bar Mechanism Assembly and b) Compliant Mechanism

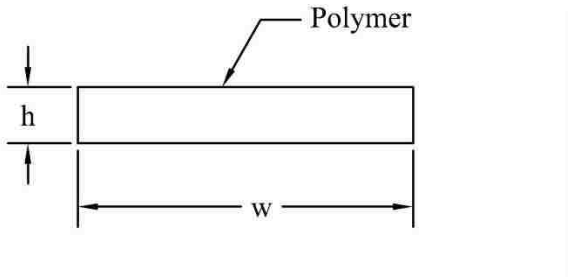

Figure 3: Cross-Section of a Homogeneous Compliant Segment [8]

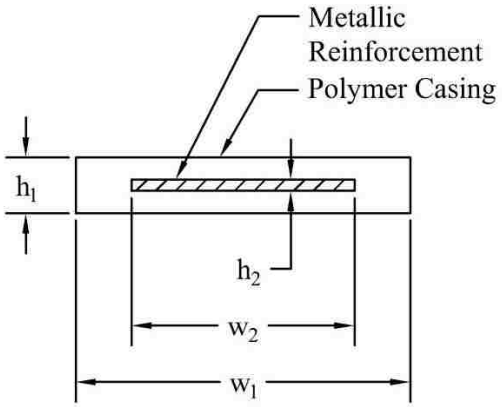

Figure 4: Cross-Section of a Reinforced Compliant Segment [8]

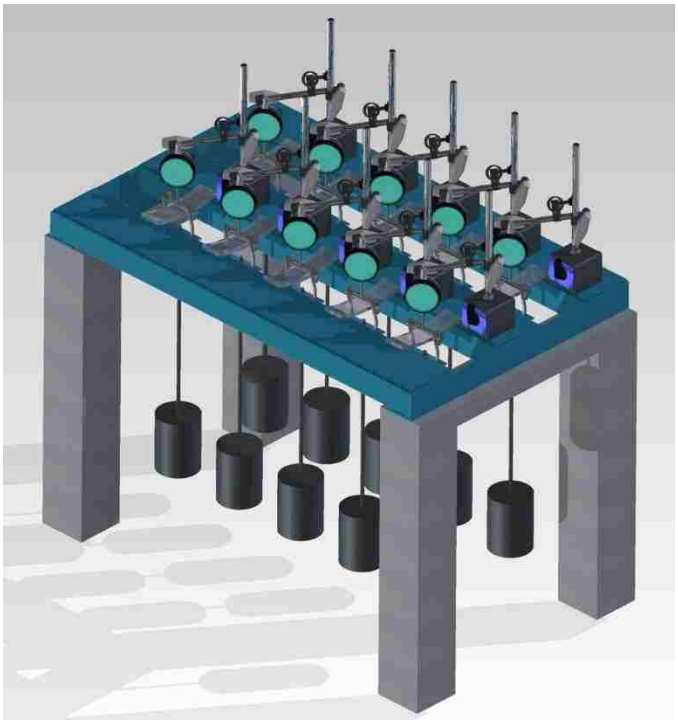

Figure 5: Three-Point-Bend Creep Testing System

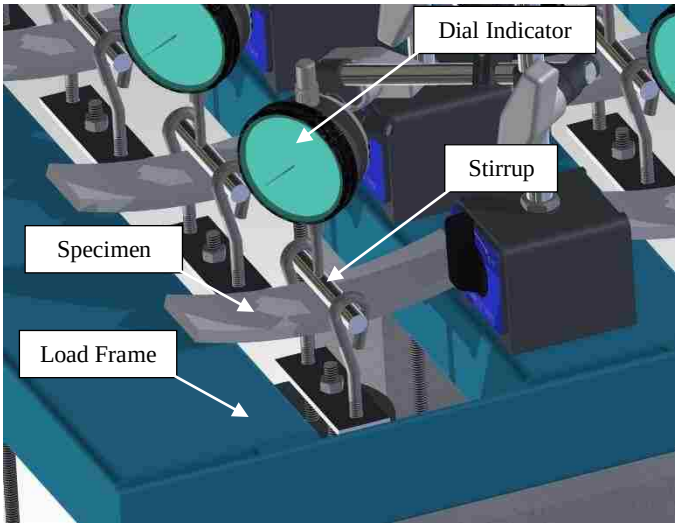

Figure 6: Close-up View of Load Frame, Stirrup and Dial Indicator

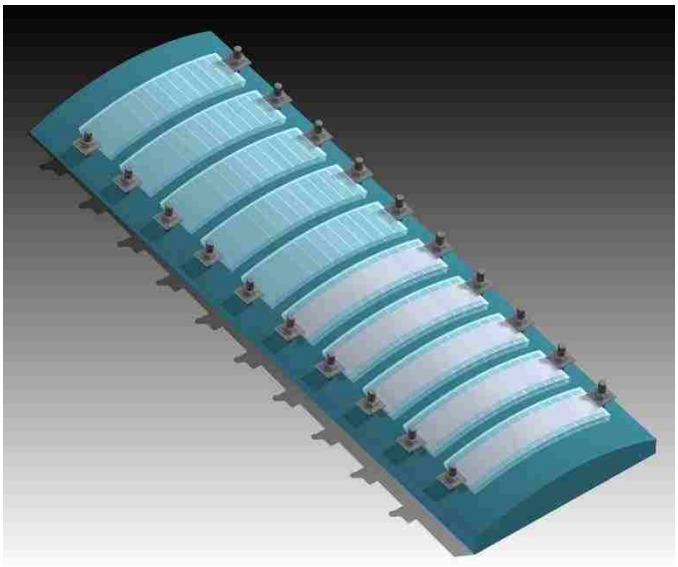

Figure 7: Stress Relaxation Mandrel

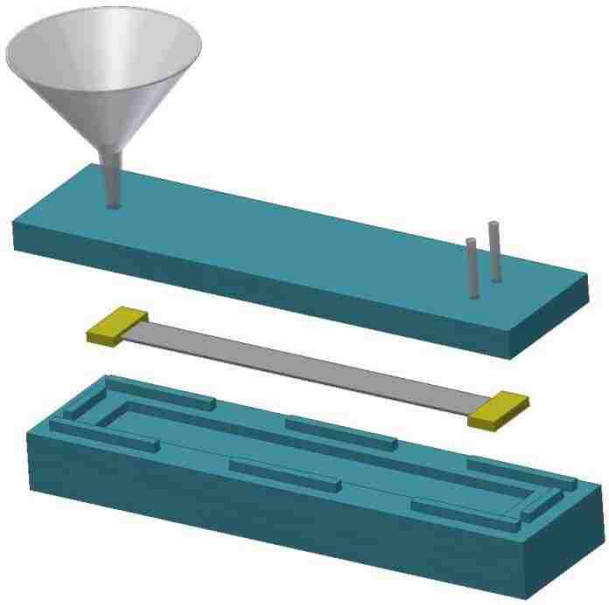

Figure 8: Assembly View of Silicone Mold used for Casting IE-3075 Urethane [8]

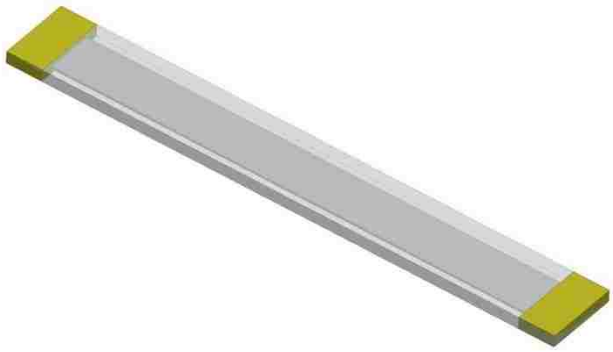

Figure 9: Cast IE-3075 Urethane Fixed-Free Compliant Segment [8]

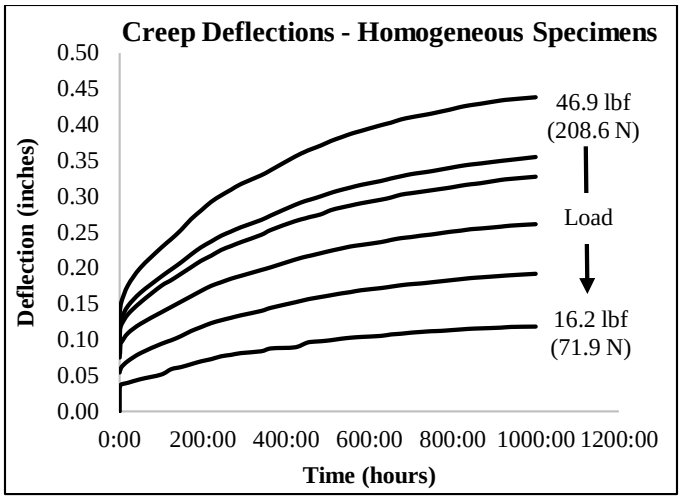

Figure 10: Deflections of Homogeneous Creep Specimens Tested at Different Load Levels

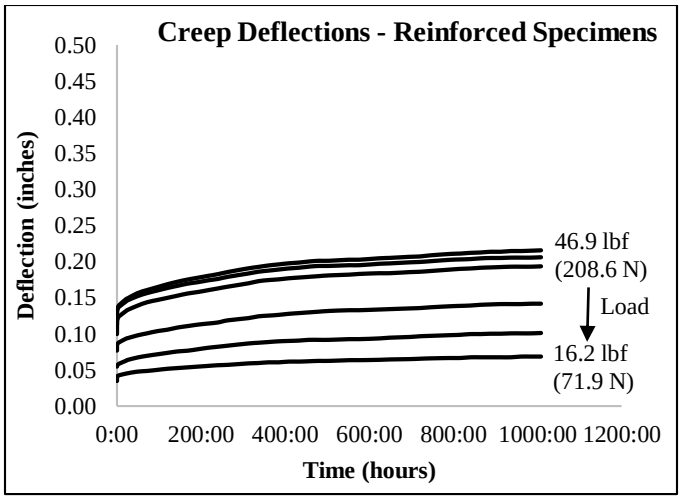

Figure 11: Deflections of Reinforced Creep Specimens Tested at Different Load Levels

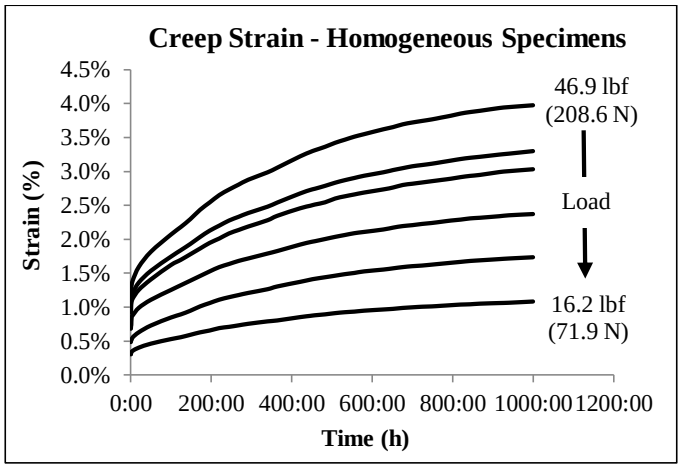

Figure 12: Strain for Homogeneous Creep Specimens Tested at Different Load Levels

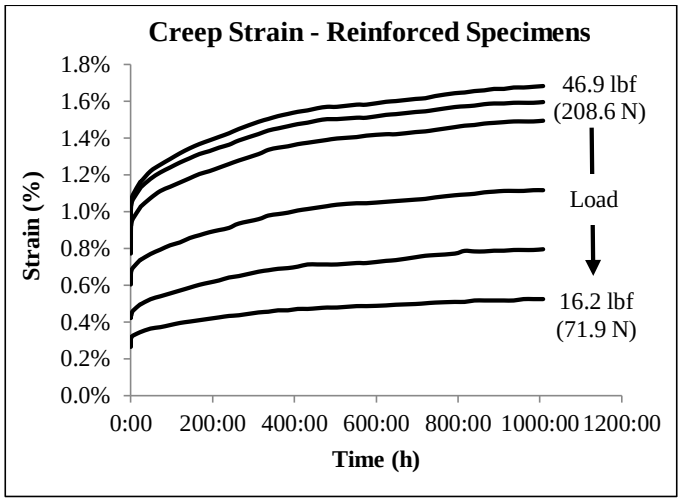

Figure 13: Creep Strain for Reinforced Specimens Tested at Different Load Levels

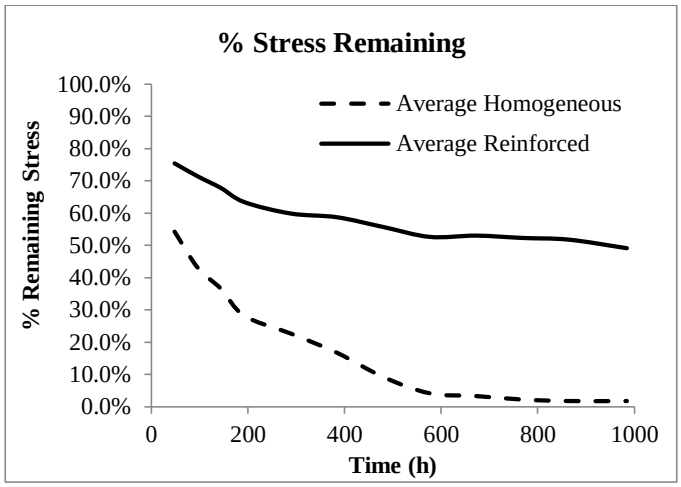

Figure 14: Percentage of Remaining Stress in Test Specimens

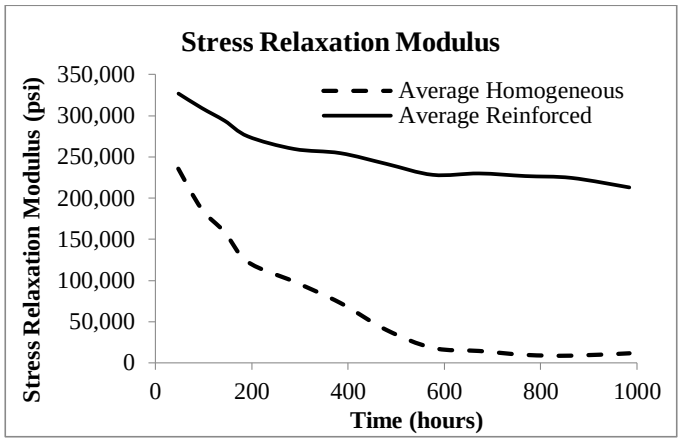

Figure 15: Stress Relaxation Modulus of Homogeneous and Reinforced Stress Relaxation Specimens

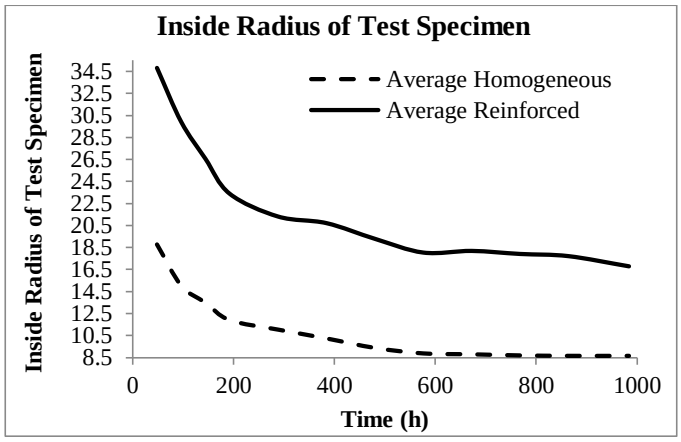

Figure 16: Inside Radius of Test Specimens after Removal from Mandrel

Table 1: Properties & Outside Dimensions of Homogeneous Stress Relaxation Test Specimens

	Stress Relaxation Specimens		Creep Specimens	
	Homogeneous	Reinforced (casing)	Homogeneous	Reinforced (casing)
Material	Polyurethane Thermoset			
L, in. (mm)	5.5 (139.7)	5.5 (139.7)	5.5 (139.7)	5.5 (139.7)
w, in. (mm)	1.497 (38.02)	(w_1) 1.500 (38.10)	1.500 (38.10)	(w_1) 1.502 (38.16)
h, in. (mm)	0.244 (6.20)	(h_1) 0.211 (5.37)	0.244 (6.20)	(h_1) 0.208 (5.28)
E_1, ksi (MPa)	433.843 (2985.43)	433.843 (2985.43)	433.843 (2985.43)	433.843 (2985.43)

Table 2: Properties & Dimensions of Metallic Reinforcing Elements

Metallic Reinforcement Properties and Dimensions	
Material	1095 Spring Temper Steel
L, in. (mm)	5.5 (139.7)
w_2, in. (mm)	1.003 (25.48)
h_2, in. (mm)	0.050 (1.27)
E_2, ksi (MPa)	30,000 (206.8)

Table 3: Initial Deflections of Homogeneous and Reinforced Creep Test Specimens

Load lbf (N)	Initial Deflection in (mm)		% Difference
	Homogeneous	Reinforced	
16.2 (72.1)	0.034 (0.86)	0.035 (0.89)	2.9%
25.6 (113.9)	0.054 (1.37)	0.055 (1.40)	1.8%
33.8 (150.3)	0.075 (1.91)	0.077 (1.96)	2.6%
41.7 (185.5)	0.099 (2.51)	0.100 (2.54)	1.0%
44.7 (198.8)	0.110 (2.79)	0.113 (2.87)	2.7%
46.9 (208.6)	0.132 (3.35)	0.130 (3.29)	-1.9%

V. FATIGUE AND FAILURE BEHAVIOR OF HOMOGENEOUS AND REINFORCED COMPLIANT MECHANISM SEGMENTS

J. Crews, L.R. Dharani[1], and A. Midha

Department of Mechanical and Aerospace Engineering, Missouri University of Science and Technology, Rolla, MO, 65409-0050

ABSTRACT: This paper presents a comprehensive study of the fatigue and failure behavior of both homogeneous and metallic-reinforced compliant segments. Baseline test results are presented for a homogeneous, fixed-free compliant segment constructed of thermoset urethane. The advantages of both polymeric and metallic materials for compliant mechanism construction are leveraged by designing and testing compliant test specimens containing a polymer casing and a metallic reinforcing element. Results obtained from fatigue testing of fixed-free compliant segments in a cyclic loading configuration show that the metallic-reinforced compliant specimens offer superior fatigue performance when compared to the homogeneous baseline specimens. Fractography, both macroscopic and microscopic, is used for a qualitative assessment of the failure behavior.

Keywords: compliant segment, compliant mechanism, thermoset, fatigue, fractography

[1] Corresponding author

E-mail address: dharani@mst.edu

1. INTRODUCTION

A mechanism is comprised of at least two components or links such that the motion of each is related [1]. Automotive suspension systems often contain mechanisms as shown in Figure 1. The each side of the rear suspension depicted in Figure 1 contains a 4-bar mechanism, dampener, and spring. The suspension components work together to ensure that the axle follows the desired path and that the vehicle behaves in a predictable and stable manner. The shock absorber dampens the motion of the axle by slowing the suspension's reaction to road conditions. The spring offers resistance to motion to ensure that the axle translates the desired distance based on anticipated terrain. The 4-bar mechanism ensures that the axle follows the desired path to provide both stability and the desired performance characteristics.

A compliant mechanism is a type of mechanism that achieves its functionality by transferring motion, force, or energy through the deformation of its interconnected links or segments [2]. Figure 2 depicts another possible design for the rear suspension of an automobile, which includes a compliant 4-bar mechanism. The compliant portion of the 4-bar mechanism consists of a single component containing two compliant links connected by a rigid link. The links are connected to mounting points on the vehicle that provide the ground link of the mechanism. The deformation of the compliant links offers resistance as the axle translates, performing the function of the spring shown in Figure 1. Damping may be provided by careful selection of a polymeric material for construction of the compliant mechanism. The redesign of the mechanism shown in Figure 1 to include compliance, as shown in Figure 2, allows for the reduction in moving parts, reduction in weight, and reduction in maintenance.

Compliant mechanisms are designed to transfer motion, force, or energy through deflection of their members [2], [3], [4]. It would be unusual for a mechanism to be designed for a single load cycle. Mechanisms are often designed to accomplish a single task or a set of similar tasks in a repeated fashion. As such, it is often understood that mechanisms are used in machine design applications or consumer products where deflection, and associated stress cycles will occur many times in a relatively predictable fashion [4]. Repeated stress cycles can result in fatigue failure.

The consistent nature of the stress cycles in compliant mechanisms lends well to fatigue analysis using the stress-life model [4]. The stress-life approach to fatigue analysis is based upon the relationship between cyclic stress and the number of cycles to failure. This approach assumes that all stress excursions are within the elastic limit. The relationship between stress and number of cycles to failure for a particular material is represented by its associated Wöhler fatigue curve. The Wöhler fatigue curve (S-N curve) plots the number of cycles to failure (N) versus stress amplitude (S).

Compliant mechanisms are often constructed using engineering plastics [4], [5]. One critical disadvantage of compliant mechanisms constructed of engineering plastics is poor fatigue resistance [4].

Fatigue is generally defined as the degradation and failure of a material caused by stresses applied in a cyclic fashion [6]. It has been estimated that at least half of all mechanical failures are due to fatigue, most of which were unexpected [6].

Fatigue of engineered products is a serious problem that ultimately impacts both the economy as well as consumer confidence. The extent to which fracture impacts the economy of the United Stated was researched and documented in 1983 [7]. The scope of

the study included metals, ceramics and glass, polymers, wood and composites. The study found the cost of fracture to be approximately $99.0 billon, in 1978 dollars [7]. While the cost of fracture includes all fracture mechanisms, including overload, fatigue and others, the findings indicate that money could be saved by using proper design and materials.

This paper presents an experimental evaluation of high-cycle fatigue performance of both homogeneous and metallic-reinforced compliant segments. Applications of compliant mechanisms often require both repetitive motion and a constant force-deflection behavior. Fatigue fractures may limit the use of compliant mechanisms in applications requiring a constant force-deflection behavior because the stiffness of the compliant segments decreases as the fatigue fracture grows. The reduction in stiffness caused by a fatigue fracture often degrades the performance of the compliant mechanism such that it is unusable even if the mechanism links are still physically connected.

2. MATERIAL AND METHODS

Fatigue testing of both homogeneous and reinforced compliant segments was performed using a custom designed fatigue tester to apply a 2.01 inch (51.05 mm) vertical deflection at the tip of a fixed-free, or cantilever compliant segment.

The bending stiffness was monitored to provide an indication of fracture propagation or material degradation. The reduction in bending stiffness that occurs in deflection-controlled fatigue testing enables failure to be defined as a percentage reduction in bending stiffness.

Test specimen design and construction, as well as test machine configuration are detailed in the following subsections.

2.1 TEST SPECIMEN DESIGN

The dimensions of the homogeneous test specimens were selected based on preexisting molds and materials, as well as to provide relevance to creep and stress relaxation test results obtained in other research efforts [5].

The force-deflection behavior of the homogeneous and metallic-reinforced segments was designed to be equal to provide a comparison of two possible designs that could be introduced into a compliant mechanism without altering the overall functionality [5]. This was accomplished by matching the bending stiffness of the metallic reinforced segment to that of the homogeneous segment.

Cross sections of homogeneous and reinforced compliant segments are shown in Figure 3.

2.2 TEST SPECIMEN CONSTRUCTION

Engineering plastics are used in compliant mechanism construction because they are inexpensive, corrosion resistant, lightweight and have a high strength-to-modulus ratio relative to metals [4], [5]. However, polymeric materials generally exhibit lower endurance limits than metallic materials. The endurance limit is the cyclic stress under which no failure will occur due to fatigue [6]. The endurance limit for polymer materials is estimated to be approximately 25% to 30% of the materials static tensile strength [8]. The endurance limit for metallic materials is estimated to be 50% of the static tensile strength [6].

This paper aims to leverage the advantages of both plastic and metal by testing segments that contains a polymer casing containing a metallic reinforcing element. Kuber introduced the concept of placing a strong reinforcing material within a compliant casing constructed of a relatively weak casing material in an effort to prevent creep and fatigue failures [9].

IE-3075, a room-temperature casting urethane, was selected as the material of construction for test specimens. The flexural modulus and flexural strength are similar to other engineering plastics, such as Acetal [5]. IE-3075 is cast in a custom silicone mold made using readily available construction supplies.

The mold making process for compliant segments, both homogeneous and reinforced was described by Crews [5]. This method has been used in experimental evaluations of stress relaxation and creep as for comparison of deflections between homogeneous and metallic-reinforced compliant mechanisms [5]. A brief overview of the process is given in the following paragraphs.

A silicone mold is constructed by casting silicone over a pattern in a mold box in two steps to produce a two piece mold. The mold contains both fill and vent ports. A mixed solution containing urethane resin and hardener is poured into the fill tube until it emerges in the vent tubes. Upon curing, the mold is split and the test specimen is removed from the mold.

A reinforced compliant segment can be constructed using the same bottom mold half as the original, unreinforced compliant segment [5]. A metallic reinforcing element is held by two plastic insert holders which are then placed into the mold as an assembly. The plastic insert holders were custom designed and constructed from thermoplastic using additive manufacturing. Figure 4 shows an exploded assembly view of a mold setup for casting a metallic reinforced specimen [5]. A completed, reinforced compliant segment created using the example mold is shown in Figure 5.

Properties and dimensions of fatigue test specimens are included in Table 1. Table 2 shows the bending stiffness, EI, of each fatigue test specimen. The bending stiffness proportion related to the polymer and metallic components of the reinforced specimens is included. Complete failure of the polymer casing would result in a 61% reduction in the bending stiffness of the compliant segment.

Fatigue testing of both homogeneous and reinforced compliant segments was performed using the custom designed fatigue tester shown in Figure 6. The fatigue tester contains a rigid specimen holder to provide a fixed boundary condition for the test specimen. A NEMA 34 stepper motor, microstepping driver, and power supply provide the force to deflect the fixed-free specimen. A cam is attached to the motor shaft.

A cam follower, guided by a linear bearing, applies a load directly to the free end of the test specimen. The load applicator applies an upward force on the free end of the segment. The cam is circular in shape with an eccentric mounting hole which produces a sine function displacement curve. The maximum load applicator displacement is 2.010 inches (54.1 mm). The displacement of the cam follower is shown in Figure 7.

This loading configuration is not fully-reversed bending, but is a fluctuating stress where the minimum stress is zero. The R-Ratio or stress ratio is the ratio of minimum stress to maximum stress [10]. This testing device provides an R=0 stress ratio, meaning that the stress varies between zero and maximum. The fluctuating loading configuration described above is more common in compliant mechanisms than the R=-1, fully reversed loading configuration [4].

The use of a cam and follower ensures that the load is non-following. A non-following load does not change orientation with respect to the base coordinate system as the specimen deflects. Consistency in the loading configuration between the starting position and deflected position are depicted in Figure 8.

The stepper motor is highly suited to this application because it is rotates through discrete steps thus ensuring that the force measurements are taken at the same deflection at each data collection point. The motor driver supplies power to the stepper in a specified number of pulses to achieve the desired angular rotation. The motor and driver used in this test effort were configured to require 400 pulses to achieve one rotation of the motor shaft. Collection of data from the load cell occurred every 200,000 pulses, or 500 rotations of the motor shaft. Measurement of the force required to achieve the specified

deflection at the end of the fixed-free compliant segment enables trending of the bending stiffness as a function of cycle count.

Control of the angular velocity and acceleration of the motor is provided by an Arduino Uno microcontroller board. Force measurements are provided by an s-beam load cell placed in line with the load applicator. Strain gage signal amplification was performed using an HX711 24-bit analog-to-digital converter calibrated using test weights applied to the load applicator. The output of the HX711 was connected to a digital input of the Arduino Uno.

A software program was developed and installed on the Arduino Uno that provides pules to the stepper motor driver to rotate the stepper motor at a test frequency of 2 Hz, or two cycles per second. The load output from the HX711 was recorded at 500 cycle intervals, starting at cycle 0. Recording the test load intermittently provides a trend in the test load with respect to time or number of cycles, which is directly related to the bending stiffness of the specimen. The bending stiffness decreases as the fatigue fracture size increases due to the associated reduction in cross-sectional area at the fracture location. The bending stiffness was calculated at 500 cycle intervals using the PRBM force-deflection relationship [11]:

$$\mathrm{EI} = \frac{\mathrm{P}\gamma \mathrm{l}^2 \cos(\Theta)}{2.258\Theta} \tag{1}$$

Where P is the measured load at maximum deflection, l is the free length or distance from the load applicator to the fixed end of the test specimen, γ is a characteristic radius factor equal to 0.85 for a cantilever, and Θ is the pseudo-rigid-body angle. The test

machine provides a fixed free length, *l*. The pseudo-rigid-body angle is also constant because the load measurements occurred at the same tip deflection every 500 cycles.

Test setup includes measuring the cross-sectional dimensions of each fatigue test specimen and installing it into the fixed base of the fatigue tester. The load cell is activated and load values are displayed while the cam is rotated manually to identify the top of the load cycle. This establishes the starting point for the fatigue test. The aforementioned software program is initiated and testing commences with the simultaneous start of motor and data collection from the load cell. Figure 9 shows a homogeneous test specimen at maximum deflection.

3. RESULTS AND DISCUSSION

3.1 FATIGUE TEST RESULTS

The fatigue performance of a material is represented in the form of a plot of the number of cycles to failure versus the applied stress. The focus of this paper was to compare the fatigue performance of homogeneous compliant segments and metallic-reinforced compliant segments for a single deflection level.

Bending stiffness was recorded at 500 cycle intervals during the fatigue test. A trend of bending stress, as a percentage of the original stiffness, provides an indication of the degree of material degradation. A decrease in bending stiffness indicates a decrease in the moment of inertia of the compliant segment associated with material degradation.

Trends in bending stiffness of the homogeneous specimens revealed that minimal reductions in bending stiffness preceded total failure, or complete separation of the specimens into two pieces. The homogeneous specimen did not contain noticeable fractures upon intermittent visual inspection during testing. This sudden fracture is not uncommon in thermoset polymers [12]. Homogeneous Specimens 1 and 3 experienced complete failure at 105,500 and 98,000 cycles, respectively. Homogeneous Specimen 2 failed prematurely at 58,500 cycles possibly due to an internal flaw. All three homogeneous specimens exhibited similar trends in bending stiffness prior to failure, as shown in Figure 10.

The reinforced specimens did not fracture completely across the cross-sectional area. The fatigue tester was programmed to run until the bending stiffness of each specimen reduced to 50% of the value measured on the first cycle. A 50% reduction in bending stiffness was chosen to represent a stiffness that would drastically alter the

functionality of a compliant mechanism. Testing of the first reinforced test specimen revealed that the reinforced specimens would not endure total separation of the polymer casing in a reasonable test duration. Reinforced specimen 1 showed little reduction in bending stiffness upon completion of 275,000 cycles. The subsequent test specimens, Reinforced specimens 2 and 3 were tested to 320,000 and 375,000 cycles, respectively, to monitor the reduction in bending stiffness.

Upon inspection, it was determined that reinforced specimen 3 contained a fracture that extended through the entire cross section on the tensile side and below the metallic reinforcement. Reinforced specimens 1 and 2 exhibited cracking on the tensile side of the cross section which propagated from the edge thickness inward to the location of the metallic reinforcement. A detailed discussion of fracture surfaces is given in the next section.

All three metallic-reinforced specimens exhibited similar trends in bending stiffness prior to failure, as shown in Figure 11. The reinforced test specimens followed a similar percent reduction in bending stiffness when compared to the homogeneous test specimens, but at significantly higher cycle counts. For example: homogeneous specimen 1 and reinforced specimen 2 both exhibited a bending stress reduction of approximately 15%, but the associated cycle count for the reinforced specimen was 320,000 compared to 105,500 for homogeneous specimen 1.

3.2 FRACTURE SURFACE ANALYSIS

Visual and microscopic examination revealed that the fracture surfaces of the fatigue samples exhibited brittle behavior. Brittle fracture behavior is common in thermoset polymers [13]. Fracture surfaces of a homogeneous fatigue specimen and a

homogeneous static specimen are shown in Figure 12a and 12b, respectively. Visual inspection revealed that the fracture surface of the fatigue specimen was distinctly different from the fracture surface of a fixed-free compliant segment that underwent static deflection to failure. The fracture surface is notable smoother than the static fracture surface, with the exception of the hackle region associated with increased fracture velocity. The fracture surface of the fatigue specimen contained initiation, mirror, mist, and hackle regions commonly found in polymer fracture surfaces [14]. However, no significant surface area of the fatigue fracture contained intact fatigue striations or beach marks.

While the homogeneous specimens failed completely, resulting in two separate pieces, the reinforced specimens experienced fracture of the casing without complete separation. A thumbnail-shaped fracture was observed across the tensile side of the fixed-free compliant segment. Fractures also extended around the metallic reinforcement, but arrested in the cross-sectional area above the reinforcement. Figure 13 shows the fracture surface of a polymer casing from a metallic reinforced segment after fatigue testing. The cross-sectional area above the metallic reinforcement remained intact after fatigue testing and was subsequently fractured in the laboratory to separate the two fracture surfaces.

Optical microscopy was used to perform fractography to identify characteristic features on the fracture surfaces. Microscopic examination revealed that the fractures in the homogeneous specimens initiated at an internal flaw near a corner of the tensile cross section. The fracture initiation location of a homogeneous specimen is shown in Photographs 4 and 5. The fracture initiated at an internal flaw and propagated left-to-right

in the fracture surface shown in Figure 14 and Figure 15. The mirror region adjacent to the initiation location is representative of a relatively slow fracture velocity [14]. The mist region adjacent to the mirror region is representative of an increase in fracture velocity [14] [15]. The final fracture region, which contains hackles, is identified by relatively rough features [14].

Microscopic examination revealed that the fractures in the selected, reinforced specimen initiated at a group of pores located near the corner of the tensile cross section. The fracture initiation location of a reinforced specimen is shown in Figure 16. The fracture propagated right-to-left in the fracture surface shown in Figures 14-16. The fracture propagated around the metallic reinforcement with little change in fracture surface topography. This indicates that the local stress resulting from the edge of the slot did not significantly alter the propagation velocity. Figure 17 shows that the slot in the polymer casing does not contain sharp corners. The spring steel was supplied with a rounded edge, which provided a rounded slot as the resin was cast around the reinforcing element. The rounded edge in the slot reduces the local stresses at the corners.

4. CONCLUSIONS

This paper provides results from an experiential investigation of fatigue in homogeneous compliant segments constructed of thermoset plastic, as well as thermoset segments containing spring steel reinforcement. It was highlighted that fatigue is of concern to designers of compliant mechanisms because mechanisms are often designed to accomplish tasks in a repeated fashion.

Fatigue testing showed that failure of homogeneous specimens resulted in two separate pieces which is notably different than the fracture behavior observed in metallic reinforced specimens. Metallic-reinforced specimens experienced fracture of the casing without complete separation. The reinforced test specimens attained a similar percent reduction in bending stiffness when compared to the homogeneous test specimens, but at significantly higher cycle counts.

While no significant surface area of the fatigue fracture contained intact fatigue striations or beach marks, Fractography revealed that the fracture surface of the fatigue specimen was distinctly different from the fracture surface of a fixed-free compliant segment that underwent static deflection to failure. Fracture surface features such as mirror and mist regions identified on the fatigue fracture surfaces of the fatigue specimens which are indicative of relatively slow fracture propagation.

Future work in this research area may include an experiential investigation of fatigue in homogeneous compliant segments constructed of thermoplastic materials, as well as thermoset segments containing spring steel reinforcement.

5. REFERENCES

[1] Baumeister, T, and Marks, L., Standard Handbook for Mechanical Engineers, 7th ed. McGraw Hill, New York, New York, 1967

[2] Midha, A., T. W. Norton and L. L. Howell, "On the Nomenclature, Classification, and Abstractions of Compliant Mechanisms," Journal of Mechanical Design, Trans. ASME, Vol. 116, No. 1, March 1994, pp. 270-279.

[3] Salamon, B. A., "Mechanical Advantage Aspects in Compliant Mechanisms Design," MS Thesis, Purdue University, October 1989.

[4] Howell, L. L., Compliant Mechanisms, John Wiley & Sons, Inc., New York, New York, 2001.

[5] Crews, J. A., "Methodology for Analysis of Stress, Creep and Fatigue Behavior of Compliant Mechanisms," Doctoral Dissertation. Missouri University of Science and Technology, 2016.

[6] Stephens, R.I., et al. *Metal Fatigue in Engineering*, 2nd Ed., John Wiley & Sons, Inc., New York, New York, 2001.

[7] Reed, R.P., et al. "The Economic Effects of Fracture in the United States," United States Department of Commerce, National Bureau of Standards, Special Publication 647, 1983.

[8] Lazan, B.J. and Yorgiadis, A., "Symposium on Plastics," ASTM Technical Publication Number 59, Pg. 66, 1944.

[9] Kuber, Raghvendra Sharadchandra, "Development of a methodology for pseudo-rigid-body models of compliant segments with inserts, and experimental validation," Master's Theses. Paper 5363. Missouri University of Science and Technology, 2013.

[10] Gedeon, M., "Fatigue and Stress Ratios," Technical Tidbits, Issue 53, Materion Brush, Inc. Mayfield Heights, Ohio, 2013

[11] Howell, L.L., Magleby, S.P., Olsen, B.M., *Handbook of Compliant Mechanisms*, John Wiley & Sons, Ltd., West Sussex, United Kingdom, 2013.

[12] A.J. Kinloch & R.J. Young, *Fracture Behaviour of Polymers*, Applied Science Publishers, London, UK, 1983.

[13] Knauss, W.G. "Time Dependent Fracture of Polymers," Graduate Aeronautical Laboratories, California Institute of Technology, Pasadena, CA., 1989.

[14] Fracture of Plastics, *Failure Analysis and Prevention*, Vol 11, ASM Handbook, ASM International, 2002, pgs 650-661.

[15] Difrancesco, S., "Quantitative Fractography: A Comparative Study for Polymer Toughness Evaluation," Master's Thesis, University of Florida, 2006.

6. FIGURES AND TABLES

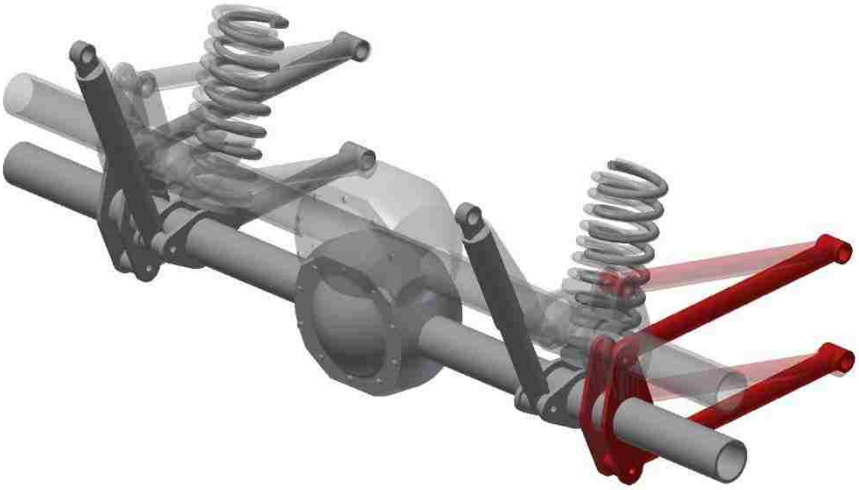

a)

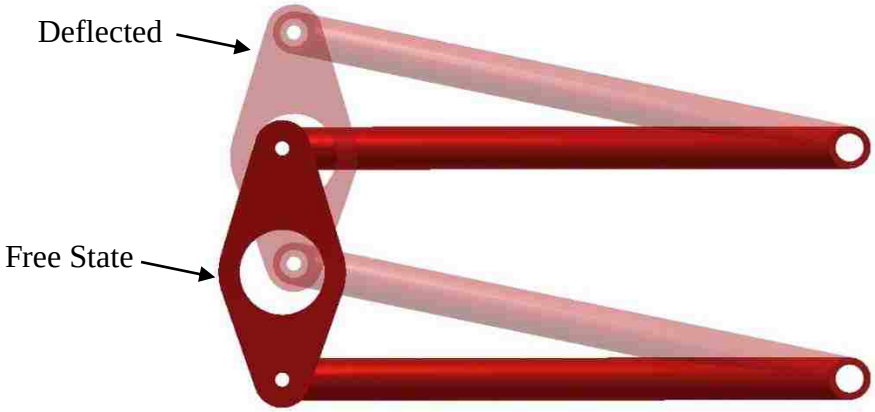

b)

Figure 1: Automotive Suspension Rigid-body Mechanism Example a) Rigid-body 4-bar Mechanism Assembly and b) Rigid-body Mechanism

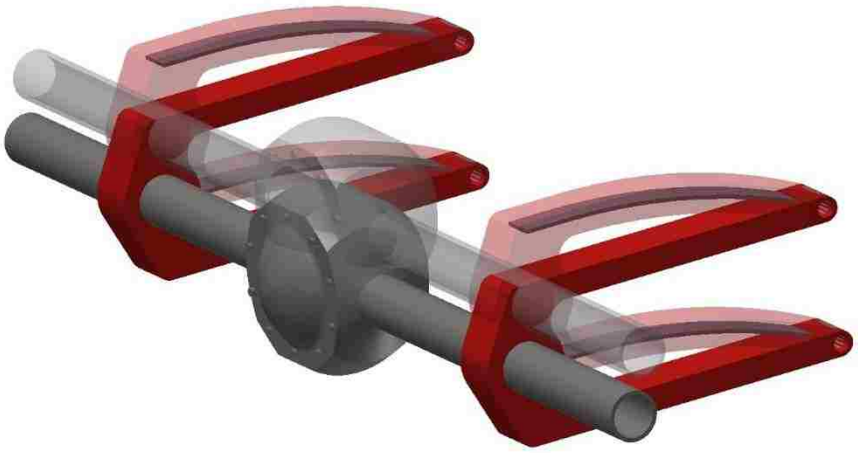

a)

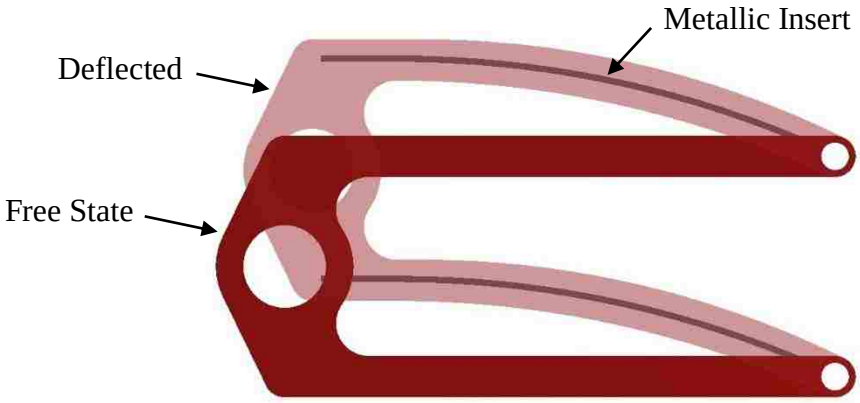

b)

Figure 2: Automotive Suspension Compliant Mechanism Example a) Compliant 4-bar Mechanism Assembly and b) Compliant Mechanism

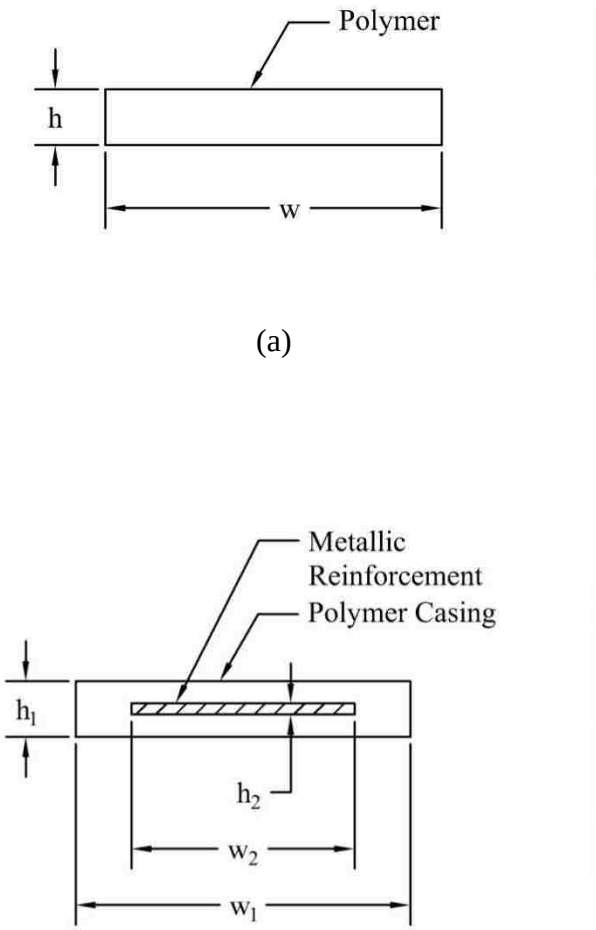

Figure 3: Cross-Section of (a) Homogeneous and (b) Reinforced Compliant Segments [8]

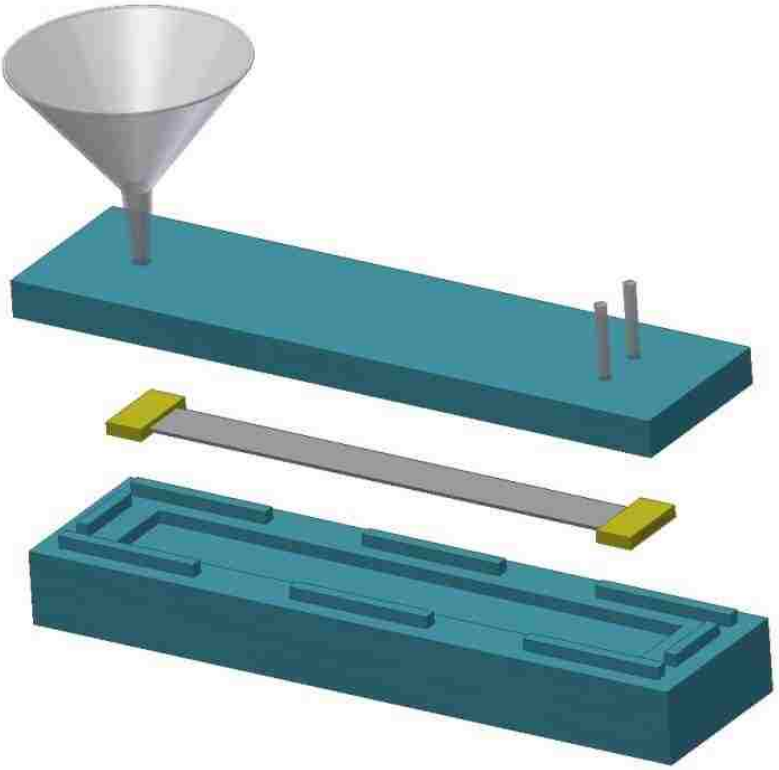

Figure 4: Assembly View of Silicone Mold used for Casting IE-3075 Urethane [8]

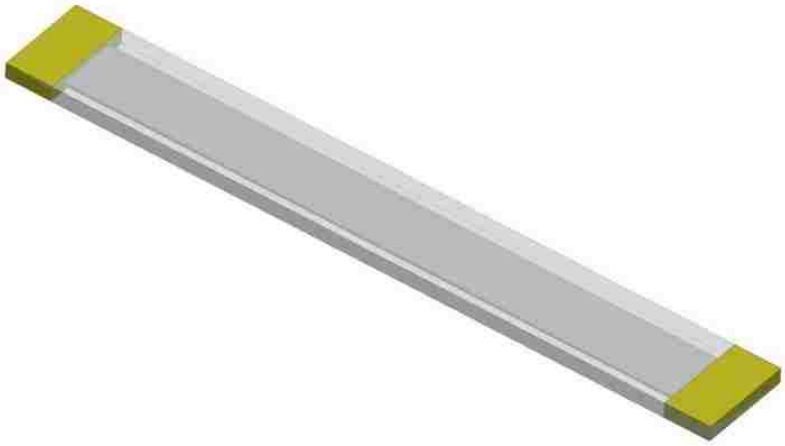

Figure 5: Cast IE-3075 Urethane Fixed-Free Compliant Segment [8]

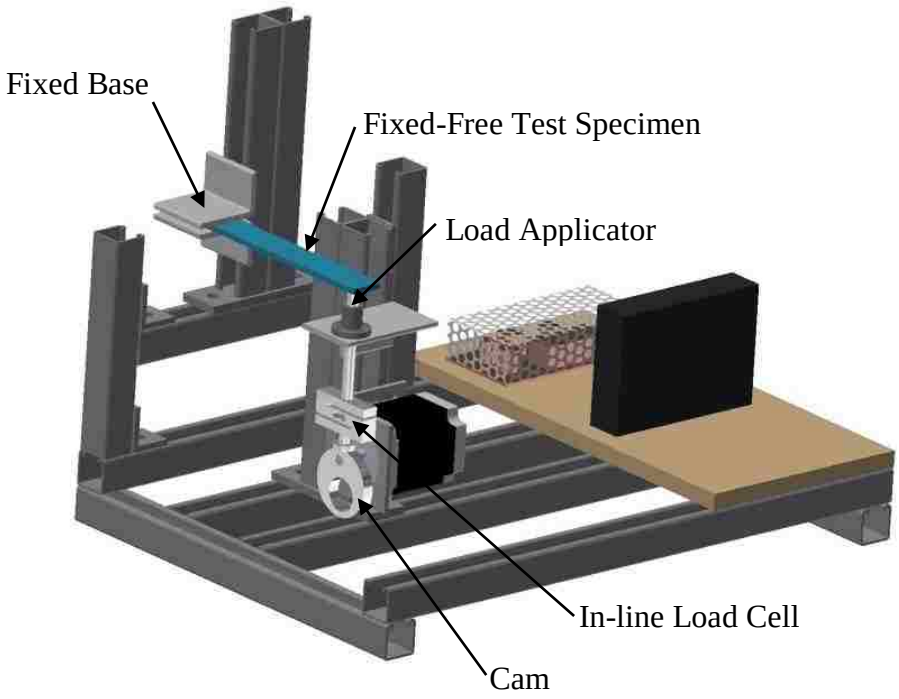

Figure 6: Fatigue Tester for Fixed-Free Compliant Segments

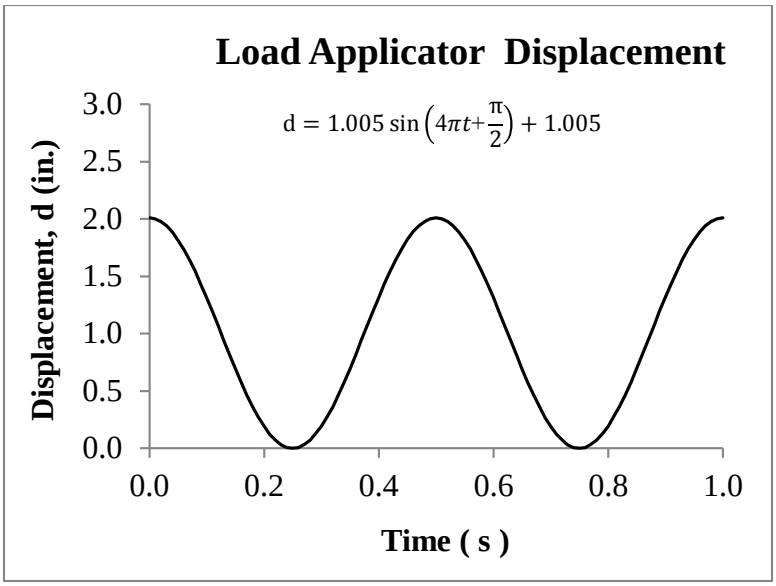

Figure 7: Sinusoidal Displacement of Load Applicator

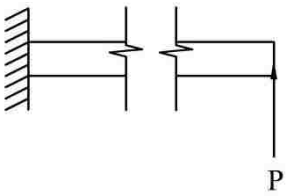

(a)

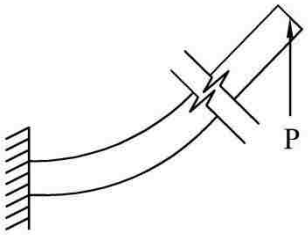

(b)

Figure 8: End-Load, P Applied to Fixed-Free Compliant Segment in the (a) Free State and (b) Deflected State

Figure 9: Homogeneous Test Specimen Shown at Maximum Displacement

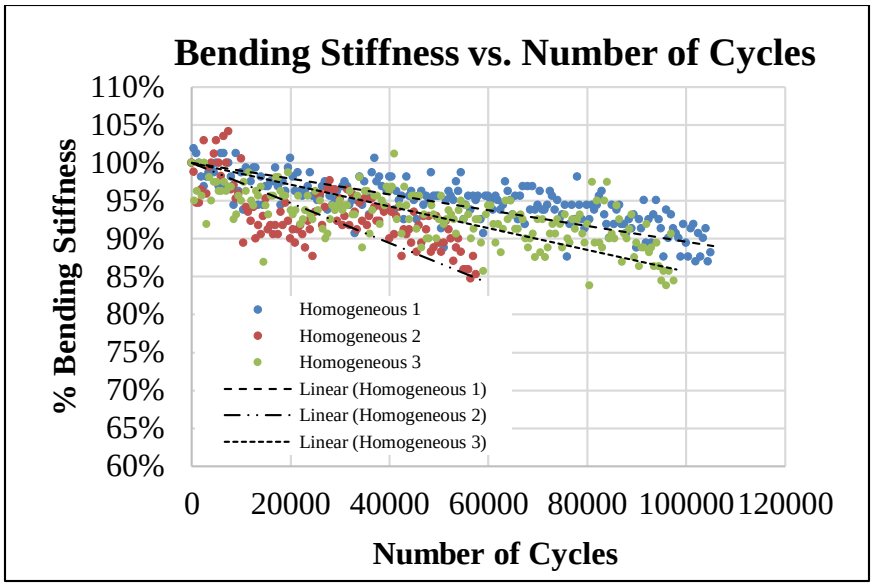

Figure 10: Bending Stiffness vs. Number of Cycles for Homogeneous Specimens

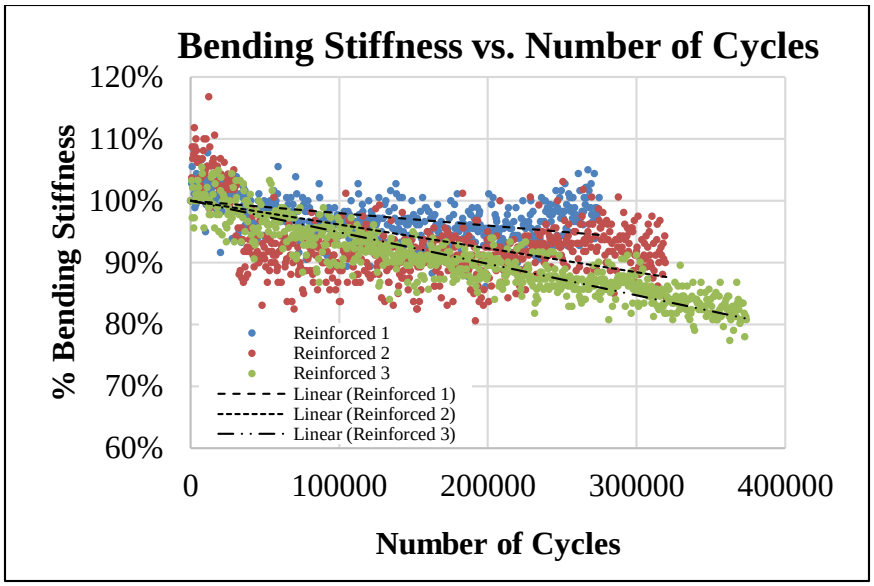

Figure 11: Bending Stiffness vs. Number of Cycles for Reinforced Specimens

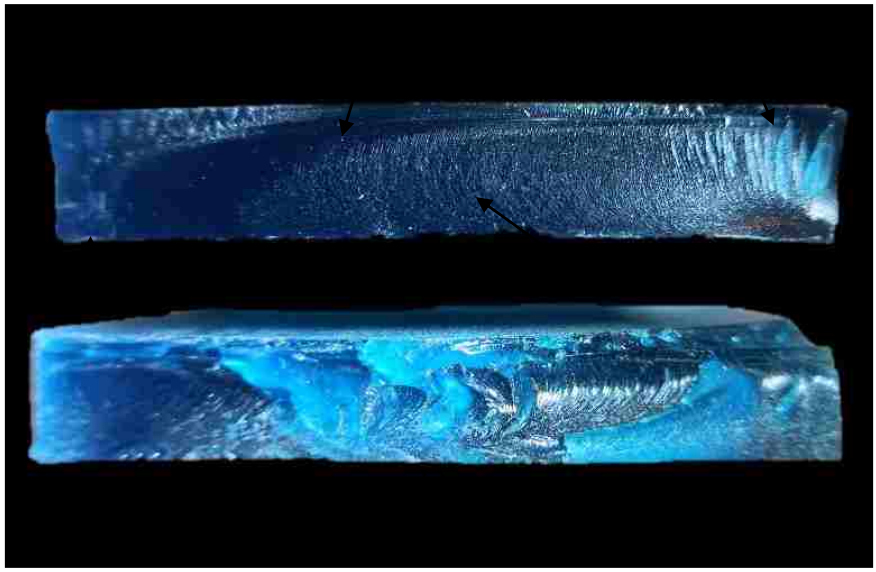

Figure 12: Fracture Surfaces of Homogeneous Samples a) Fatigue and b) Static Bending

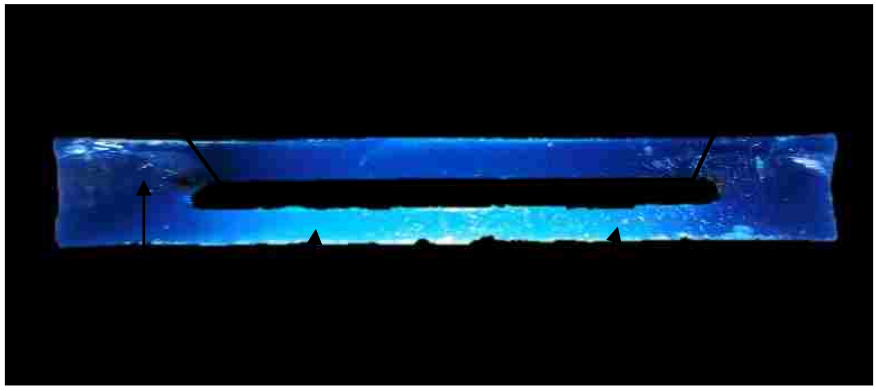

Figure 13: Fracture Surface of Casing from Metallic Reinforced Compliant Segment After 375,000 Stress Cycles

Figure 14: Fracture Initiation of a Homogeneous Fatigue Specimen

Figure 15: Close-up View of Fracture Initiation of a Homogeneous Specimen

Figure 16: Fracture Initiation of a Metallic Reinforced Specimen

Figure 17: Fracture Surface Surrounding the Metallic Reinforcement Slot

Table 1: Properties & Dimensions of Polymer Portions of Fatigue Test Specimens

	Polymer		
Specimen	Thickness in. (mm)	Width in. (mm)	Moment of Inertia $in.^4$ (mm^4)
Homogeneous 1	0.240 (6.10)	1.497 (38.02)	0.00173 (720.08)
Homogeneous 2	0.239 (6.07)	1.498 (38.04)	0.00171 (711.756)
Homogeneous 3	0.239 (6.07)	1.498 (38.04)	0.00171 (711.756)
Reinforced 1	0.208 (5.28)	1.506 (38.25)	0.00112 (466.179)
Reinforced 2	0.208 (5.28)	1.506 (38.25)	0.00111 (462.017)
Reinforced 3	0.209 (5.31)	1.510 (38.35)	0.00113 (470.342)

Table 2: Bending Stiffness Information for Fatigue Test Specimen

		% of Bending Stiffness	
Specimen	Total Bending Stiffness in^2-lbf (mm^2-kN)	Polymer	Metal
Homogeneous 1	749 (2,149)	100%	
Homogeneous 2	743 (2,132)	100%	
Homogeneous 3	743 (2,131)	100%	
Reinforced 1	799 (2,293)	61%	39%
Reinforced 2	797 (2,286)	61%	39%
Reinforced 3	805 (2,310)	61%	39%

SECTION

2. CONCLUSIONS

A method was presented for analysis of stress in fixed-free compliant segments as well as small-length flexural pivots, subjected to end loads or displacement boundary conditions. The analysis method builds upon key outputs from the pseudo-rigid-body models (PRBM) previously developed for force-deflection analysis. Simplified equations for stress were presented for both homogeneous and metallic-reinforced segments. Stress in both the polymer compliant segment, and the metallic reinforcing element was addressed, thus providing a comprehensive stress analysis tool. The stress analysis method and equations were demonstrated using two example design cases: one homogeneous compliant segment and one reinforced with a spring steel reinforcing element. The results showed that the introduction of metallic reinforcement increases the flexural rigidity, but does not reduce the bending stress in the casing unless the cross-sectional thickness is reduced.

A straightforward method was developed to redesign a baseline compliant segment to reduce stress without requiring additional redesign of the whole mechanism. The need to redesign the entire mechanism was eliminated by matching the force-deflection response of the redesigned segment to that of the failed segment.

The method enables researchers and designers of compliant segments to redesign segments that are overstressed and have experienced creep, stress relaxation, or fatigue. It was shown that the bending stress in the polymer portion of the compliant segment can be indirectly reduced by the introduction of a high-modulus insert because the distance

from the neutral axis to the extreme fiber of the polymer is reduced to maintain a consistent deflection behavior.

Room-temperature urethane casting was introduced as a simple and economical construction technique for compliant mechanisms. This manufacturing technique enabled the production of both homogeneous and reinforced compliant mechanisms at ambient temperature using relatively inexpensive materials and equipment. A unique, simple, and accurate deflection testing device was introduced that enabled experimental testing and validation of the force-deflection response of fixed-free compliant segments.

Equivalence between results obtained using the parallel spring and equivalent area methods showed that the degree of bonding between the insert and casing does not affect the bending stiffness if the reinforcement and casing share a common neutral axis due to symmetry about the horizontal axis.

Creep and stress relaxation were examples as they relate to compliant mechanisms. Results were presented from creep and stress relaxation tests. Creep test results showed that metallic-reinforced compliant segments exhibit improved creep resistance over homogeneous compliant segments of similar function. Experimental testing showed that the introduction of metallic reinforcement and optimization of the cross-sectional thickness of the segment reduced the creep strain by 50% during a 1,000-hour creep test. Similar improvements in stress relaxation performance were realized by the introduction of metallic reinforcement. The homogeneous specimens had relaxed to near-zero stress approximately 800 hours after they were restrained to the mandrel. The reinforced specimens retained approximately 50% of the initial stress after 1,000 hours.

Results were presented from an experiential investigation of fatigue in homogeneous compliant segments constructed of thermoset plastic, as well as thermoset segments containing spring steel reinforcement. It was highlighted that fatigue is of concern to designers of compliant mechanisms because mechanisms are often designed to accomplish tasks repeatedly.

Fatigue testing showed that failure of homogeneous specimens resulted in two separate pieces, which is notably different than the fracture behavior observed in metallic reinforced specimens. Metallic-reinforced specimens experienced fracture of the casing without complete separation. The reinforced test specimens attained a similar percent reduction in bending stiffness when compared to the homogeneous test specimens, but at significantly higher cycle counts.

While no significant surface area of the fatigue fracture contained intact fatigue striations or beach marks, fractography revealed that the fracture surface of the fatigue specimen was distinctly different from the fracture surface of a fixed-free compliant segment that underwent static deflection to failure. Fracture surface features such as mirror and mist regions that were identified on the fatigue fracture surfaces of the fatigue specimens are indicative of relatively slow fracture propagation.

Future work in this research area should include an experiential investigation of fatigue in homogeneous compliant segments constructed of thermoplastic materials, as well as thermoset segments containing spring steel reinforcement. Additional studies should be conducted to assess thermoset polymers for exploitation in the field of compliant mechanisms.

BIBLIOGRAPHY

[1] Budynas, R. and Nisbett K., Shigley's Mechanical Engineering Design, McGraw-Hill Education. New York, New York, 2015.

[2] Howell, L. L., Compliant Mechanisms, John Wiley & Sons Inc., New York, New York, 2001.

[3] Salamon, B. A., "Mechanical Advantage Aspects in Compliant Mechanism Design," M.S. Thesis, Purdue University, 1989.

[4] Midha, A., Howell, L. L. and Norton T. W., "On the Nomenclature, Classification and Abstractions of Compliant Mechanisms", Journal of Mechanical Design, Trans ASME Vol 116, No. 1. - 1994. - pp. 270-279.

[5] Howell, L. L. and Midha, A., "A Method for the Design of Compliant Mechanisms with Small-Length Flexural Pivots," Journal of Mechanical Design, Trans. ASME, Vol. 116, No. 1. - 1994. - pp. 280-290.

[6] Bapat, S. G., "On the Design and Analysis of Compliant Mechanisms using the Pseudo-Rigid-Body Model Concept," Doctoral Dissertation. Paper 2376. Missouri University of Science and Technology, Rolla, Missouri, 2015.

[7] Kuber, R. S., "Development of a Methodology for Pseudo-Rigid-Body Models of Compliant Segments with Inserts, and Experimental Validations," Master's Thesis. Paper 5363. Missouri University of Science and Technology, 2013.

[8] Howell, L. L., "The Design and Analysis of Large-Deflection Members in Compliant Mechanisms," Master's Thesis. Purdue University, 1991.

[9] Howell, L. L. and Midha, A., "Parametric Deflection Approximations for End-Loaded, Large-Deflection Beams in Compliant Mechanisms", Journal of Mechanical Design, Trans ASME, Vol 117, No. 1. - 1995. - pp. 156-165.

[10] Howell, L. L., "A Generalized Loop Closure Theory for the Analysis and Synthesis of Compliant Mechanisms," Doctoral Dissertation Thesis. Purdue University, 1993.

[11] Pauly, J. and Midha, A, "Improved Pseudo-Rigid-Body Model Parameter Values for End-Force-Loaded Compliant Beams," Proceedings of the 28th Biennial ASME Mechanisms and Robotics Conference. - Salt Lake City, Utah. September 2004, Vols. DETC57580-1-5.

[12] Midha, A. and Kuber, R., “Closed-Form Elliptic Integral Solution for Initially-Straight and Initially-Curved Small-Length Flexural Pivots,” Proceedings of the ASME 2014 International Design Engineering Technical Conferences & Computers and Information in Engineering Conference, Buffalo, NY, 2014, Vols. DETC35268-1-7.

VITA

Joshua A. Crews was born in St. Charles, Missouri. He received his Bachelor of Science degree in mechanical engineering in 2008 from the University of Missouri-St. Louis/Washington University in St. Louis Joint Undergraduate Engineering Program. After completion of his undergraduate work, he joined Ameren Missouri as a hydro engineer responsible for mechanical projects related to hydroelectric power generation. He received his Graduate Certificate in engineering mechanics in 2011 from the Missouri University of Science and Technology. He gained the Project Management Professional certification from the Project Management Institute in 2011. He received his Master of Science degree in 2012 from the Missouri University of Science and Technology. He became a licensed professional engineer (PE) in the State of Missouri in 2012 after passing the Principals and Practice of Engineering exam focusing on materials and machine design. After becoming a PE, he joined Briem Engineering as a consulting engineer responsible for failure analysis and forensic engineering. He joined GKN Aerospace in 2014 as a technology engineer and is currently employed as the Technology Center Manager in North America. He received his Doctor of Philosophy degree in mechanical engineering in December 2016 from the Missouri University of Science and Technology.